

A Detailed Geochemical Study of Island Arc Crust: The Talkeetna Arc Section, South-central Alaska

**ANDREW R. GREENE^{1*}, SUSAN M. DeBARI², PETER B. KELEMEN³, JUREK
BLUSZTAJN⁴ AND PETER D. CLIFT⁵**

¹ DEPARTMENT OF EARTH AND OCEAN SCIENCES, UNIVERSITY OF BRITISH COLUMBIA,
VANCOUVER, BC, V6T1Z4, CANADA

² DEPARTMENT OF GEOLOGY, WESTERN WASHINGTON UNIVERSITY, BELLINGHAM, WA, 98225, USA

³ LAMONT-DOHERTY EARTH OBSERVATORY, COLUMBIA UNIVERSITY, PALISADES, NY, 10964, USA

⁴ DEPARTMENT OF GEOLOGY AND GEOPHYSICS, WOODS HOLE OCEANOGRAPHIC INSTITUTION,
WOODS HOLE, MA, 02543, USA

⁵ DEPARTMENT OF GEOLOGY AND PETROLEUM GEOLOGY, UNIVERSITY OF ABERDEEN, ABERDEEN,
AB24 3UE, UK

* Corresponding author.
Email: agreene@eos.ubc.ca

ABSTRACT

The Early to Middle Jurassic Talkeetna Arc section exposed in the Chugach Mountains of south central Alaska is 5-18 km wide and extends for over 150 km. This accreted island arc includes exposures of upper mantle to volcanic upper crust. The section comprises six lithologic units, in order of decreasing depth: (1) residual upper mantle harzburgite (with lesser proportions of dunite); (2) pyroxenite; (3) basal gabbro-norite; (4) lower crustal gabbro-norite; (5) mid-crustal plutonic rocks; and (6) volcanic rocks. The pyroxenites overlie residual mantle peridotite, with some interfingering of the two along the contact. The basal gabbro-norite overlies pyroxenite, again with some interfingering of the two different units along their contact. Lower crustal gabbro-norite (≤ 10 km thick) includes abundant rocks with well developed modal layering. The mid-crustal plutonic rocks include a heterogeneous assemblage of gabbroic rocks, dioritic to tonalitic rocks (30-40% area), and concentrations of mafic dikes and chilled mafic inclusions. The volcanic rocks (~ 7 km thick) range from basalt to rhyolite.

Many of the evolved volcanic compositions are a result of fractional crystallisation processes whose cumulate products are directly observable in the lower crustal gabbro-norites. For example, Ti and Eu enrichments in lower crustal gabbro-norites are mirrored by Ti and Eu depletions in evolved volcanics. In addition, calculated parental liquids from ion microprobe analyses of clinopyroxene in lower crustal gabbro-norites indicate that the clinopyroxenes crystallised in equilibrium with liquids whose compositions were the same as the compositions of volcanic rocks. The compositional variation of the main series of volcanic and chilled mafic rocks can be modeled through fractionation of observed phase compositions and phase proportions in lower crustal gabbro-norite (i.e. cumulates).

Primary, mantle-derived melts in the Talkeetna Arc underwent fractionation of pyroxenite at the base of the crust. Our calculations suggest that more than 25 wt % of the primary melts crystallised as pyroxenites at the base of the crust. The discrepancy between the observed proportion of pyroxenites (less than 5% of the arc section) and the proportion required by crystal fractionation modeling (more than 25%) may be best

understood as the result of gravitational instability, with dense ultramafic cumulates, probably together with dense garnet granulites, foundering into the underlying mantle during the time when the Talkeetna Arc was magmatically active, or in the initial phases of slow cooling (and sub-solidus garnet growth) immediately after the cessation of arc activity.

KEYWORDS: *island arc crust; layered gabbro; Alaska geology; island arc magmatism; lower crust*

INTRODUCTION

A major obstacle to our understanding the sources of island arc magmas is the effect of crustal evolution on the erupted volcanic products (Leeman, 1983). Studies of volcanic rocks in active island arcs often suggest the existence of large sections of complementary cumulates in the lower crust (e.g. Kay & Kay, 1985). To improve our understanding of the lower crust in island arcs, studies often use plutonic xenoliths (e.g. Arculus & Wills, 1980; Conrad *et al.*, 1983; DeBari *et al.*, 1987), partial crustal exposures (e.g. Kawate & Arima, 1998; DeBari *et al.*, 1999; Spandler *et al.*, 2003), or seismic velocity measurements (e.g. Suyehiro *et al.*, 1996; Fleidner & Klemperer, 1999; Holbrook *et al.*, 1999). These provide indirect evidence of the magmatic processes in the deep crust of island arcs.

Exposures of island arc crust provide an opportunity to directly observe relationships not normally observable in active systems. Unfortunately there are few examples of well-exposed, island arc crust (e.g. Kohistan section, Pakistan (Tahirkheli, 1979); Darb Zubaydah, Saudi Arabia (Quick, 1990); Hokkaido section, Japan (Takashima, 2002)). The Talkeetna Arc section in south-central Alaska has been recognized as the crust and upper mantle of an accreted, Early to Middle Jurassic island arc (Burns, 1985; DeBari &

Coleman, 1989; Plafker *et al.*, 1989) and hence offers a rare opportunity to directly compare volcanic rocks and their complementary deep and middle crustal plutonic equivalents.

The Talkeetna Arc has a fairly consistent north-dipping stratigraphy along strike with deepest rocks in the south and shallower rocks in the north (Fig. 1). The deepest level of the arc consists of residual mantle peridotite, overlain by pyroxenite, in turn overlain by gabbro-norite. The lower crust is dominated by layered gabbro-norite (≤ 10 km thick). Mid-crustal exposures are a heterogeneous assemblage of dioritic to tonalitic rocks mixed with gabbroic rocks and areas of abundant mafic dikes and chilled mafic inclusions. The upper crust of the arc is comprised of thick sequences of lavas, tuffs and volcanoclastic debris-flow deposits of the Talkeetna Volcanic Formation (~ 7 km thick) ranging from basalt to rhyolite.

This study examines a diverse suite of Talkeetna Arc rocks from the Chugach and Talkeetna Mountains using mineral and whole-rock chemistry to assess the nature of the relationship between the cumulate gabbro-norite and volcanic and upper-level plutonic rocks. These observations have been used to model the magmatic processes that link the volcanic and plutonic complements of this island arc and to place constraints on the nature of parental magmas.

DESCRIPTION OF THE ARC

The Talkeetna Arc represents the northernmost exposure of an island arc system that may have extended continuously along the entire western margin of North America during the Early to Middle Jurassic (Plafker *et al.*, 1989). The arc is part of the Peninsular Terrane,

which formed the over-riding plate during subduction of the oceanic Farallon Plate (Plafker *et al.*, 1989). The Peninsular Terrane has been thrust to the south over the accretionary rocks of the Chugach Terrane.

Early to Middle Jurassic plutonic and volcanic rocks of the Talkeetna Arc extend for more than 1000 km across southern Alaska. This study looks at a 150 km segment in the eastern portion of the arc in the Chugach Mountains (Fig. 1) but includes references to parts of the arc in the Talkeetna Mountains and on the Alaska Peninsula. Arc activity may have initiated between ~210 and 200 Ma and continued in an oceanic setting until at least 180 Ma, whereafter magmatism may have shifted northward (Clift *et al.*, 2005).

The earliest ages for the volcanic deposits from the Talkeetna Arc are 200 Ma (Pálffy *et al.*, 1999) and 207 ± 3 Ma (J. Amato, personal communication) based on zircons. The Tuxedni Formation, unconformably overlying the Talkeetna Volcanics in the Talkeetna Mountains, contains Early Bajocian mollusks dated at ~172 Ma (Imlay & Detterman, 1973; Imlay, 1984; Hillebrandt *et al.*, 1992). Thus the volcanic rocks constrain the age of the arc to be between 207 Ma and 172 Ma. Zircon ages from plutonic rocks in the Chugach Mountains generally agree with these constraints (~201 to 181 Ma), but extend to younger ages for plutonic rocks further west on the Alaska Peninsula (183-164 Ma) and further north in the Talkeetna Mountains (177-156 Ma) (Rioux *et al.*, 2001; 2002; 2004).

The buoyant arc crust was incorporated into the North American plate by the Late Jurassic or Middle Cretaceous (Plafker *et al.*, 1989). Up to 1000 kilometers of Cenozoic strike-slip displacement may have transported the Talkeetna Arc to its present position (Plafker *et al.*, 1989).

Previous studies and our continuing work in the eastern part of the arc have not identified an older, pre-arc, felsic crustal component within the section (Martin *et al.*, 1915; Grantz *et al.*, 1963; Detterman & Harstock, 1966; Newberry *et al.*, 1986; Millholland *et al.*, 1987; Plafker *et al.*, 1989; Nokleberg *et al.*, 1994; Rioux *et al.*, 2001; 2002; 2004). For this reason, the Talkeetna section is interpreted as having formed in an island arc within oceanic crust, as distinct from an arc emplaced within pre-existing continental material. In contrast, the western part of the arc (not part of this study) may have intruded into pre-existing Paleozoic basement of the Peninsular Terrane. In this western region there are some (detrital?) zircons in volcanic rocks on the Alaska Peninsula (Pálffy *et al.*, 1999) and possible inheritance in zircons from Jurassic plutonic rocks on Kodiak Island (Roeske *et al.*, 1989)

Most of the rocks examined for this study are exposed in the Chugach Mountains between Scarp Mountain and the Matanuska Glacier (Fig. 1), with additional volcanic rocks from the southern Talkeetna Mountains to the northwest. The exposures extend over an area 5-18 km wide (perpendicular to the Border Ranges Fault) and nearly 150 km long (parallel to the Border Ranges Fault). The rocks analysed in this study comprise four lithologic units, in order of decreasing depth: (1) basal gabbro-norite exposed on Scarp and Bernard Mountains that directly overlies mantle rock (Fig. 1); (2) lower crustal gabbro-norites exposed between Tazlina Lake and Barnette Creek; (3) mid-crustal plutonic rocks primarily between the Nelchina and Matanuska Glaciers that consist of gabbro-norite, gabbro, amphibole gabbro-norite, diorite, quartz diorite, tonalite and very minor amounts of granodiorite, all with dikes and inclusions of chilled mafic rocks; and

(4) volcanic rocks from the length of the study area between Scarp Mountain and the Matanuska Glacier, plus a small group from the Talkeetna Mountains.

The boundary between lower crustal gabbro-norite and mid-crustal plutonic rocks is inferred, from geochemistry and field relationships, to be between the extensive section of layered gabbro-norites showing distinct modal layering (lower crust) and the heterogeneous assemblages of mafic to felsic plutonic rocks (mid-crust). In addition, high-level amphibole gabbro-norite forms a homogeneous pluton closely associated with volcanic rocks on Pippin Ridge, and an intrusion into volcanic rocks on Sheep Mountain.

Ultramafic rocks, not analysed as part of this study, are exposed on four isolated hills (each 1-2 km²) at the eastern edge of the exposed arc section. In this locality, basal gabbro-norite, garnet gabbro, pyroxenite and residual mantle peridotite form a layered crust-mantle boundary about 200 m thick separating outcrops with >90% gabbro-norite from outcrops with >95% harzburgite and dunite (DeBari & Coleman, 1989).

South of these rocks, the base of the arc section is cut by the Border Ranges Fault that separates the arc rocks of the Peninsular Terrane from the accretionary sequences of the Chugach Terrane to the south (MacKevett & Plafker, 1974; Page *et al.*, 1986). The Border Ranges Fault has a history as both a thrust and right lateral strike-slip fault, which has been interpreted as the megathrust or backstop during accretion (Plafker *et al.*, 1989).

Internally, the Talkeetna Arc section is disrupted by a network of arc-parallel faults and there is no continuous exposure from the base to upper crust. However, throughout the length of the arc section, the volcanics and mid-crustal plutonic rocks lie to the north of the lower crustal gabbro-norites, with Moho and residual mantle sections even further to the south.

The arc crust also appears to have been tectonically thinned. Pressure estimates from garnet gabbros at the base of the crust are 850-1000 MPa, indicating a crustal thickness of 25-30 km (DeBari & Coleman, 1989; Mehl *et al.*, 2001; Kelemen *et al.*, 2003b). However, the exposed section has a maximum width of only 18 kilometers, perpendicular to the strike of the Border Ranges Fault and to internal lithological contacts, which dip at steep to shallow angles to the north. Thus, the section has a present day structural thickness of less than 18 kilometers (Fig. 1).

The lithologies examined in this study and petrographic characteristics for 144 out of 159 plutonic rock samples collected are summarized in Table 1 and Figure 2. Phase proportions in Table 1 are expressed as volume %, based on visual estimates. A representative suite of 83 volcanic rocks from the Talkeetna Arc were also analysed for whole-rock chemistry (Clift *et al.*, 2005).

ANALYTICAL METHODS

Minerals in 21 samples (18 gabbro-norites & 3 mafic dikes) were analyzed using a JEOL 733 electron microprobe at Massachusetts Institute of Technology and the University of Washington. Compositions from cores and rims in clinopyroxene, orthopyroxene, plagioclase, amphibole, spinel and olivine were measured with 15-keV accelerating voltage and 10-nA beam current. Element peaks/backgrounds were counted for 20-40 s and data were processed according to the Bence and Albee (1968) matrix correction as modified by Albee and Ray (1970). Analytical error is <2% relative for major elements and <15% relative for trace elements. Averages for the analyses from each sample are listed in Table 2 (the full data set is available at <http://www.petrology.oupjournals.org>).

Trace element concentrations in clinopyroxene and plagioclase were measured using the Cameca IMS-3F ion microprobe at Woods Hole Oceanographic Institution (WHOI). Analytical techniques are summarized by Shimizu and Hart (1982). A 20-30 nA primary beam of negative oxygen ions was focused to a 30 μ m diameter. After preliminary sputtering, the emitted positive secondary ions were analyzed by a double focusing mass spectrometer using energy filtering with a secondary accelerating voltage of 4500keV offset to -60eV for the Rare Earth Elements (REE) and -90eV for other trace elements (Ti, V, Sr, Y, Zr). Analytical error is estimated as <10% relative to the concentrations. Averages for the analyses from each sample are shown in Table 3A (clinopyroxene-REE), 4B (clinopyroxene-trace elements), and 4C (plagioclase-REE) (the full data set is available at <http://www.petrology.oupjournals.org>).

Whole-rock analyses have been acquired for 77 plutonic rocks from the Talkeetna Arc. Fifty-two analyses, with the major elements calculated on a volatile-free basis, are presented in Table 4. Samples were analyzed for 22 major and trace elements by X-Ray Fluorescence (XRF) and 27 trace elements by Inductively-Coupled Plasma Mass Spectrometry (ICP-MS) at the Washington State University (WSU) GeoAnalytical Laboratory. The preparation techniques and analytical methods for XRF (Johnson *et al.*, 1999) and ICP-MS (Knaack *et al.*, 1994) are available from WSU GeoAnalytical Lab (<http://www.wsu.edu/~geology/Pages/Services/Geolab.html>).

Nd isotopic ratios for 11 samples (6 gabbro-norites, 3 chilled mafic rocks, and 2 intermediate-felsic plutonic rocks) were measured at WHOI using a ThermoFinnigan MC-ICPMS Neptune and are presented in Table 5. Between 50 and 300 mg of rock powders were spiked with Sm-Nd spike (enriched in ¹⁴⁹Sm and ¹⁵⁰Nd) and dissolved in a

mixture 4:1 HF and HClO₄. After drying, 6.2N HCl was added, samples were evaporated to dryness, and this was repeated. Then 0.5 ml of 2.5N HCl was added to the samples, left to stand for several hours, and transferred for column separation. The first columns separate light REE (LREE) (technique as in Hart & Brooks, 1977) and second columns separate Nd from Sm (technique as in Richards *et al.*, 1976). Samples were loaded, washed, and separated by time with 0.25N HCl for Nd and 0.6N HCl for Sm. Concentrations of Sm were determined on a ThermoFinnigan ICP-MS Element. Nd isotopic compositions were normalized to $^{146}\text{Nd}/^{144}\text{Nd}=0.7219$ and all results are corrected against the La Jolla Nd standard $^{143}\text{Nd}/^{144}\text{Nd}=0.511847$.

MODAL MINERALOGY AND MINERAL CHEMISTRY

Samples from lower crustal gabbro-norites (between Tazlina Lake and Barnette Creek) were collected in north-south transects in order to characterize mineral compositions and evaluate vertical variations in mineral chemistry. Phase proportions (in weight percent) for 16 of the gabbro-norites were calculated using a least-squares method based on mass balance of whole-rock and mineral chemistry (Table 6).

Clinopyroxene

Gabbro-norites contain 1.80-22.0 wt % clinopyroxene, with an average of 13.4 wt % (Table 6). Clinopyroxene from lower crustal gabbro-norite has a narrow compositional range. It is Mg-rich (13.1-15.7 wt % MgO) and shows minimal Fe-enrichment with differentiation (Table 2). Magnesium number (Mg#) $[\text{Mg\#} = \text{molar MgO}/(\text{MgO} + \text{FeO}^{\text{total}}) \times 100]$, in which FeO^{total} refers to all Fe expressed as FeO] ranges

from 73.6 to 81.3 (mean 77.3) and Al_2O_3 contents range from 1.32 to 3.24 wt % (Fig. 3A). Clinopyroxene from basal gabbronorite (Scarp and Bernard Mountains) has high Al_2O_3 (4.69-7.31 wt %) compared to clinopyroxene in lower crustal gabbronorite with the same Mg#s. Clinopyroxene in amphibole gabbronorite, as part of the mid-crustal assemblage, has a range of Al_2O_3 contents similar to clinopyroxene in lower crustal gabbronorite, but with generally lower Mg#s (Pippin Ridge 69.2-70.7; Little Lake 71.5-75.4) (75.4-78.3) (Fig. 3A). TiO_2 contents are <0.59 wt % and Na_2O contents are <0.49 wt % in clinopyroxenes from all the gabbronorites.

Clinopyroxene phenocrysts from two mafic dikes have Mg#s (72.1-80.5) similar to clinopyroxene in lower crustal gabbronorite (Fig. 3A). Alumina contents in the phenocrysts range from 2.11 to 6.08 wt %, and have greater core to rim variation than clinopyroxene in gabbronorite (Table 2). The phenocrysts have Cr_2O_3 contents as high as 0.67 wt %, whereas clinopyroxene in gabbronorite has <0.15 wt % Cr_2O_3 (except for two clinopyroxene analyses from basal gabbronorite sample 1710A4b that are higher).

Chondrite-normalised (N) REE patterns for clinopyroxene from lower crustal gabbronorite samples are parallel, with positive-sloping LREE segments ($\text{La/Sm(N)}=0.05\text{-}0.17$; mean 0.11) and flat heavy REE (HREE) segments ($5\text{-}25\times$ chondrite; mean $10\times$ chondrite)(Fig. 4A). Ion microprobe analyses (3-8 per sample) showed minimal core-to-rim and grain-to-grain variation within samples, with a median standard deviation of less than $1\times$ chondrite. Rare earth element patterns for nine out of thirteen lower crustal gabbronorite samples form a distinct band, with similar abundances. Clinopyroxene in four samples (mid-crustal amphibole gabbronorite 1709A2, 1723A5; lower crustal gabbronorite 1712A7, 1722A7) have noticeably higher

REE abundances and negative Eu anomalies. Clinopyroxene in two basal gabbronorite samples (1710A4b, 1710A4d; dashed patterns in Fig. 4A) have LREE abundances that cross the band of patterns and have pronounced positive Eu anomalies. Clinopyroxene in one of these samples also has a positive Sr anomaly. Clinopyroxene phenocrysts in one mafic dike (1728A2) have similar major-element compositions and nearly identical REE abundances to clinopyroxene in lower crustal gabbronorites (Figs 2 and 3).

In a chondrite-normalised trace-element diagram for clinopyroxene (Fig. 4B), Zr is depleted relative to LREE and Ti is depleted relative to the HREE. The clinopyroxene with higher REE abundances have negative Sr anomalies as well as negative Eu anomalies. Four samples with the highest REE abundances in clinopyroxene are also enriched in Zr, Y, Ti, and V in clinopyroxene. Analyses of clinopyroxene from each of these samples form isolated trends in plots of Zr versus Y and Sr (Fig. 4C, D).

Orthopyroxene

Orthopyroxene compositions correlate with co-existing clinopyroxene compositions in the same samples, but have slightly lower Al_2O_3 (0.82-2.09 wt %) and Mg# (Fig. 3B). The Mg#s for orthopyroxene are more variable than clinopyroxene Mg#s in lower crustal gabbronorite (65.0-74.9; mean 69.9), and are also lower for orthopyroxene in mid-crustal amphibole gabbronorite (Pippin Ridge 57.4-59.6; Little Lake 57.9-62.7; Sheep Mountain 65.6-65.8) (Table 2). TiO_2 contents are <0.49 wt % and Na_2O contents are <0.44 wt %. From mass balance calculations, gabbronorites contain 1.71-45.7 wt % orthopyroxene (Table 6), averaging 13.4 wt %, the same as the average clinopyroxene proportion.

DeBari and Coleman (1989) estimated equilibrium conditions for basal gabbronorite of approximately 800-925°C at 0.95-1.05 GPa. Temperature estimates of co-existing pyroxenes for the suite of gabbronorites in this study, using the QUILF program (Andersen *et al.*, 1993) with pressure set at 0.7 GPa yielded temperatures ranging from 740-930°C and at 0.3 GPa yielded temperatures ranging from 700-920°C. The calculated temperatures for pyroxenes from Barnette Creek were slightly lower than those from Tazlina Lake. Amphibole gabbronorite from Pippin Ridge, Little Lake, and Sheep Mountain yielded similar temperatures to those from Barnette Creek (~800-820 °C).

Plagioclase

Plagioclase is the most abundant phase in the gabbronorites, ranging from 29 to nearly 80 wt % (Table 6). There is minimal intragrain zoning or variation in anorthite content. The anorthite content ranges from An_{91.8} to An_{77.7} in basal gabbronorite and An_{94.7} to An_{75.0} in lower crustal gabbronorite from Tazlina Lake and Barnette Creek (Table 2). There is a considerable gap between the plagioclase compositions in mid-crustal amphibole gabbronorite from Pippin Ridge and Little Lake (An_{65.5}-An_{59.8}) and the deeper gabbronorite. Most of the analysed gabbronorites show reverse zoning in plagioclase, with rims of most grains slightly more calcic than the cores. Plagioclase REE patterns have negative-sloping LREE segments, with relatively low abundances, and pronounced positive Eu anomalies (Fig. 4E). Samples with the highest REE abundances (e.g. mid-crustal amphibole gabbronorite samples 1709A2, 1723A5) have the lowest An contents.

Amphibole

Amphibole in the gabbronorites constitutes between 0.97 and 50.1 wt % (mean 19.1 wt %) (Table 6). The amphibole is pargasitic to actinolitic hornblende, with some edenite component (nomenclature of Leake, 1978). Mg#s for the amphibole range from 53.2 to 78.2, with slightly lower Mg#s in amphiboles from mid-crustal amphibole gabbronorites (Table 2). Mg#s in amphibole correlate with co-existing clinopyroxene Mg#s; clinopyroxene Mg#s are mostly higher than amphibole, with the exception of one sample from Scarp Mountain (1710A4e). The amphibole in basal gabbronorites from Scarp Mountain also has higher Al₂O₃ than other amphibole, analogous to the pyroxene. As noted by Burns *et al.* (1991), amphibole in gabbronorite samples is interstitial, and so is interpreted as a late magmatic or high temperature hydrothermal mineral.

Spinel

The proportion of Cr-Al-Mg-Fe-Ti oxide in gabbronorite ranges from 0.15 to 12.3 wt % (Table 6). With the exception of one sample from Scarp Mountain (1710A4d) which contains Fe-Ti oxide, spinels in basal gabbronorite are all Mg-Al pleonastes. All the other gabbronorites contain exsolved magnetite-ilmenite pairs. Lower crustal gabbronorites from Tazlina Lake average 10.2 wt % Fe-Ti oxide. TiO₂ contents in magnetite from lower crustal gabbronorites average 3.30 wt % (Table 2).

Olivine

Olivine is present in only one gabbroic sample (Tazlina 1712A4). This sample has whole-rock chemistry similar to the other gabbronorites. The olivine grains are not zoned and are mostly resorbed. Thin sections reveal symplectite intergrowths of amphibole and

magnetite between olivine and orthopyroxene. The olivine Mg#s in this sample range from 69.9 to 72.7 (Table 2).

Summary of mineral chemistry

The compositions of minerals from lower crustal gabbronorite between Tazlina Lake and Barnette Creek are consistent with a common igneous parentage, limited interaction with percolating evolved interstitial liquids, and/or re-equilibration of cores and rims through intracrystalline diffusion (Tribuzio *et al.*, 1999). There is no discernable vertical variation (from north-south transects), nor is there any consistent core to rim variation in clinopyroxene, orthopyroxene or amphibole from any of the gabbronorites or chilled mafic rocks.

Plagioclase in the layered gabbronorite has distinctly high An contents (mean 86.1), characteristic of plagioclase crystallised from hydrous arc magmas (e.g. Sisson & Grove, 1993). In hydrous arc magmas, clinopyroxene crystallises before plagioclase as a result of the suppression of plagioclase crystallisation due to water dissolved in the melt. Thus, the most primitive clinopyroxene (high Mg#, low Yb) will have negligible Eu anomalies, and more evolved clinopyroxene will have more pronounced negative Eu anomalies (Plank *et al.*, 2004). This is reflected by the presence of pronounced positive Eu anomalies in plagioclase and the absence of negative Eu anomalies in clinopyroxene (in all but two lower crustal gabbronorites, see below). The rims of plagioclase in samples from Tazlina and Barnette are slightly more calcic than the cores, by an average of 1.5 mole % An. This reverse zoning may be the result of several factors, such as an increase of pH₂O in

interstitial liquid (Arculus & Wills, 1980) or diffusion of Na from plagioclase into late crystallising amphibole (Khan *et al.*, 1989).

Clinopyroxene may have acquired REE characteristics from subsolidus breakdown of plagioclase + olivine to form pyroxenes, spinel, and garnet at the base of the crust. As previously described, clinopyroxene in basal gabbronorite samples has positive Eu anomalies and flatter LREE segments than clinopyroxene in lower crustal gabbronorite, and one of these samples possesses a positive Sr anomaly (Fig. 4B). Positive Eu anomalies and elevated LREE in clinopyroxene from gabbro-derived granulites from the Northern Apennines have also been attributed to redistribution of REE during granulite-facies recrystallisation (Montanini & Tribuzio, 2001).

The higher Al₂O₃ contents of pyroxene in the basal gabbronorite, compared to pyroxene in underlying pyroxenite, were attributed by DeBari and Coleman (1989) to Al increase in the liquid as a result of pyroxenite crystallisation. Although we believe pyroxenite crystallisation may have been extensive (see pyroxenite fractionation section, below), Al contents in pyroxenes in basal gabbronorites are six to eight times higher than in underlying pyroxenite. Pyroxenite crystallization was not likely sufficient to cause a six- to eight-fold increase in incompatible element abundances. Thus, if the Al contents of pyroxene in basal gabbronorites and pyroxenites were both formed in equilibrium with liquid, this suggests the presence of both high- and low-Al melts entering the Talkeetna Arc crust through the Moho. Alternatively, the high Al content in pyroxene in basal gabbronorites may result from metamorphic reactions involving breakdown of plagioclase ± olivine. In addition to high-Al pyroxene in basal gabbronorite, high-Al clinopyroxenes are found in several mafic dikes (Fig. 3A). This suggests that either some

high-Al pyroxene formed as igneous phases, or that the high-Al pyroxene grains in the dikes are xenocrysts derived from granulite facies rocks near the base of the arc crust.

Several lower crustal gabbro-norite samples with anomalous clinopyroxene trace-element chemistry (Fig. 4) possess distinct mineralogy. Tazlina sample (1712A7) has <2 wt % clinopyroxene, 12.3 wt % magnetite, and 40.9 wt % amphibole and a sample from Barnette Creek (1722A7) has >45 wt % orthopyroxene (Table 6). The high proportion of mafic minerals may be responsible for the enrichment of Zr in clinopyroxene rims from these samples, due to the incompatibility of Zr in Fe-Ti oxides and amphibole (e.g. Tribuzio *et al.*, 1999). Clinopyroxene rim compositions are enriched in Zr in mid-crustal amphibole gabbro-norite. In this case, the rims likely crystallised from a more evolved magma and/or retained a greater proportion of trapped melt, enriched in incompatible elements. Low Sr contents and negative Eu anomalies in clinopyroxene from mid-crustal amphibole gabbro-norite clearly reflect prior removal of plagioclase from the melt that crystallised the clinopyroxene (Fig. 4B).

WHOLE-ROCK CHEMISTRY

Major- and trace-element compositions

Mid-crustal intermediate to felsic plutonic rocks from the Talkeetna Arc have remarkably similar major- and trace-element concentrations to the volcanic rocks, while lower crustal “cumulate” gabbro-norites have systematically different major-element compositions, but many comparable trace-element characteristics. Major-element variations in whole-rocks are plotted in Figure 5, along with previously published results for the Talkeetna Arc and published analyses from the Mesozoic Kohistan Island arc in Pakistan. Talkeetna Arc

samples possess 38.0-77.9 wt % SiO_2 , with considerable overlap between the volcanic and intermediate to felsic plutonic rocks (Fig. 5). Al_2O_3 , CaO , and MgO decrease with increasing SiO_2 . There is very little overlap in SiO_2 between the gabbroic rocks (dominantly cumulates) and the volcanic and intermediate to felsic plutonic rocks. Al_2O_3 contents are high (mostly >15 wt % for samples with <65 wt % SiO_2) for all lithologies; in particular, gabbroic rocks contain 12.3-28.1 wt % Al_2O_3 with a mean of 18.9 wt % (Fig. 5). TiO_2 contents are low (primarily <1.5 wt %) for Talkeetna volcanic and intermediate to felsic plutonic rocks, with concentrations decreasing with increasing SiO_2 . Gabbroic rocks also define a broad, steeply-decreasing trend of TiO_2 with decreasing SiO_2 , at lower SiO_2 values. $\text{FeO}^{\text{total}}$ (not shown) behaves in the same way as TiO_2 and defines a similar trend versus SiO_2 . There is minimal overlap in CaO and MgO between the gabbroic rocks and other lithologies, with most of the gabbroic rocks having higher abundances. Gabbroic rocks generally have lower K_2O and Na_2O (not shown) than the volcanic and intermediate to felsic plutonic rocks.

Overall, compositions from the Talkeetna Arc for most of the major elements are similar to those for Kohistan Island Arc rocks, though many of the Kohistan samples have higher SiO_2 at about the same Mg\# (Fig. 5E). A broad band of data points overlaps the tholeiitic and calc-alkaline fields in Mg\# versus SiO_2 (using the classification scheme of Miyashiro (1974), expressed using Mg\#), with the majority of the basaltic volcanics lying within the tholeiitic field. Mg\# s range from 38.1 to 77.4 (mean 57.2) for the gabbroic rocks and are mostly lower for the volcanic (14.5-62.6; mean 42.8) and intermediate to felsic plutonic rocks (16.4-67.6; mean 41.8). The chilled mafic rocks

define steeply-decreasing trends for both MgO and Mg# versus SiO₂, with MgO from 3.5-12.4 wt % (mean 7.2 wt %) and Mg# from 39.7-69.8 (mean 56.3).

Concentrations of Ni, V, and Sr are, on average, higher in cumulate gabbronorites than in volcanic and intermediate to felsic plutonic rocks (Figs 5G, 5H, and 5I), but similar to those in the chilled mafic rocks. Zr concentration increases from very low levels in cumulate gabbronorite to higher concentrations in volcanic and intermediate to felsic plutonic rocks, with a distinct group of volcanic rocks diverging from the main trend to even higher concentrations.

Chondrite-normalised REE patterns for the range of different lithologies from the Talkeetna Arc (volcanic rocks, intermediate to felsic plutonic rocks, chilled mafic rocks, and gabbroic rocks) are remarkably parallel and increase in abundance systematically from the basal gabbronorite and lower crustal gabbronorite (1-10×chondrite) through the volcanic upper crust (8-38×chondrite) (Figs 5A and 5B). The patterns are flat through the middle and heavy REE, with very few crossing patterns. The gabbronorites with lower abundances are noticeably LREE-depleted and have distinct positive Eu anomalies. The LREE segments progressively flatten with increasing REE abundance in gabbroic rocks. Patterns for the mid-crustal gabbros, and several chilled mafic rocks and intermediate to felsic plutonic rocks, are nearly flat with small Eu anomalies.

The REE patterns for the volcanic samples throughout the arc section form a distinct band with parallel middle to heavy REE segments. However, three lavas, out of the 84 analyzed, are strongly depleted in HREE, similar to a single HREE-depleted volcanoclastic sample reported by Plafker *et al.* (1989) (Fig. 6A). The patterns in the main band are progressively LREE-enriched with increasing abundance and samples with

higher abundances generally have more pronounced negative Eu anomalies. REE patterns for volcanic and chilled mafic rocks found in close proximity (<1 km) are nearly identical. Several of the intermediate to felsic plutonic rocks are slightly LREE-enriched and most of these patterns overlap volcanic rock REE patterns.

N-MORB-normalised trace-element patterns are characterized by high concentrations of large-ion-lithophile elements (LILE) Ba, K, and Pb and lower abundances of high-field-strength elements (HFSE) Nb, Ta, Zr, Hf, Ti, Y (Figs 5C and 5D). The concentrations of virtually all incompatible elements rise incrementally, from basal gabbro-norites through the upper volcanic rocks, with noticeably parallel patterns. Positive Pb and Sr spikes, relative to adjacent elements, are present for all lithologies, with the exception of 8 volcanic rock samples with high trace element concentrations which have negative Sr and Eu anomalies. Ti concentrations are higher relative to HREE in cumulate gabbro-norites from the Tazlina and Barnette areas, while Ti is depleted relative to HREE in most of the volcanic and intermediate to felsic plutonic rocks.

Summary of whole-rock chemistry

The major- and trace-element whole-rock chemistry for Talkeetna Arc rocks is consistent with evolution as part of a co-magmatic differentiation sequence related to similar parental magmas. The whole-rock patterns reflect variability which may be related primarily to fractional crystallisation, where REE and HFSE increase and Mg# decreases with differentiation. The representative suite of volcanic rocks span the range of SiO₂ contents, from 48-80 wt % SiO₂. Sixty-three of the 83 volcanic rocks from throughout the arc have evolved compositions, with Mg# <50.

The importance of plagioclase fractionation is reflected by variation in whole-rock major and trace-element compositions. Plagioclase represents the dominant phase in the cumulate gabbronorites (Table 6) and trends of Al_2O_3 and CaO in the volcanic rocks are primarily the result of plagioclase fractionation. Positive Eu anomalies for layered gabbronorite clearly reflect their cumulate nature, assuming mantle-derived, parental arc magmas possess no Eu anomaly prior to crystallisation of plagioclase. Kelemen *et al.* (2003a) postulated that the high Pb and Sr in cumulate gabbroic rocks from the Talkeetna Arc result from a combination of (a) high plagioclase/liquid distribution coefficients for Pb and Sr, and (b) the presence of Pb and Sr spikes in parental Talkeetna Arc liquids.

Crystallisation of Fe-Ti oxides in lower crustal gabbroic cumulates was an important control on the composition of erupted arc lavas (see also, e.g. Osborn, 1959; Gill, 1981; Woodhead, 1988). Fe-Ti oxides represent a major phase within the lower and mid-crustal gabbronorites from the Talkeetna Arc, and clearly affected the whole-rock TiO_2 budget for other lithologies in the arc crust. This is particularly evident in the trace-element patterns, where all of the Fe-Ti oxide-bearing lower crustal gabbronorite samples from the Tazlina-Barnette area have pronounced positive Ti anomalies and nearly all of the volcanic and intermediate to felsic plutonic rocks have distinct negative Ti anomalies (Fig. 6). These complementary Ti anomalies imply that crystallisation of Fe-Ti oxides within the layered gabbronorite caused liquids forming the volcanic and intermediate to felsic plutonic rocks to be depleted in TiO_2 . There probably was no Ti anomaly relative to HREE in primitive Talkeetna Arc magmas.

Yb can be used as a proxy for differentiation for the various arc lithologies given the systematic increase in concentrations from basal gabbronorite through the most

evolved volcanics, and the flat HREE patterns in almost all samples. When plotted versus East-West distance along the Talkeetna Arc section (meters, from Universal Transverse Mercator (UTM) coordinates), Yb(N) provides a means for visualizing the “chemical stratigraphy” of the Talkeetna Arc crust (Fig. 7). The easternmost exposures represent the deepest portion of the arc crust, where basal gabbronorites overlying and interlayered with pyroxenite have the lowest whole-rock Yb(N), highest Mg#, and high An contents. Most of the lower crustal gabbronorites from the Tazlina-Barnette area have similar chemical characteristics and show a slight sympathetic variation between Yb(N) and An, as expected for cumulates created during fractional crystallisation. Mid-crustal amphibole gabbronorites from Pippin Ridge have higher Yb(N), lower An and Mg#, and small Eu anomalies. The chilled mafic rocks and intermediate to felsic plutonic rocks clearly overlap the compositions of the nearby volcanic rocks for all elements, and likely represent liquid compositions (Kelemen *et al.*, 2003a). The volcanic rocks extend to more evolved compositions in the eastern part of the arc section. However, intermediate to felsic plutonic rocks are either unexposed or missing in this area.

Neodymium isotopic compositions

Nd isotopic compositions ($^{143}\text{Nd}/^{144}\text{Nd}$) for 11 plutonic samples of different lithologies (basal gabbronorite, lower crustal gabbronorite, chilled mafic rocks and intermediate to felsic plutonic rocks) range from 0.512960 to 0.513047 (Table 5). These samples have a narrow isotopic range and most of the 11 samples have the same ratio within analytical error. $^{143}\text{Nd}/^{144}\text{Nd}$ ratios for 6 volcanic samples (listed for comparison in Table 5) range from 0.512919 to 0.512998 (Clift *et al.*, 2005). $^{143}\text{Nd}/^{144}\text{Nd}$ ratios for additional plutonic

samples in the Chugach Mountains (mid-crustal gabbro-norite, and intermediate to felsic plutonic rocks) range from 0.512857 to 0.512988 (Rioux *et al.*, 2004). Nd isotopic ratios from the Talkeetna Mountains have a slightly greater range (0.512815-0.513304) (Rioux *et al.*, 2004).

Initial ratios were calculated at an age of 182 Ma. This age is based on the average of a range of U-Pb zircon ages from similar samples in close proximity in the Chugach Mountains (Rioux *et al.*, 2001; 2002; 2004), and a Sm-Nd isochron age (the best-fitting isochron fit 8 of 11 samples) (Table 5).

As shown in Figure 8, the initial Nd isotopic compositions are close to those of Jurassic Atlantic MORB (0.51276 to 0.51278) (Hoernle, 1998) and Jurassic Pacific MORB (0.51290 to 0.51301) (Hauff *et al.*, 2003) and thus were derived from a mantle source very similar to the MORB source. The small difference between the initial Nd isotopic compositions in Talkeetna rocks and Jurassic MORB is similar to the small difference in Nd isotopes between Marianas arc lavas and present-day MORB.

Two chilled mafic rocks (1728A3, 1719A11) have the highest Mg#s for noncumulate samples and represent the most primitive samples analysed in the Talkeetna Arc. The fact that these samples have Nd isotopic compositions similar to the other lithologies indicates that assimilation of older crustal material with different Nd isotope ratios was minimal to nonexistent during the chemical differentiation of the Talkeetna Arc.

The Nd isotopic characteristics of the Talkeetna Volcanic Formation are consistent with an oceanic subduction-related origin, with no evidence of collision with North America during arc activity (Clift *et al.*, 2005). Also, to a first order approximation, the

Nd isotopic data are consistent with derivation of the entire arc section from one type of primary magma derived from a mantle source with a fixed proportion of “subduction components”. However, ongoing research on the Talkeetna Arc recently revealed slightly enriched Sr isotopic ratios in the younger plutonic rocks of the Talkeetna Mountains (north of the study area), which may reflect intrusion of rocks younger than ~177 Ma into recently accreted continental material or into a pre-existing crustal boundary (Rioux *et al.*, 2004).

CALCULATED EQUILIBRIUM LIQUIDS FOR GABBRONORITES

Field and petrographic observations, and mineral and whole-rock chemistry described above, are strong evidence that the layered gabbronorites are cumulates that formed from partial crystallisation of a magma from which the remaining liquid was subsequently removed. This remaining liquid was most likely erupted as the basalts and basaltic andesites of the volcanic section. This assumption can be tested by determining whether the cumulate, layered gabbronorites crystallised in equilibrium with liquids that formed the volcanic rocks.

Determining the trace-element composition of “equilibrium liquids” can be done by utilizing trace element compositions of clinopyroxene from the gabbronorite cumulate rocks and clinopyroxene/liquid partition coefficients. However, this assumes that the clinopyroxenes from the gabbronorite cumulates have retained their igneous trace element characteristics. Sixteen of the 18 gabbronorite samples have parallel, LREE-depleted trace element patterns, and hence have indeed retained their igneous character.

In contrast, clinopyroxenes from the basal gabbronorites have been re-equilibrated under granulite facies conditions.

Liquid REE concentrations calculated to be in equilibrium with clinopyroxene in 18 gabbronorites and 2 mafic dikes are shown in Figure 9A, along with a shaded area representing 80 of the 83 REE patterns for volcanic rocks throughout the arc (from Fig. 6A, omitting 3 anomalous LREE-enriched, HREE-depleted lavas). Calculated equilibrium liquids for all but two of the lower crustal gabbronorite samples between Tazlina Lake and Barnette Creek lie within the range of volcanic rock compositions (8 to 38 \times chondrite; mean Ce/Yb(N)=1.45) (Fig. 9B). Ten out of fourteen calculated liquids from lower crustal gabbronorite samples form a band of REE patterns between \sim 11 and 18 \times chondrite (mean Ce/Yb(N)=1.10). A suite of eight chilled mafic rocks also range from \sim 8 to 18 \times chondrite with an average Ce/Yb(N) of 1.15.

The above-described evidence from calculated liquids links many of the layered gabbronorites and volcanic rocks through crystal fractionation, such that the cumulate gabbronorites crystallised in equilibrium with liquids that were extracted and erupted to produce the volcanic rocks.

Some but not all of the lower crustal gabbronorite samples in apparent cpx/liquid REE exchange equilibrium with a given volcanic rock composition are also in cpx/liquid Fe/Mg exchange equilibrium with that same volcanic rock composition. However, ten volcanic samples (Mg# >54) have Mg#s too high for equilibrium with any of the lower crustal gabbronorites. This suggests that they formed in equilibrium with more primitive cumulates, either pyroxenites or gabbronorites that were not sampled during our study. It should be noted that Fe/Mg partitioning between clinopyroxene and melt is linked to

$\text{Fe}^{3+}/\text{Fe}^{2+}$ through $f\text{O}_2$ and for calculations involving the layered gabbro-norites, the values of Sisson & Grove (1993) were used: $\text{Fe}/\text{Mg } K_{\text{d}_{\text{cpx/liquid}}}$ of 0.23 calculated with total $\text{Fe}_{\text{liquid}}$. This assumption is a source of uncertainty, but it remains the case that for any reasonable combination of $\text{Fe}^{3+}/\text{Fe}^{2+}$ and $\text{Fe}/\text{Mg } K_{\text{d}_{\text{cpx/liquid}}}$, about 10 of the volcanic samples have Mg\# 's too high for Fe/Mg equilibrium with lower crustal gabbro-norite.

A plot of Yb(N) versus Mg\# shows that most of the volcanic rocks form a trend of increasing Yb(N) with decreasing Mg\# (Fig. 10), as expected for crystal fractionation. In contrast, clinopyroxenes in the lower-crustal gabbro-norites have nearly constant Mg\# and a wide range of Yb . Therefore, the calculated liquids in equilibrium with these clinopyroxenes do not show the same trend of Yb(N) versus Mg\# as the volcanic rocks.

Interestingly, several of the volcanic rocks have a high Mg\# , high Yb signature, similar to calculated liquids for several gabbro-norites (Fig. 10). The clinopyroxenes with this signature are from the mid-crustal amphibole gabbro-norite and from orthopyroxene-rich (>40 wt %) sections of the lower crustal gabbro-norite. It is possible that the high Mg\# , high Yb clinopyroxenes and high Mg\# , high Yb lavas represent complementary products of the same process. This signature could be the result of several processes: reaction of migrating, evolved melt \pm aqueous fluids and mafic cumulates (e.g. Costa *et al.*, 2002), magma mixing, and/or fractionation of very oxide-rich cumulates. Mid-crustal amphibole gabbro-norite samples have high REE abundances (patterns which overlap volcanic rock compositions), negative Sr and Eu anomalies in clinopyroxenes, and low An content in plagioclase. Clinopyroxene from mafic layers in the layered gabbro-norite possesses high REE abundances, negative Sr and Eu anomalies, and higher concentrations of trace elements (Zr, Y, Ti, V). High Mg\# and high Yb values for these

calculated liquids may be linked to the formation of the mafic layers. In the case of the lavas, the high Mg#, high Yb samples could also be produced by mixing of evolved melt (low Mg#, high Yb) and primitive melt (high Mg#, low Yb). Mixed melts could then precipitate high Mg#, high Yb cumulates.

DISCUSSION

Magma compositions for the Talkeetna Arc

The geological evidence and chemical characteristics of the Talkeetna Arc are consistent with the hypothesis that the bulk of the crust formed during arc magmatism in an intra-oceanic setting. Almost all samples appear to be related to a single type of parental magma through processes of intracrustal differentiation. Most of the volcanic rocks have evolved compositions, with nearly 75% of the representative suite having >53 wt % SiO₂ and Mg# <50. Many of the evolved volcanic compositions are a result of cumulate processes recorded by middle to lower crustal gabbro-norites.

One of our goals in this study is to determine the parental melt composition(s) for the cumulate gabbroic rocks and evolved lavas in the arc. This provides us with crucial information about magmatic fluxes into arc systems. However, this parental magma composition also provides us with starting points for two types of modeling which are described in subsequent sections of the paper: (1) crystal fractionation modeling, to quantify the processes and proportions of rock types involved in crustal differentiation; and (2) pyroxenite addition models, to determine the composition of hypothetical primary arc melts in equilibrium with residual peridotite. In order to do this, we have assessed the

most primitive magma compositions preserved in the Talkeetna Arc by selecting sampled primitive basaltic compositions (high Mg#, Ni, Cr) (Table 4). In Table 4 we have only tabulated the volcanic samples with Mg# >60, along with the mafic dikes and inclusions from this study. For the complete set of volcanic rock analyses see Clift *et al.* (2005).

As an overview, of the 83 volcanic rocks and 8 chilled mafic rocks analysed as a representative suite within the arc, 6 volcanic rocks and 2 chilled mafic rocks have Mg# >60. Fourteen volcanic rocks have Mg# 50-60. Of the 20 volcanic rocks with Mg#s between 50 and 70, SiO₂ contents range from 47 to 76 wt % (with 11 <53 wt % SiO₂, 2 between 53 and 57 wt % SiO₂, 2 between 57 and 63 wt % SiO₂, and 5 >63 wt % SiO₂). All 5 of the 8 chilled mafic rocks with Mg# >50 are basaltic in composition.

In the process of surveying the suite of volcanic samples for potential parental melt compositions, several interesting observations arise. The volcanic samples with Mg#s greater than 50 are not uniformly distributed throughout the study area. They are primarily concentrated in two areas, one in the easternmost exposures near Stuck Mountain and the other in the Little Oshetna River area, the most northerly of the sampled volcanics, in the Talkeetna Mountains (see Clift *et al.* (2005) for descriptions). Fifteen of the 20 volcanic samples with Mg# >50 are from these two areas.

Five of the six lavas with Mg# >60 are from these two areas and were not selected as potential parental melt compositions. The Little Oshetna River area is dominated by basaltic lavas and is unconformably overlain by Middle Jurassic sandstone in close proximity (Clift *et al.*, 2005). These lavas have trace-element compositions that are characteristic of eruption in an off-axis setting (Clift *et al.*, 2005). Several lavas from Stuck Mountain have distinct trace element chemistry (with high La/Yb, see discussion

below) and were not used as parental compositions. The remaining lava, which has the highest Mg# (62.6), has ~57 wt % SiO₂ and therefore it probably cannot be parental to evolved basalts and basaltic andesites. This eliminated all six lavas with Mg# >60 as initial liquids for the crystal fractionation modeling.

The two primitive chilled mafic rocks with Mg# >60 (1719A11-mafic pillow, 1728A3-mafic dike) are basaltic, with MgO contents of 8.35 and 8.09 wt %, Mg#s of 64.0 and 61.9, and Al₂O₃ contents of 18.5 and 19.3 wt %, respectively (Table 4). They also possess high Cr concentrations (296 and 188 ppm) and variable Ni (205 and 73 ppm). The REE patterns for these primitive samples lie just below a field of calculated liquid REE for lower crustal gabbro-norite, using cpx/liquid coefficients of Hart and Dunn (1993). However, in detail the relationship of calculated liquids to actual liquids depends on the selection of partition coefficients, which is uncertain. The REE pattern for the chilled mafic pillow, and a second, basaltic mafic pillow with Mg# 57.0, lie close to the calculated primary magma composition of DeBari and Sleep (1991). However, the REE patterns for these chilled mafic rocks have small positive Eu anomalies. Calculations from whole rock and plagioclase REE concentrations measured on Talkeetna samples during this study indicate that the Eu anomalies can be accounted for by as little as 3 wt % accumulated plagioclase, with an insignificant effect on the major element composition. In summary, we chose the two primitive chilled mafic rocks as potential compositions of primitive melts, parental to more evolved basalts and basaltic andesites, and perhaps to most andesites, dacites and rhyolites as well. Burns *et al.* (1991) also reported three mafic dikes from within the study area with 9.05-12.1 wt % MgO and Mg#s of 64.3-69.8. Two of these samples contain <14 wt % Al₂O₃, which may further

indicate that they represent relatively unfractionated melts which quenched within the upper crust.

The five primitive dacites (>63 wt % SiO₂) are interesting for various reasons, but we did not use them as parental liquids for most of the crystal fractionation and pyroxenite addition calculations because we do not believe primitive andesites and dacites can evolve by crystal fractionation to low Mg# basalts and basaltic andesites. Two volcanic samples from Stuck Mountain are high Mg# dacites (Mg# 59.0-62.0; 67.5-68.0 wt % SiO₂). One of these high Mg# dacites (in addition to a dacite breccia (68.5 wt % SiO₂, Mg# 53.6) and a volcanoclastic sample from Plafker *et al.* (1989) from the same area) have trace-element chemistry with distinctly high La/Yb ratios that are different from the rest of the arc samples (Fig. 6A). These compositions imply either very different crystal fractionation processes (probably involving garnet) or a distinctly different parental melt, which in turn may have been derived from a source with residual garnet, or a source with different trace element composition. Other samples with distinctive HREE concentrations are preserved in the Klanelneechena Klippe, where garnet- and pyroxene-bearing, quartz diorites and tonalites are thrust over accretionary complex assemblages south of the Border Ranges Fault (Fig. 1). These plutonic rocks have distinctly HREE-enriched trace element patterns and could represent cumulates or restites in equilibrium with LREE-enriched, HREE-depleted lavas (Kelemen *et al.*, 2003a). Evolved, strongly HREE-depleted silicic melts could mix with primitive basalts to produce moderately HREE-depleted, high Mg# andesites and dacites. The HREE-depleted volcanic samples are fairly rare and were not incorporated into our modeling of primary magma compositions or crystal fractionation trends for the bulk of the Talkeetna Arc samples.

Effects of crustal fractionation

Numerous petrologic studies predict the existence of large sections of lower crustal cumulates to explain the observed geochemical variation in evolved volcanic rocks (e.g. Kay & Kay, 1985). Volcanic differentiation trends in several active arcs have been related through fractionation of lower crustal cumulates using the composition of xenoliths (e.g. Conrad & Kay, 1984). Exposures of complementary volcanic and plutonic sections of island arc crust from the Talkeetna Arc provide an exceptional opportunity to quantitatively test models relating volcanic suites and lower crustal cumulates through fractional crystallisation. Burns (1985) recognized the similarities between the exposed layered gabbro-norite from the Tazlina-Barnette area and plutonic xenoliths from island arc lavas, and cited this evidence in support of the plagioclase-orthopyroxene/olivine-augite-magnetite (POAM) fractionation model emphasized by Gill (1981). Gill (1981) proposed a dominant role for POAM fractionation to account for the derivation of the basalt-andesite-dacite-rhyolite series in island arc settings. The calculated phase proportions of minerals in our layered gabbro-norite samples indicate plagioclase + orthopyroxene + clinopyroxene + Fe-Ti oxide \pm amphibole represent the bulk of the residual cumulates (Table 6).

Trace-element ratios allow a clear distinction between cumulate gabbroic rocks on the one hand, and evolved plutonic and volcanic samples on the other hand, and illustrate the effect of POAM fractionation in the Talkeetna Arc. The group of cumulate gabbro-norites is easily distinguishable in Figure 11 because it has lower silica contents than evolved

plutonic and volcanic samples. The volume of cumulates in lower crustal exposures may be large enough to drive primitive basaltic liquid compositions to higher SiO_2 , as explored quantitatively in the least squares fractional crystallisation modeling section, below. With the exception of two high Sr/Y dacites (same as high La/Yb samples described above), trends in Sr/Y appear generally to be the result of plagioclase fractionation (Fig. 11). The variation in Ti, Zr and V within the suite of arc rocks is clearly related to the nature and proportion of crystallising phases (Pearce & Norry, 1979). Crystallisation of V-rich, Fe-Ti oxides within the layered gabbro-norite is reflected by a trend of decreasing Ti/Zr and V/Ti for residual melts (e.g. Pearce & Norry, 1979; Nielsen *et al.*, 1994). Zr concentrations appear to be controlled almost exclusively by fractionation (also see Fig. 6). Zr enrichment relative to Sm is often attributed to amphibole fractionation (Thirlwall *et al.*, 1994), and Zr/Sm in the layered gabbro-norites is distinctly lower than the other arc rocks. However, augite fractionation (Thirlwall *et al.*, 1994) and magnetite fractionation (Tribuzio *et al.*, 1999) may also exert an influence on the Zr/Sm ratio.

Studies of inclusions from the Lesser Antilles document cumulate-textured xenoliths containing 5-15 modal % magnetite and attribute many of the chemical trends within suites of island arc rocks to magnetite fractionation (Arculus & Wills, 1980). Magnetite-ilmenite gabbro-norite is prevalent in lower crustal gabbro-norites between Tazlina Lake and Barnette Creek. Whole rock trace element patterns for these cumulate rocks are enriched in Ti relative to the HREE, whereas volcanic and upper-level plutonic rocks, presumably the derivative liquids, are distinctly depleted in Ti (Fig. 6).

The precipitation of amphibole, in addition to POAM fractionation, is also often cited to explain geochemical variations within arc volcanic suites (e.g. Gill (1981) and references therein). However, the perthitic hornblende in lower crustal gabbro-norite in the Talkeetna Arc appears to be primarily a late magmatic phase from progressive fluid enrichment (DeBari & Coleman, 1989), the result of subsolidus re-equilibration (Burns, 1985), from the reaction of clinopyroxene and melt as suggested by Foden and Green (1992), and/or formed by reactions between cumulus minerals and evolved melts \pm aqueous fluids (Costa *et al.*, 2002).

Plagioclase accumulation is an important process within island arc crust (e.g. Woodhead, 1988). Eu anomalies in island arc magmas are at least partly due to the accumulation of plagioclase (Vukadinovic, 1993). In the Talkeetna Arc, correlation between Eu/Eu^* (log scale) and $\text{Yb}(\text{N})$ reflects the strong effect of plagioclase fractionation and minimal effect of trapped liquids on Yb concentrations (Fig. 12A). Eu and Sr anomalies show a clear positive correlation for the range of the Talkeetna Arc lithologies (Fig. 12B), indicating plagioclase accumulation is largely responsible for enriched Sr concentrations in cumulate gabbro-norites. However, primary Talkeetna magmas probably did have an initial enrichment in Sr/Nd compared to MORB (Kelemen *et al.*, 2003a).

Least squares fractional crystallisation modeling

Least squares calculations are commonly used to quantify the possible relationship of a series of volcanic rocks through fractional crystallisation (e.g. Arculus & Wills, 1980).

Cumulate sections from the middle and lower crust of the Talkeetna Arc provide a broad range of mineral compositions and proportions with which to quantify the possible relationship of volcanic and chilled mafic rock compositions through fractionation of observed cumulate gabbro. The goal of this modeling is to determine if the most primitive volcanic and chilled mafic rocks ($Mg\# > 60$) can be related to more evolved volcanic rocks through fractional crystallisation of gabbros, and to constrain the relative proportions of crystal and liquid products required by this hypothesis.

Initially, it is important to assess Fe/Mg and REE equilibrium between the cumulus phases and volcanic rocks to determine appropriate fractionation assemblages for the least squares calculations. Using an Fe/Mg $K_{d_{cpx/liquid}}$ of 0.23, calculated with total Fe_{liquid} (Sisson & Grove, 1993), clinopyroxene $Mg\#$ is plotted in Figure 13, in a panel adjacent to a plot of $Mg\#$ versus SiO_2 for volcanic and chilled mafic rocks. Clinopyroxene from Talkeetna pyroxenite, plagioclase pyroxenite, garnet gabbro, basal gabbro, lower crustal gabbro, and mid-crustal amphibole gabbro covers most of the range of equilibrium compositions required for the lavas and mafic inclusions (Fig. 13). This diagram was used to evaluate potential equilibrium pairs of clinopyroxene-bearing rocks and corresponding liquid compositions. When available, REE clinopyroxene/liquid equilibria were assessed in conjunction with Fe/Mg equilibria. For example, in step 3 of the least squares modeling, calculated liquid REE concentrations from clinopyroxene in lower crustal gabbro (0718A4; Dy(N) 17.7, Yb(N) 15.8) are close to REE abundances in the parent basaltic andesite (0709P2A; Dy(N) 18.3, Yb(N) 14.5).

The compositional variation for a series of volcanic and chilled mafic rocks was modeled by relating observed compositions through fractionation of phases in cumulate

gabbro. Parent/daughter pairs of liquid compositions were selected based on decreasing Mg#, increasing SiO₂, and increasing REE concentrations. Phase compositions (but not phase proportions) were chosen from cumulate Talkeetna samples with clinopyroxene in Fe/Mg exchange equilibrium (and, sometimes, REE exchange equilibrium) with the parent liquid. The outputs include % crystallised, weight proportions of fractionated phases, and residuals for each of the oxides. Solutions from three steps of least squares fractionation modeling are shown in Table 7 and illustrated in 13B. Phase proportions from cumulate gabbros (from Table 6) are compared to model solutions from steps 2 and 3 (Fig. 13C). Observed and calculated REE provide an additional test for the three steps of the fractionation modeling (Fig. 13D).

Differentiation of three consecutive parent/daughter pairs was modeled:

Step 1- A primitive chilled mafic rock (1728A3) was selected as the parent composition for the first step based on its high Mg# (61.9), despite its slightly LREE-depleted whole rock REE pattern. Another primitive, chilled mafic rock (Mg# 64.0) did not yield acceptable solutions for the first step of the series. Possible solutions include assemblages of cpx+opx+plag+sp (Table 7, with mineral abbreviations defined) and oliv+plag (not shown). Both yield solutions with ~20% crystallisation. The ol+plag solution requires proportions of ~25% olivine and 75% plagioclase. Such troctolite compositions are not present in the Talkeetna Arc section. The cpx+opx+plag+sp solution includes a lot of aluminous spinel (18%), and only 32% plagioclase. However, plagioclase is necessary in this step to attain a solution (cpx+opx+sp or ol+cpx+opx+plag+sp are not workable assemblages). Even though phase proportions in the cpx+opx+plag+sp solution from this step represent a pyroxene-rich gabbro, the only rock with clinopyroxene Mg# appropriate

for Fe/Mg equilibrium with the parent composition in this step is a plagioclase pyroxenite. Plagioclase pyroxenite is rare in the Talkeetna Arc, but was sampled from Scarp Mountain. Sample 1709P11 is a spinel-rich, plagioclase pyroxenite with clinopyroxene Mg#s of 84.4 to 87.0 (Table 2), which partially bridge the gap in Mg# between more common plagioclase-free pyroxenites (Mg#s from 87 to 91) and basal gabbronorites (Mg#s from 65 to 83) (Figs 2 and 12). We reiterate, however, that plagioclase pyroxenites are very rarely exposed in the Talkeetna Arc.

Step 2- The daughter composition from step 1 was used as the parent for step 2. The daughter liquid in step 2 was a basaltic andesite (0709P2A), chosen on the basis of lower Mg# (49.4) and higher SiO₂ and REE. Again, only clinopyroxene from the plagioclase pyroxenite has Mg# high enough for Fe/Mg equilibrium with the parent composition in step 2. However, solutions using this clinopyroxene composition yield *phase proportions* that are consistent with calculated modes of cumulate gabbronorites and require 39% crystallisation (Fig. 13C).

Step 3- The daughter composition from step 2 was used as the parent for step 3. The daughter liquid in step 3 was an andesite (0709P2C), again chosen on the basis of lower Mg# (43.1) and higher SiO₂ and REE. Using a variety of phase compositions observed in lower crustal gabbronorites, all chosen to be close to Fe/Mg and REE equilibrium with the parental liquid for step 3, yields model results which span the range of observed phase proportions in lower crustal gabbronorites. Solutions consistently yield extremely low residuals ($\sum R^2=0.0000-0.0015$). Using different lower crustal gabbronorite phase compositions for the fractionation assemblage produces a range of outputs requiring 30-45% crystallisation. However, phase assemblages yielding solutions at the lower end of

this range (~30% crystallisation) have low proportions of orthopyroxene (<3 wt %), and slightly higher proportions of clinopyroxene (20-26 wt %) and hornblende (35-45 wt %) than observed gabbro-norites. Solutions that require close to 45% crystallisation (Table 7) have phase proportions which closely match observed phase proportions (Fig. 13; Table 6).

REE abundances for the three daughter compositions increase in each step. The calculated and observed REE patterns are similar for steps 2 and 3 (Fig. 13C). The calculated REE concentrations are dependent on the selection of crystal/liquid partition coefficients and phase proportions from solutions (which vary slightly in alternative solutions).

Cumulative results for the overall percent crystallised and melt remaining for the three least squares steps are also shown in Table 7 (bottom right of each step), assuming no eruption of the remaining liquid at each step (all remaining liquid is used for the parent magma in the subsequent step). These calculations indicate 73.1% crystallisation (26.9% melt remaining), by weight, after the three steps.

Attempts to model the formation of more evolved andesites and dacites through fractional crystallisation were unsuccessful. Solutions capable of producing dacites and rhyolites, using other evolved basaltic andesite and andesite compositions and a range of cumulate gabbro fractionation assemblages (e.g. opx+cpx+plag+amph+sp), were also unattainable. In addition, fractionation of observed phase compositions from high Mg# andesites and dacites to form evolved andesite-dacite-rhyolite was surprisingly difficult to model. Using a high Mg# dacite parent yielded one possible solution out of 10 parent-daughter combinations. However the solution, requiring 15% crystallisation of the

assemblage cpx+opx+plag+sp+hbl, would have minimal effect on La/Yb and is inconsistent with the difference between parent and daughter REE patterns.

The free energy minimization program MELTS (Ghiorso & Sack, 1995) was used as an independent method for comparison with results from least squares fractional crystallisation modeling. Liquid compositions from four fractional crystallisation MELTS calculations at 0.5 and 1 GPa and temperatures from ~1250 to 1000 °C are shown in Figure 13B. Using the parent composition from step 1 of the least squares fractionation modeling, MELTS models are shown for 2 wt % H₂O and fO₂ of NNO+1 at 0.5 GPa and 1 wt % H₂O and fO₂ of FMQ+1, 2 wt % H₂O and FMQ+2, and 3 wt % H₂O and FMQ+2 at 1 GPa. Although we tried other runs, the MELTS calculations presented in this Figure have the closest results to either observed volcanic rock compositions or observed phases in the lower crustal gabbro-norites for reasonable H₂O contents and fO₂.

The liquid compositions for runs with 2 and 3 wt % H₂O at FMQ+2 at 1 GPa are closest to the general trend of the volcanic rock compositions. However, fractionated solid assemblages from these two MELTS runs are not the same as observed phase proportions in the lower crustal gabbro-norites or to results from least squares fractional crystallisation modeling. 1 wt % H₂O, FMQ+1 and 2 wt % H₂O, FMQ+2 solid assemblages include sp+garnet+plag+cpx, while solid assemblages for 3 wt % H₂O, FMQ+2 include only sp+cpx.

For calculations with pressure set at 0.5 GPa, the fractionated solid proportions predicted in MELTS calculations are close to observed phase proportions in the lower crustal gabbro-norites and to results from least squares fractional crystallisation modeling, but the evolving liquid composition from these MELTS runs does not match the observed

trend of volcanic rock compositions as closely. Results for 2 wt % H₂O, NNO+1 and NNO+2 at 0.5 GPa include fractionated solids with opx+cpx+plag+sp in proportions in the range observed in our samples.

Thus, using a variety of pressures, water contents and oxygen fugacities, we find that the MELTS calculations do not reproduce both liquid compositions and fractionated phase proportions observed in the Talkeetna section. In contrast, the least squares models - by design - simultaneously fit both solid and liquid compositions better than the MELTS calculations. One possible conclusion is that the phase proportions produced by the least squares models are not, in fact, equilibrium proportions of co-crystallizing minerals in arc magmas. However, given that isotope and petrologic data indicate a genetic link between the plutonic and gabbroic rocks in the Talkeetna section, we believe that the least squares models probably do yield realistic phase proportions, and thus provide better constraints on igneous differentiation within the Talkeetna section, compared to the MELTS calculations. This is quite understandable, given the very limited number of experimental data on water-undersaturated crystallisation of primitive, basaltic magmas in the pressure range from 0.2 to 1.0 GPa that are available to calibrate thermodynamic parameters used in MELTS.

Pyroxenite fractionation

Even the most primitive chilled mafic rocks in the Talkeetna Arc are not in Fe/Mg equilibrium with residual mantle peridotite, and so are probably not primary, mantle-derived melts. Instead, they probably formed via fractionation of primitive cumulates from a primary magma. The obvious primitive cumulates in the Talkeetna Arc section are

pyroxenites present between residual mantle peridotites and basal gabbro-norites in the Tonsina area. Alternatively, DeBari and Sleep (1991) implied that primary Talkeetna magmas might have undergone extensive fractionation of olivine to form cumulate dunites. However, the proportion of dunites in the Talkeetna mantle section is small, and many of the dunites that are present may be relict or the result of incomplete peritectic reactions, rather than cumulates. Primitive hydrous melts in equilibrium with mantle peridotite at 1 GPa are in a reaction relationship with olivine (peritectic reaction: olivine + liquid \rightarrow pyroxene) and are pyroxene-saturated (e.g. Müntener *et al.*, 2001). In keeping with this result, most of the websterites in the Tonsina area are olivine-free. Further, Talkeetna mantle dunites do not have Mg#s less than 89, as required to explain the evolution of primary melts to the lower Mg#s observed in the most primitive Talkeetna lavas. Instead, Tonsina pyroxenites have pyroxene Mg#s that overlap those in the residual mantle peridotites. Specifically, pyroxenites in the Tonsina area of the Talkeetna Arc have clinopyroxene compositions with Mg# 87-91 and 0.6-1.0 wt % Cr₂O₃ (R. Workman, unpublished data; DeBari & Coleman, 1989). Clinopyroxene in dunite and harzburgite has Mg# 90-94, and slightly lower Cr₂O₃ contents (0.5-0.7 wt %) (DeBari & Coleman, 1989). Thus, we conclude that pyroxenites, not dunites, were the most primitive cumulates in the Talkeetna Arc section.

To account for the crystallisation of pyroxene at the base of the crust and estimate a primary magma composition for the Talkeetna crustal section, we modeled pyroxenite fractionation by incrementally adding pyroxene and spinel to the most primitive liquid compositions obtained from lavas and mafic inclusions, until the estimated melt was in equilibrium with clinopyroxene with Mg# of 92. The clinopyroxene Mg# of 92 was

chosen as a typical value for clinopyroxene in residual mantle peridotite. The most primitive chilled mafic rocks and lavas in the Talkeetna Arc are in equilibrium with clinopyroxene compositions with Mg#s of ~85-88.

Although clinopyroxene-bearing orthopyroxenites are present in 10% of the outcrop area, the majority of websterites in the Tonsina area have 70-75% clinopyroxene, 25-30% orthopyroxene, and less than 2% spinel (Kelemen *et al.*, 2003a; DeBari & Coleman, 1989). Websterite with these mineral proportions, in Fe/Mg exchange equilibrium with the initial melt, was added to two primitive chilled mafic rock and two basaltic lava compositions in increments of 0.2 weight percent, while calculating a new clinopyroxene and orthopyroxene based on Fe/Mg equilibrium with the new melt composition at each step (using a constant Cr-Al spinel composition). Due to the uncertainties involving cpx Fe/Mg Kd's and $\text{Fe}^{3+}/\text{Fe}^{2+}$, two sets of values for each are used to show the range of possible results (cpx Fe^{2+}/Mg Kd's of ~0.27 (Sisson & Grove, 1993) and ~0.33 (Müntener *et al.*, 2001); $\text{Fe}^{3+}_{\text{liquid}}$ of 0.14 and 0.20). Estimated primary magma compositions and the weight percent added pyroxenite are presented in Table 8.

To attain a primary liquid composition in equilibrium with clinopyroxene having a Mg# of 92, the required proportion of added pyroxenite is substantial. With a cpx Fe^{2+}/Mg Kd of 0.27 and $\text{Fe}^{3+}_{\text{liquid}}$ of 0.14, the proportion of pyroxenite (with phase proportions of 70% cpx: 28% opx: 2% sp) added to the four primitive compositions ranges from ~26 to 33 wt % (Table 8). A slightly higher proportion of pyroxenite is required using 75% cpx: 23% opx: 2% sp for all the calculations. Varying the cpx/melt Kd from 0.27 to 0.33 has a dramatic effect, increasing the required proportion of pyroxenite by ~15-18 wt %. With increasing $\text{Fe}^{3+}_{\text{liquid}}$ (from 0.14 to 0.20), the required

proportion of pyroxenite decreases by ~5-8 wt %. If we stop at an estimated melt in equilibrium with clinopyroxene with Mg# of 90, this decreases the required proportion of pyroxenite by ~10 wt %. Using these different values is intended to provide bounds on the potential amount of pyroxenite fractionation. In almost every case where preferred values are used, more than 25 wt % pyroxenite is required to achieve a liquid composition in Fe/Mg exchange equilibrium with clinopyroxene in mantle peridotite (Table 8). Despite the substantial uncertainties involved in these calculations, this provides an approximate minimum estimate for the amount of pyroxenite fractionation that potentially occurred at the base of the arc crust.

The estimated primary magma compositions after pyroxenite addition calculations (Table 8) are similar to the calculated primary magma composition for the Talkeetna Arc of DeBari and Sleep (1991). Our calculated primary melts have ~14-16 wt % Al_2O_3 and 11-12 wt % MgO. CaO contents range from ~11 to 14 wt %, and are slightly higher than expected (13-14 wt %) for calculations using sample 1728A3 (Table 8). This sample, with 12 wt % CaO, likely has a small amount of accumulated plagioclase and/or clinopyroxene, which is also reflected in its whole-rock REE pattern. The calculated primary magma composition of DeBari and Sleep (1991) was a high-Mg (11.3 wt %), low-Al (15.0 wt %) basaltic composition (51.1 wt % SiO_2) with a flat REE pattern (also listed in Table 8).

This is a dramatic corroboration of DeBari and Sleep's first order approach. Recall that we have derived our primary melt compositions from the most primitive of observed lavas and mafic inclusions, considering only pyroxenite addition to reach a primary melt in Fe/Mg equilibrium with residual mantle peridotite. In contrast, DeBari and Sleep

(1991) used a mass-balance of all the exposed arc rocks, in their estimated proportions, to calculate an approximate bulk composition for the Talkeetna Arc crust. As such, they interpreted the bulk composition as the integrated mass flux from mantle to crust, after assuming that there was some dunite fractionation in the mantle. The trace element and isotopic data presented in this paper are consistent with crystallisation of the entire arc section along a single liquid line of descent from a homogeneous primary melt. Therefore, the bulk crust composition of DeBari and Sleep might be expected to correspond to the primary magma composition inferred from our data.

However the apparent agreement between our estimates and those of DeBari and Sleep mask some essential differences. While DeBari and Sleep assumed that the arc process produced 18 wt % ultramafic rocks (45.5 wt % dunite) below the Moho, with the remainder of the arc magma flux present as gabbroic and volcanic rocks in the crust, we infer that primary melts crystallised at least one quarter of their mass as primitive pyroxenite cumulates, probably along the Moho where appropriate pyroxenite compositions are exposed in the Talkeetna section. In fact, in comparison to DeBari and Sleep, we derive a very different composition for the gabbroic to volcanic crust overlying this Moho-level pyroxenite.

Estimates of the type and proportion of ultramafic cumulates in island arcs have important consequences. The proportion of ultramafic cumulates directly affects estimates of the bulk composition of arc crust. The degree of fractional crystallisation from primary, mantle-derived melts below the Moho is also crucial to our understanding the formation of high-Al basalts parental to plagioclase-bearing crustal rocks. Our calculations suggest that more than 25 wt % of primary melts crystallised as pyroxenites

at the base of the crust. The experiments of Müntener *et al.* (2001) show that up to 50% of primary, mantle-derived melts could crystallise as pyroxenites prior to plagioclase saturation. If olivine is incorporated into our pyroxenite addition calculations, so ultramafic cumulate with between 10 and 80% olivine is added to the primitive liquid compositions, 18-30 wt % ultramafic cumulate is required to achieve a liquid composition in Fe/Mg exchange equilibrium with clinopyroxene in mantle peridotite. Previous studies using least-squares fractionation models require 21% (Conrad & Kay, 1984) and 16-26% (Gust & Perfit, 1987) crystallisation of ultramafic cumulates to produce high-Al basalt in island arcs.

However, exposures of pyroxenites in the Tonsina area represent a thickness of less than one kilometer. Thermobarometry on overlying garnet granulites require that the crust above the pyroxenites was 30-35 km thick at one time (DeBari & Coleman, 1989). There are small ultramafic intrusions into the lower crustal gabbro-norites at several places in the Talkeetna section (e.g. Rose, 1966; Clarke, 1972; Pavlis, 1983; Burns, 1985) but altogether pyroxenites represent less than 3% of the outcrop area in the plutonic parts of the Talkeetna Arc section. The discrepancy between the amount of pyroxenite fractionation deduced from crystallisation modeling and the amount of pyroxenite observed in the Talkeetna section is probably not due to gaps in the section due to faults or missing outcrop. Although the total outcrop area is small, Moho level outcrops in the Tonsina area expose several unfaulted, high temperature contacts between underlying mantle peridotites, primitive pyroxenites (clinopyroxene Mg# 90 to 85), and overlying gabbro-norites (clinopyroxene Mg# less than 85). Thus, the thin layer of pyroxenite is

bounded on either side by high temperature, arc-aged contacts with Talkeetna upper mantle and lowermost crust.

Instead, the discrepancy between the observed proportion of pyroxenites and the proportion required by crystal fractionation modeling may be explained by “delamination” (Kay & Kay, 1985; Kay & Kay, 1988; 1990; 1991; Arndt & Goldstein, 1989; Turcotte, 1989; DeBari & Sleep, 1991; Jull & Kelemen, 2001). Although many treatments of “delamination” have called upon the presence of abundant garnet in eclogites or garnet granulites, Arndt & Goldstein (1989) noted that ultramafic cumulates have lower Mg# than residual mantle peridotites, and so are generally denser than underlying mantle. Jull & Kelemen (2001) and Müntener *et al.* (2001) quantified this. They showed that calculated densities for an olivine clinopyroxenite xenolith from the Aleutians (bulk Mg# of 84) and an experimentally produced pyroxenite (bulk Mg# of 82) are $\sim 50 \text{ kg/m}^3$ higher than the density of fertile lherzolite, and $\sim 75 \text{ kg/m}^3$ denser than depleted oceanic peridotite, at 1 GPa and temperatures from 900 to 1200°C. These are the PT conditions which were present beneath the Talkeetna Arc while it was magmatically active. At the higher end of this temperature range, the density contrast and relative viscosities would allow pyroxenites to delaminate almost as quickly as they formed (Jull and Kelemen, 2001).

Garnet granulites are found in a narrow horizon in the Talkeetna area, immediately above the pyroxenites (DeBari & Coleman, 1989). Jull & Kelemen (2001) found that garnet granulites with the composition of Tonsina garnet granulites would be $\sim 100 \text{ kg/m}^3$ denser than the underlying mantle at Tonsina Moho PT conditions. For a Moho temperature of 1000°C, Jull & Kelemen (2001) found that a layer of ultramafic cumulates

and garnet granulites varying in thickness from 1 to 2 km would become gravitationally unstable and “drip” into the underlying mantle in a few thousand to a few million years (non-Newtonian dry olivine rheology with background strain rates from 10^{-14} to 10^{-18} /s; abundant, dissolved H₂O would shorten instability times still further).

Thus, the discrepancy between the observed proportion of pyroxenites (less than 5% of the arc section) and the proportion required by crystal fractionation modeling (more than 25%) is best understood as the result of gravitational instability, with dense ultramafic cumulates, probably together with dense garnet granulites, foundering into the underlying mantle during the time when the Talkeetna Arc was magmatically active, or in the initial phases of slow cooling (and sub-solidus garnet growth) immediately after the cessation of arc magmatism. Alternatively, either the small proportion of pyroxenite in Talkeetna Arc outcrops is not representative of the true proportion of rocks which originally comprised the arc section, or pyroxenite “sills” within the mantle wedge were present at depths greater than the maximum depth of exposure.

If the interpretation is correct that the bulk composition of island arc crust is close to the integrated mass flux from mantle to crust, then the bulk composition of the Talkeetna Arc crust is probably close to the composition of the most primitive arc lavas and mafic inclusions. Compared to the crustal bulk composition estimated by DeBari and Sleep (1991) (also shown in Table 4) the most primitive chilled mafic rocks have higher Mg# and lower SiO₂.

CONCLUSION

Geochemistry of a diverse suite of volcanic and plutonic rocks from the Talkeetna Arc crust is consistent with the linked magmatic origin of these different lithologies. Exposures of layered, lower crustal gabbro-norite represent cumulates that crystallised in equilibrium with liquids that were extracted and yielded volcanic rocks of the Talkeetna Arc. Fractional crystallisation of layered gabbro-norite in the middle and lower crust was the predominant process in the formation of the lithologically heterogeneous Talkeetna Arc crust. Plagioclase + orthopyroxene + clinopyroxene + Fe-Ti oxide \pm amphibole lithologies represent the bulk of the cumulate rocks that are complementary to the erupted lavas and noncumulate plutonic rocks. The compositional variation of a series of volcanic and chilled mafic rocks can be modeled through fractionation of cumulus phases within the range of their observed proportions, with a few notable exceptions.

Primitive volcanic samples have ~8 wt % MgO and possess REE concentrations similar to calculated parental magma compositions for layered gabbro-norites. However, magmas parental to layered gabbro-norites had already been fractionated themselves, forming as a result of fractionation of pyroxenites from primary magmas at the base of the crust. Calculations indicate that more than 25 wt % of primary, mantle-derived melts in the Talkeetna Arc may have crystallised as pyroxenites below the Moho. The considerable discrepancy between these results and the observed proportion of pyroxenites in the Talkeetna section may be best explained by delamination of dense pyroxenites into the less dense, underlying residual mantle.

ACKNOWLEDGEMENTS

This study was supported by National Science Foundation Grant EAR-9910899. Analytical work for this study was made possible with assistance from Karen Hanghøj, Nobu Shimizu, Graham Layne, Nilanjan Chatterjee, Scott Kuehner, Diane Johnson and Charles Knaack. Field work was assisted by Terry Pavlis, Greg Hirth, Brad Hacker, Luc Mehl, Matt Rioux, Jim Mattinson, and Nik Christensen. Assistance with back-fraction routines was provided by Bill Leeman. Additional electron probe data was furnished by Rhea Workman, Brad Hacker, and Luc Mehl. The authors appreciate the thorough and insightful reviews by Richard Arculus and Mike Dungan. A. Greene appreciates the patience and encouragement from James Scoates while revising the manuscript.

REFERENCES

- Albee, L. A. & Ray, L. (1970). Correction factors for electron microprobe analysis of silicates, oxides, carbonates, phosphates, and sulfates. *Analytical Chemistry* **42**, 1408-1414.
- Anders, E. & Grevesse, N. (1989). Abundances of the elements: Meteoritic and solar. *Geochimica et Cosmochimica Acta* **53**, 197-214.
- Andersen, D. J., Lindsley, D. H. & Davidson, P. M. (1993). QUILF: A Pascal program to assess equilibria among Fe-Mg-Mn-Ti oxides, pyroxenes, olivine, and quartz. *Computers & Geosciences* **19**, No. 9, 1333-1350.
- Arculus, R. J. & Wills, K. J. A. (1980). The petrology of plutonic blocks and inclusions from the Lesser Antilles island arc. *Journal of Petrology* **21**, 743-799.
- Arndt, N. T. & Goldstein, S. L. (1989). An open boundary between lower continental crust and mantle; its role in crust formation and crustal recycling. *Tectonophysics* **161**, 201-212.
- Bence, A. E. & Albee, L. A. (1968). Empirical correction factors for the electron microanalysis of silicates and oxides. *Geology* **76**, 382-403.

- Burns, L. E. (1985). The Border Ranges ultramafic and mafic complex, south-central Alaska: cumulate fractionates of island-arc volcanics. *Canadian Journal of Earth Sciences* **22**, 1020-1038.
- Burns, L. E., Pessel, G. H., Little, T. A., Pavlis, T. L., Newberry, R. J., Winkler, G. R. & Decker, J. (1991). Geology of the northern Chugach Mountains, south-central Alaska. *Alaska Division of Geological and Geophysical Surveys Professional Report* **94**, 63 pp., 2 sheets.
- Clarke, S. H. B. (1972). The Wolverine Complex, a newly discovered layered ultramafic body in the western Chugach Mountains, Alaska. *U. S. Geological Survey Open-file Report* **522**, scale 1:63,360, 10 pp., 1 sheet.
- Clift, P., Draut, A., Kelemen, P. B., Blusztajn, J., Greene, A. R. (2005). Stratigraphic and geochemical evolution of an oceanic arc upper crustal section: The Jurassic Talkeetna Volcanic Formation, south-central Alaska. *Geological Society of America Bulletin* **117**, no. 7/8, 902-925.
- Conrad, W. K. & Kay, R. W. (1984). Ultramafic and mafic inclusions from Adak Island: Crystallization history, and implications for the nature of primary magmas and the crustal evolution in the Aleutian arc. *Journal of Petrology* **25**, 88-125.
- Conrad, W. K., Kay, S. M. & Kay, R. W. (1983). Magma mixing in the Aleutian arc: Evidence from cognate inclusions and composite xenoliths. *Journal of Volcanology and Geothermal Research* **18**, 279-295.
- Costa F., Dungan, M. A. & Singer, B. S. (2002). Hornblende- and phlogopite-bearing gabbroic xenoliths from Volcán San Pedro (36°S), Chilean Andes: Evidence for melt and fluid migration and reactions in subduction-related plutons. *Journal of Petrology* **43**, 219-241.
- DeBari, S. M., Anderson, R. G. & Mortensen, J. K. (1999). Correlation amongst lower to upper crustal components in an island arc: the Jurassic Bonanza Arc, Vancouver Island, Canada. *Canadian Journal of Earth Sciences* **36**, 1371-1413.
- DeBari, S. M. & Coleman, R. G. (1989). Examination of the deep levels of an island arc: Evidence from the Tonsina Ultramafic-Mafic Assemblage, Tonsina, Alaska. *Journal of Geophysical Research* **94**, 4,373-4,391.
- DeBari, S. M., Kay, S. M. & Kay, R. W. (1987). Ultramafic xenoliths from Adagdak volcano, Adak, Aleutian Islands, Alaska: deformed igneous cumulates from the Moho of an island arc. *Journal of Geology* **95**, 329-341.
- DeBari, S. M. & Sleep, N. H. (1991). High-Mg, low-Al bulk composition of the Talkeetna Arc, Alaska: Implications for primary magmas and the nature of arc crust. *Geological Society of America Bulletin* **103**, 37-47.

- Detterman, R. & Harstock, J. (1966). Geology of the Inikin-Tuxedni region, Alaska. *United States Geological Survey Professional Paper* **512**, 78 pp.
- Fleider, M. & Klemperer, S. L. (1999). Structure of an island arc: Wide-angle seismic studies in the eastern Aleutian Islands, Alaska. *Journal of Geophysical Research* **104**, 10,667-10,694.
- Foden, J. D. & Green, G. H. (1992). Possible role of amphibole in the origin of andesite: some experimental and natural evidence. *Contributions to Mineralogy and Petrology* **109**, 479-493.
- Ghiorso, M. S. & Sack, R. O. (1995). Chemical mass transfer in magmatic processes IV. A revised and internally consistent thermodynamic model for the interpolation and extrapolation of liquid-solid equilibria in magmatic systems at elevated temperatures and pressures. *Contributions to Mineralogy and Petrology* **119**, 197-212.
- Gill, J. (1981). *Orogenic Andesites and Plate Tectonics*. Berlin: Springer-Verlag. 390 pp.
- Grantz, A., Thomas, H., Stern, T. & Sheffey, N. (1963). Potassium-argon and lead-alpha ages for stratigraphically bracketed plutonic rocks in the Talkeetna Mountains, Alaska. *United States Geological Survey Professional Paper* **475-B**, B56-B59 pp.
- Gust, D. A. & Perfit, M. R. (1987). Phase relations of a high-Mg basalt from the Aleutian Island arc: implications for primary island arc basalts and high-Al basalts. *Contributions to Mineralogy and Petrology* **97**, 7-18.
- Hart, S. R. & Brooks, C. (1977). Geochemistry and evolution of early Precambrian mantle. *Contributions to Mineralogy and Petrology* **69**, 109-128.
- Hart, S. R. & Dunn, T. (1993). Experimental cpx/melt partitioning of 24 trace elements. *Contributions to Mineralogy and Petrology* **113**, 1-8.
- Hauff, F., Hoernle, K. & Schmidt, A. (2003). Sr-Nd-Pb composition of Mesozoic Pacific oceanic crust (Site 1149 and 801, ODP Leg 185): Implications for alteration of ocean crust and the input into the Izu-Bonin-Mariana subduction system. *Geochemistry, Geophysics, and Geosystems* **4(8)**, 8913, doi:10.10292002GC000421.
- Hillebrandt, A. v., Westermann, G. E. G., Callomon, J. H. & Detterman, R. L. (1992). Ammonites of the circum-Pacific region. In: Westermann, G. E. G. (ed.) *The Jurassic of the Circum-Pacific*. Cambridge: Cambridge University Press, pp. 342-359.

- Hoernle, K. (1998). Geochemistry of Jurassic oceanic crust beneath Grand Canaria (Canary Islands): implications for crustal recycling and assimilation. *Journal of Petrology* **39**, 859-880.
- Hofmann, A. W. (1988). Chemical differentiation of the Earth: The relationship between mantle, continental crust and oceanic crust. *Earth and Planetary Science Letters* **90**, 297-314.
- Holbrook, S. W., Lizarralde, D., McGeary, S., Bangs, N. & Diebold, J. (1999). Structure and composition of the Aleutian island arc and implications for continental crustal growth. *Geology* **27**, 31-34.
- Holland, T. J. B. & Blundy, J. D. (1994). Non-ideal interactions in calcic amphiboles and their bearing on amphibole plagioclase thermometry. *Contributions to Mineralogy and Petrology* **116**, 433-447.
- Hunter R. N. (1996). Texture development in cumulate rocks. In: Cawthorn, R. G. (ed.) *Layered Intrusions*. Amsterdam: Elsevier Science B.V., pp. 77-101.
- Imlay, R. W. (1984). Early and Middle Bajocian (Middle Jurassic) ammonites from southern Alaska. *United States Geological Survey Professional Paper* **1322**, 38 pp.
- Imlay, R. W. & Detterman, R. L. (1973). Jurassic paleobiogeography of Alaska. *United States Geological Survey Professional Paper* **801**, 34 pp.
- Johnson, D. M., Hooper, P. R. & Conrey, R. M. (1999). XRF analysis of rocks and minerals for major and trace elements on a single low dilution Li-tetraborate fused bead. *Advances in X-ray Analysis* **41**, 843-867.
- Jull, M. & Kelemen, P. B. (2001). On the conditions for lower crustal convective instability. *Journal of Geophysical Research* **106**, 6,423-6,446.
- Kawate, S. & Arima, M. (1998). Petrogenesis of the Tanzawa plutonic complex, central Japan: Exposed felsic midcrust of the Izu-Bonin-Mariana arc. *The Island arc* **7**, 342-358.
- Kay, R. W. & Kay, S. M. (1988). Crustal recycling and the Aleutian arc. *Geochimica et Cosmochimica Acta* **52**, 1351-1359.
- Kay, R. W. & Kay, S. M. (1990). Basaltic composition xenoliths and the formation, modification and preservation of lower crust. In: Salisbury, M. H. & Fountain, D. M. (eds.) *Exposed cross-sections of the continental crust: proceedings*. Boston: Reidel, pp. 401-420.
- Kay, R. W. & Kay, S. M. (1991). Creation and destruction of lower continental crust. *Geologische Rundschau* **80**, 259-278.

- Kay, S. M. & Kay, R. W. (1985). Role of crystal cumulates and the oceanic crust in the formation of the lower crust of the Aleutian arc. *Geology* **13**, 461-464.
- Kelemen, P. B., Hanghøj, K. & Greene, A. R. (2003a). One view of the geochemistry of subduction-related magmatic arcs, with emphasis on primitive andesite and lower crust. In: Rudnick, R. L. (ed.) *The Crust, Vol. 3*, Holland, H. D. and Turekian, K. K. (eds) *Treatise on Geochemistry*. Oxford: Elsevier -Pergamon, pp. 593-659.
- Kelemen P. B., Rilling J. L., Parmentier E. M., Mehl L. & Hacker B. R. (2003b). Thermal structure due to solid-state flow in the mantle wedge beneath arcs. In: Eiler, J. (ed.) *Inside the Subduction Factory. Geophysical Monograph, American Geophysical Union* **138**, 293-311.
- Kelley, K., Plank, T., Ludden, J. & Staudigel, H. (2003). Composition of altered oceanic crust at ODP Sites 801 and 1149. *Geochemistry, Geophysics, and Geosystems* **4(6)**, 8910, doi:10.1029/2002GC000435.
- Khan, M. A., Jan, M. Q., Windley, B. F., Tarney, J. & Thirlwall, M. F. (1989). The Chilas Mafic-Ultramafic Igneous Complex; The root of the Kohistan Island arc in the Himalaya of northern Pakistan. *Geological Society of America Special Paper* **232**, 75-94.
- Knaack, C., Cornelius, S. & Hooper, P. (1994) Trace element analyses of rocks and minerals by ICP-MS. <http://www.wsu.edu/~geology/Pages/Services/ICP.html>.
- Koga, K., Kelemen, P. B. & Shimizu, N. (2001). Petrogenesis of the crust-mantle transition zone and the origin of lower crustal wehrlite in the Oman Ophiolite. *Geochemistry, Geophysics, and Geosystems* **2**, Paper number 2000GC000132, 38 pp.
- Leake, B. L. (1978). Nomenclature of amphiboles. *American Mineralogist* **63**, 1023-1052.
- Leeman, W. P. (1983). The influence of crustal structure on compositions of subduction-related magmas. *Journal of Volcanology and Geothermal Research* **18**, 561-588.
- MacKevett, E. M., Jr. & Plafker, G. (1974). The Border Ranges Fault in south-central Alaska. *United States Geological Survey Journal of Research* **2**, 323-329.
- Martin, G., Johnson, B. & Grant, U. (1915). Geology and mineral resources of Kenai Peninsula, Alaska. *United States Geological Survey Bulletin Report* **B 0587**, 243 pp.
- McKenzie, D. & Onions, R. K. (1991). Partial melt distributions from inversion of rare earth element concentrations. *Journal of Petrology* **32**, No. 5, 1021-1091.

- Mehl, L., Hacker, B. H. & Hirth, G. (2001). Upper mantle deformation beneath intraoceanic island arcs: the Talkeetna Arc, south-central Alaska. *Eos Transactions. AGU*, **82(47)**, Fall Meeting Supplement, Abstract T41C-0878.
- Michard, A., Gurriet, P., Soudant, M. & Albarède, F. (1985). Nd isotopes in French Phanerozoic shales: external vs. internal aspects of crustal evolution. *Geochimica et Cosmochimica Acta* **49**, 601-610.
- Millholland, M., Graubard, C., Mattinson, J. & McClelland, W. (1987). U-Pb age of zircons from the Talkeetna Formation, Johnson River area, Alaska. *Isotopes*, **50**, 9-11.
- Miyashiro, A. (1974). Volcanic rock series in island arcs and active continental margins. *American Journal of Science* **274**, 321-355.
- Montanini, A. & Tribuzio, R. (2001). Gabbro-derived granulites from the Northern Apennines (Italy): Evidence for lower-crustal emplacement of tholeiitic liquids in post-Variscan times. *Journal of Petrology* **42**, 2259-2277.
- Müntener, O., Kelemen, P. B. & Grove, T. L. (2001). The role of H₂O during crystallization of primitive arc magmas under uppermost mantle conditions and genesis of igneous pyroxenites: an experimental study. *Contributions to Mineralogy and Petrology* **141**, 643-658.
- Newberry, R. J., Burns, L. E. & Pessel, G. H. (1986). Volcanogenic massive sulfide deposits and the "missing complement" to the calc-alkaline trend: Evidence from the Jurassic Talkeetna Island Arc of southern Alaska. *Economic Geology* **81**, 951-960.
- Nielsen, R. L., Forsythe, L. M., Gallahan, W. E. & Fisk, M. R. (1994). Major- and trace-element magnetite-melt equilibria. *Chemical Geology* **117**, 167-191.
- Nokleberg, W. J., Plafker, G. & Wilson, F. H. (1994). Geology of south-central Alaska. In: Plafker, G. & Berg, H. C. (eds) *The Geology of North America*. Boulder, CO: Geological Society of America, *The Geology of Alaska* **G-1**, pp. 311-366.
- Osborn, E. F. (1959). Role of oxygen pressure in the crystallization and differentiation of basaltic magma. *American Journal of Science* **257**, 609-647.
- Page, R. A., Plafker, G., Fuis, G. S., Nokleberg, W. J., Ambros, E. L., Mooney, W. D. & Campbell, D. L. (1986). Accretion and subduction tectonics in the Chugach Mountains and Copper River basin, Alaska: Initial results of the Trans-Alaska Crustal Transect. *Geology* **14**, 501-505.

- Pálffy, J., Smith, P., Mortensen, J. & Friedman, R. (1999). Integrated ammonite biochronology and U-Pb geochronometry from a basal Jurassic section in Alaska. *Geological Society of America Bulletin* **111**, 1537-1549.
- Pavlis, T. L. (1983). Pre-Cretaceous crystalline rocks of the western Chugach Mountains, Alaska: Nature of the basement of the Jurassic Peninsular terrane. *Geological Society of America Bulletin* **94**, 1329-1344.
- Pearce, J. A. & Norry, M. J. (1979). Petrogenetic implications of Ti, Zr, Y, and Nb variations in volcanic rocks. *Contributions to Mineralogy and Petrology* **69**, 33-47.
- Plafker, G., Nokleberg, W. J. & Lull, J. S. (1989). Bedrock geology and tectonic evolution of the Wrangellia, Peninsular, and Chugach terranes along the Trans-Alaskan Crustal Transect in the northern Chugach Mountains and southern Copper River basin, Alaska. *Journal of Geophysical Research* **94**, 4,255-4,295.
- Plank, T., Benjamin, E., Wade, J. & Grove, T. (2004). A New Hygrometer based on the Europium Anomaly in Clinopyroxene Phenocrysts in arc Volcanic Rocks. *Eos Transactions. AGU*, **84(47)**, Fall Meeting Supplement, Abstract V12A-05.
- Quick, J. E. (1990). Geology and origin of the Late Proterozoic Darb Zubaydah ophiolite, Kingdom of Saudi Arabia. *Geological Society of America Bulletin* **102**, 1007-1020.
- Richards, M. A., Shimizu, N. & Allegre, C. J. (1976). $^{143}\text{Nd}/^{144}\text{Nd}$ as a natural tracer: an application to oceanic basalts. *Earth and Planetary Science Letters* **31**, 269-278.
- Rioux, M. E., Kelemen, P. B., Mattinson, J., Hacker, B. H. & Blusztajn, J. (2004). Magmatic differentiation in the accreted Talkeetna Arc; south-central Alaska. *Eos Transactions. AGU*, **84(47)**, Fall Meeting Supplement, Abstract V13B-1482.
- Rioux, M. E., Mattinson, J., Hacker, B. H. & Grove, M. (2002). Growth and evolution of the accreted Talkeetna Arc, south-central Alaska: Solutions to the "arc paradox". *Eos Transactions. AGU*, **83(47)**, Fall Meeting Supplement, Abstract V12C-11.
- Rioux, M. E., Mehl, L., Hacker, B. H., Mattinson, J. M., Gans, P. & Wooden, J. L. (2001). Understanding island arc evolution through U/Pb and $^{40}\text{Ar}/^{39}\text{Ar}$ geochronology of the Talkeetna Arc, south-central Alaska. *Eos Transactions. AGU*, **82(47)**, Fall Meeting Supplement, Abstract T41C-0885.
- Roeske, S. M., Mattinson, J. M. & Armstrong, R. L. (1989). Isotopic ages of glaucophane schists on the Kodiak Islands, southern Alaska, and their implications for the Mesozoic tectonic history of the Border Ranges fault system. *Geological Society of America Bulletin* **101**, 1021-1037.

- Rose, A. W. (1966). Geology of chromite-bearing ultramafic rocks near Eklutna, Anchorage quadrangle, Alaska. *Alaska Division of Mines and Minerals Geologic Report* **18**, scale 1:63,360, 20 pp.
- Shimizu, N. & Hart, S. R. (1982). Application of the ion microprobe to geochemistry and cosmochemistry. *Annual Review of Earth and Planetary Science* **10**, 483-526.
- Sisson, T. W. & Grove, T. L. (1993). Experimental investigations of the role of H₂O in calc-alkaline differentiation and subduction zone magmatism. *Contributions to Mineralogy and Petrology* **113**, 143-166.
- Spandler, C. J., Arculus, R. J., Eggins, S. M., Mavrogenes, J. A., Price, R. C. & Reay, A. J. (2003). Petrogenesis of the Greenhills Complex, Southland, New Zealand: magmatic differentiation and cumulate formation at the roots of a Permian island-arc volcano. *Contributions to Mineralogy and Petrology* **144**, 703-721.
- Suyehiro, K., Takahashi, N., Ariie, Y., Yokoi, Y., Hino, R., Kanazawa, T., Hirata, N., Tokuyan, H. & Taira, A. (1996). Continental crust, crustal underplating and low-Q upper mantle beneath an oceanic island arc. *Science* **272**, 390-392.
- Tahirkheli, R. A. K. (1979). Geology of Kohistan and adjoining Eurasian and Indo-Pakistan continent, N. Pakistan. In: *Geological Bulletin University of Peshawar, Special Issue II*. pp. 1-30.
- Takashima, R., Nishi, H. & Yoshida, T. (2002). Geology, petrology and tectonic setting of the Late Jurassic ophiolite in Hokkaido, Japan. *Journal of Asian Earth Sciences* **21**, 197-215.
- Thirlwall, M. F., Smith, T. E., Graham, A. M., Theodorou, N., Hollings, P., Davidson, J. P. & Arculus, R. J. (1994). High field strength anomalies in arc lavas: Source or process? *Journal of Petrology* **35**, 819-838.
- Tribuzio, R., Tiepolo, M., Vannucci, R. & Bottazzi, P. (1999). Trace element distribution within olivine-bearing gabbros from the Northern Apennine ophiolites (Italy): evidence for post-cumulus crystallization in MOR-type gabbroic rocks. *Contributions to Mineralogy and Petrology* **134**, 123-133.
- Turcotte, D. L. (1989). Geophysical processes influencing the lower continental crust. In: Mereu, R. F., Mueller, S. & Fountain, D. M. (eds) *Properties and Processes of Earth's lower crust. Geophysical Monograph, American Geophysical Union* **51**, pp. 321-329.
- Vukadinovic, D. (1993). Are Sr enrichments in arc basalts due to plagioclase accumulation? *Geology* **21**, 611-614.

- Winkler, G. R., compilation (1992). Geologic map and summary geochronology of the Anchorage $1^{\circ} \times 3^{\circ}$ Quadrangle, southern Alaska. *United States Geological Survey Miscellaneous Investigations Series Map 1-2283*, scale 1:250,000.
- Winkler, G. R., Silberman, M. L., Grantz, A., Miller, R. J. & MacKevett, E. M., Jr. (1981). Geologic map and summary geochronology of the Valdez Quadrangle, southern Alaska. *United States Geological Survey Open-file Report 80-892-A*, scale 1:250,000.
- Woodhead, J. D. (1988). The origin of geochemical variations in Mariana lavas: a general model for petrogenesis in intraoceanic island arcs. *Journal of Petrology* **29**, 805-830.

FIGURE CAPTIONS

Figure 1. Geologic map of the Talkeetna Arc section in south-central Alaska. Compiled from Winkler (1992) and Winkler *et al.* (1981). Insets show the extent of the Talkeetna Arc section in Alaska.

Figure 2. Lithologic column and photographs. (a) Schematic lithologic column for the Talkeetna Arc section based on field relations and geobarometry. (b) Magma mingling features preserved in the Nelchina dike complex, adjacent to the Nelchina Glacier (sledgehammer is ~80 cm long). (c) Layered gabbronorite just west of Tazlina Lake, typical of exposures between Tazlina Lake and Barnette Creek. (d) Magnetite gabbronorite prevalent in the lower crust (photomicrograph is ~8 mm across).

Figure 3. Molar Mg # vs. Al_2O_3 in clinopyroxene and orthopyroxene from several different lithologies and crustal levels. Data for mid-crustal, lower crustal and basal gabbronorite are from individual analyses in this study (Table 2), along with the published work of Burns (1985) and DeBari & Coleman (1989). Additional electron probe data for pyroxenite and plagioclase pyroxenite provided by Rhea Workman (plagioclase pyroxenite analyses shown in Table 2), and for garnet gabbro by Brad Hacker and Luc Mehl.

Figure 4. REE and trace-element concentrations in clinopyroxene and plagioclase from gabbronorites and phenocrysts in mafic dikes. (a) and (b) Average REE and trace-element concentrations in clinopyroxene, normalised to C1 chondrite (Anders & Grevesse, 1989). Each REE pattern is an average of 6-8 analyses from an individual sample. Analyses showed minimal variation within each sample (median standard deviation less than 1x chondrite). (c) Y vs. Zr in clinopyroxenes. (d) Sr vs Zr in clinopyroxene. (e) Plagioclase REE concentrations. Each REE pattern represents an individual analysis. REE in parentheses were not analysed, and are interpolated values. Averages of the analyses for each sample are listed in Table 3 and all individual analyses are listed in Electronic Appendix II at <http://www.petrology.oupjournals.org>.

Figure 5. Whole rock major- and trace-element variation diagrams for volcanic and plutonic rocks from the Talkeetna Arc section with published data from the Kohistan Island Arc section. Major-element data are from analyses in this study (Table 4) and the published work of Burns (1985), Burns *et al.* (1991), and DeBari and Sleep (1991). The trace-element data are from samples in this study (Table 5). XRF analyses were used for all the elements except Sr and Zr, where ICP-MS data was used. Tholeiitic and calc-alkaline fields follow those of Miyashiro (1974), expressed using Mg#. Total Fe expressed as FeO for Mg#.

Figure 6. Whole rock REE and trace-element concentrations for volcanic rocks (panels a and b) and plutonic and chilled mafic rocks (panels c and d), normalised to C1 chondrite (Anders & Grevesse, 1989) and N-MORB (Hofmann, 1988). Note the contrast in Ti anomalies between the cumulate gabbronorites and the other lithologies (panel d). Samples from the Nelchina dike complex are not included due to extensive alteration.

ICP-MS analyses were used for all the elements except Ni, Ti, and K, where XRF data was used.

Figure 7. Geographic location and sample lithology versus chondrite-normalised whole-rock Yb. Geographic location is given in Universal Transverse Mercator East-West (UTM EW) coordinates, in meters. Yb is a proxy for differentiation in these lithologies given the flat HREE segments of the REE patterns. Average plagioclase anorthite (An) contents are listed alongside each of the gabbronorites which were analysed for mineral chemistry. Clinopyroxene Mg# and plagioclase An content from analysed gabbronorites are plotted versus whole-rock Yb(N). Clinopyroxene Mg# and plagioclase An do not correlate well with whole-rock HREE. In the case of clinopyroxene Mg#, this could be due to subsolidus exchange reactions between clinopyroxene and Fe-Ti oxides and/or orthopyroxene and/or hornblende. Plagioclase may have undergone high T exchange reactions with hornblende (e.g. Holland & Blundy, 1994).

Figure 8. Initial neodymium isotopic ratios plotted against normalised whole-rock Yb. Initial ratios for all samples were calculated at 182 Ma. Using a different age correction for calculating initial ratios for certain samples will determine whether they are within analytical error of the other samples. Two arrows show the effect of using an age of 202 Ma for two intermediate to felsic plutonic rocks. Initial values for Jurassic Atlantic MORB, age 170 Ma (Hoernle, 1998), Jurassic Pacific MORB, age 167 Ma (Hauff *et al.*, 2003), and depleted mantle (DM) (at 180 and 200Ma) are presented for comparison. Present-day values used for calculating DM at 180 and 200 Ma are $^{147}\text{Sm}/^{144}\text{Nd}=0.222$ and $^{143}\text{Nd}/^{144}\text{Nd}=0.513114$ (Michard *et al.*, 1985). Yb concentrations for Site 801 samples from Kelley *et al.* (2003). The volcanic rock with the highest initial $^{143}\text{Nd}/^{144}\text{Nd}$ is one of the distinct HREE-depleted, high Mg# dacites.

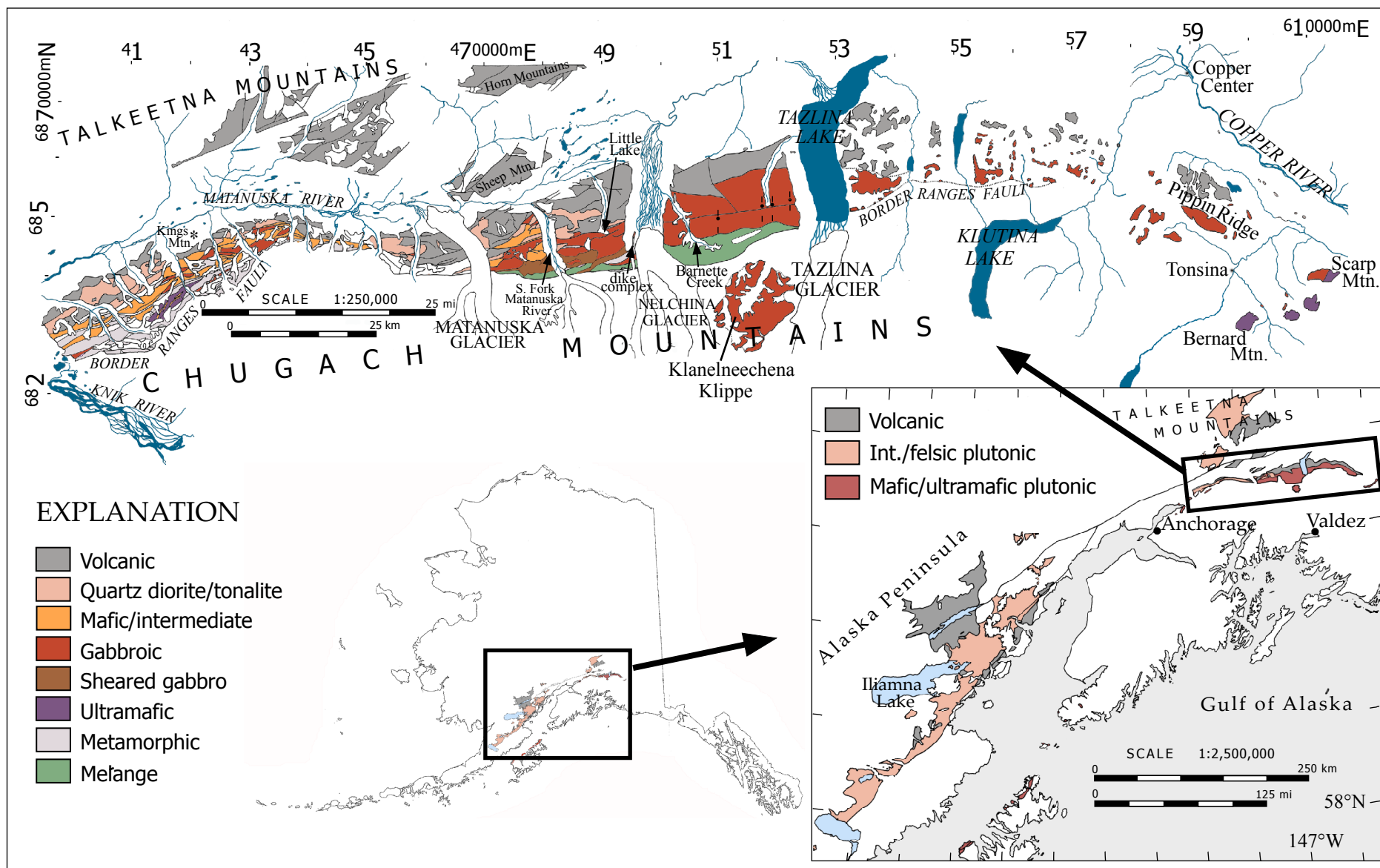
Figure 9. Calculated liquid REE concentrations compared to volcanic rock REE compositions. Calculated liquids are based on the average clinopyroxene analyses for each sample (Figure 4A) divided by clinopyroxene/liquid distribution coefficients. The coefficients of Hart and Dunn (1993) were used. The gray shaded area in both panels represents the range of volcanic rock compositions from Figure 6 (panel a). (a) Many (13 out of 18) of the calculated liquid concentrations from gabbronorite samples lie within the range of volcanic rock compositions. (b) All but two of the calculated liquids from the Tazlina-Barnette area lie within the range of volcanic rock compositions.

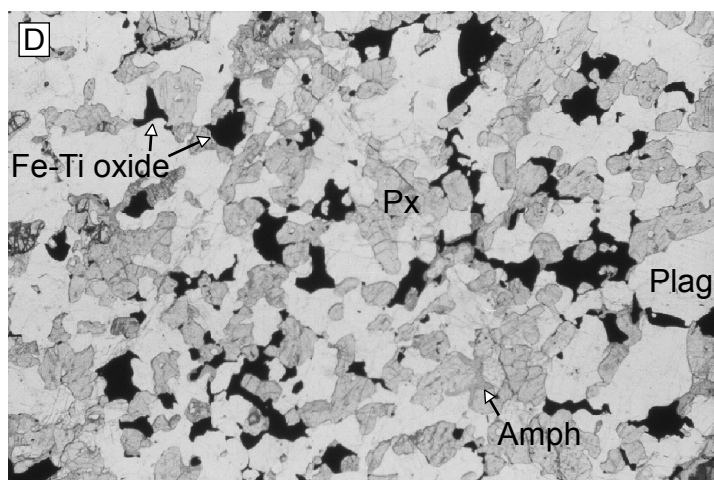
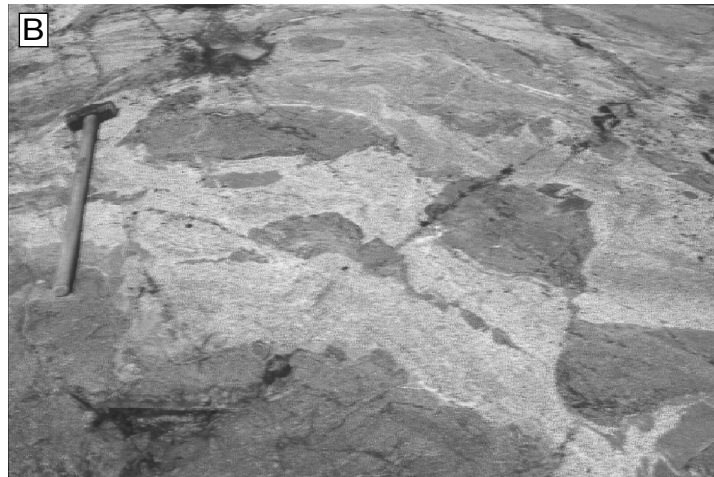
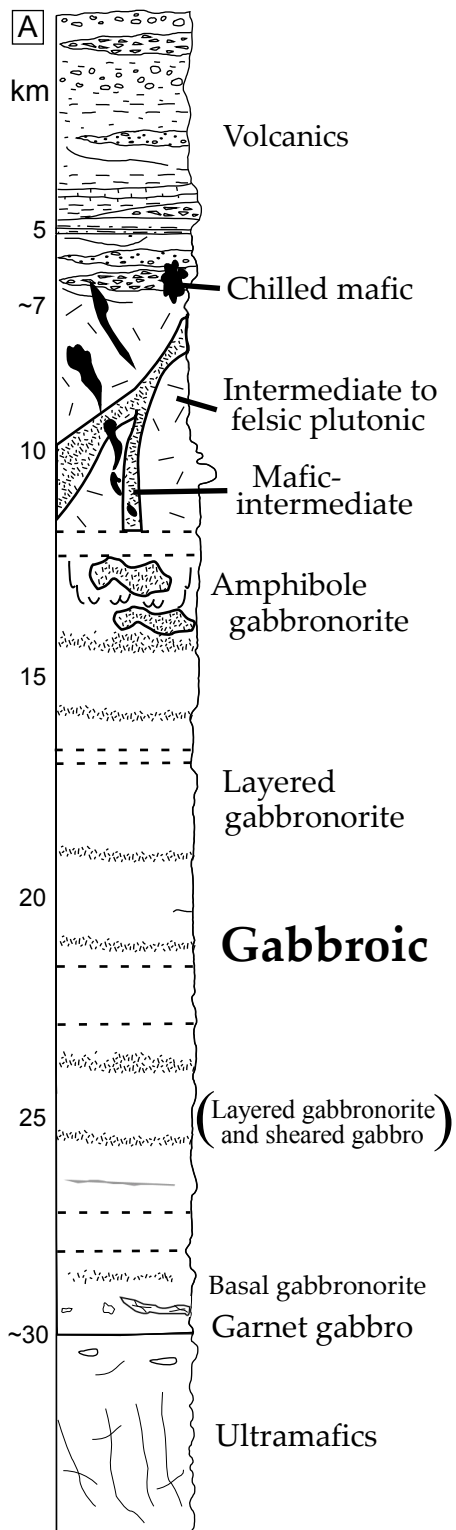
Figure 10. Variation in chondrite-normalised Yb concentration and Mg# in volcanic and chilled mafic rocks, compared with calculated liquids from clinopyroxene in gabbronorites. Calculated liquids are based on the average clinopyroxene Yb concentration for each sample divided by a clinopyroxene/liquid distribution coefficient ($D(\text{Yb})_{\text{cpx/melt}}=0.43$) (Hart & Dunn, 1993) and an Fe/Mg Kd (cpx/liquid) of 0.23, calculated with total Fe(liquid) (Sisson & Grove, 1993). There is little variation in Mg# in clinopyroxene. However, calculated liquids are similar to several of the volcanic and chilled mafic rocks. In addition to the main trend of the lava data, showing increasing Yb with decreasing Mg#, several of the volcanic rocks have high Mg# and high Yb(N), as is also observed in clinopyroxene in several gabbronorites. See text for discussion.

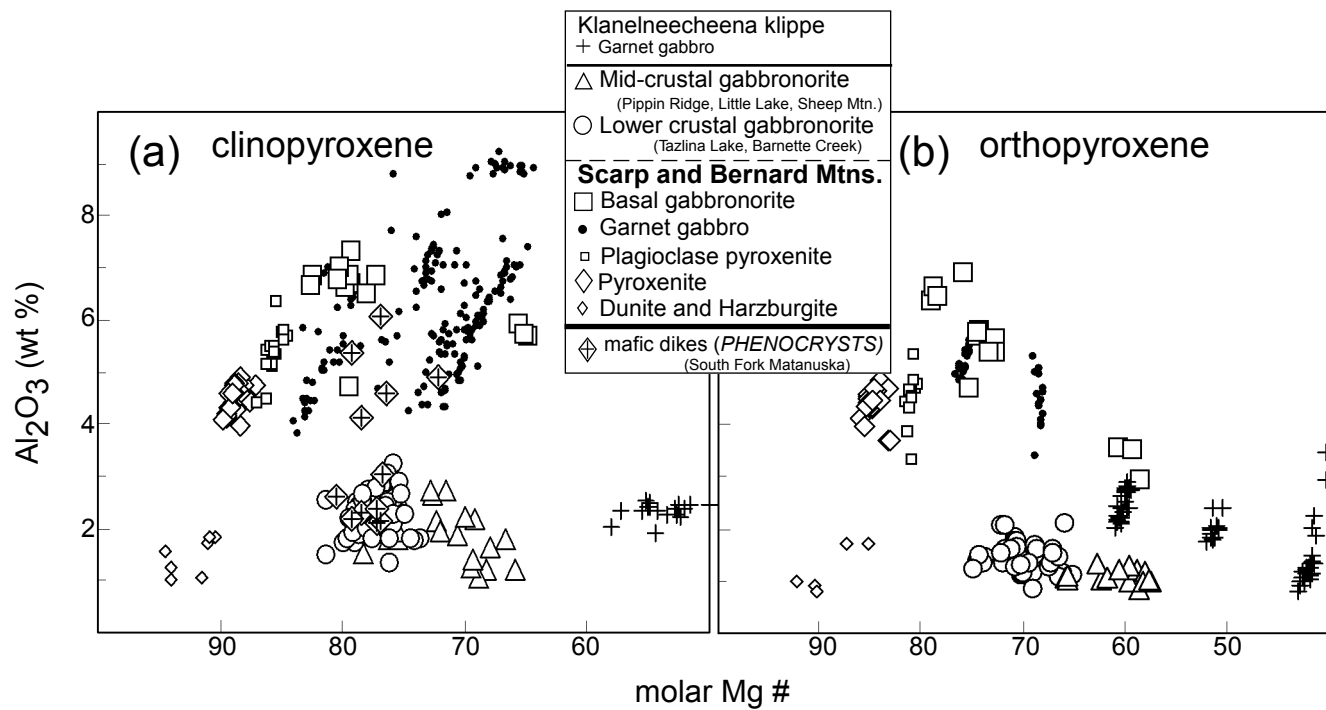
Figure 11. Whole rock trace-element ratios (log scale) plotted versus silica for volcanic and plutonic rocks from the Talkeetna Arc section. Layered gabbronorites are distinguished from gabbroic rocks without layering and, with few exceptions, clearly plot together. (a) Sr/Y reflects plagioclase fractionation within the layered gabbronorites (see Fig. 12), except for two high Mg# dacites with high La/Yb and high Sr/Y. (b) Variation in Zr/Sm is often attributed primarily to amphibole fractionation. However, clinopyroxene and magnetite fractionation may also exert an influence on this ratio. (c) and (d) Ti/Zr and V/Ti variation show a strong signature of Fe-Ti oxide fractionation, but also may have been affected by amphibole fractionation.

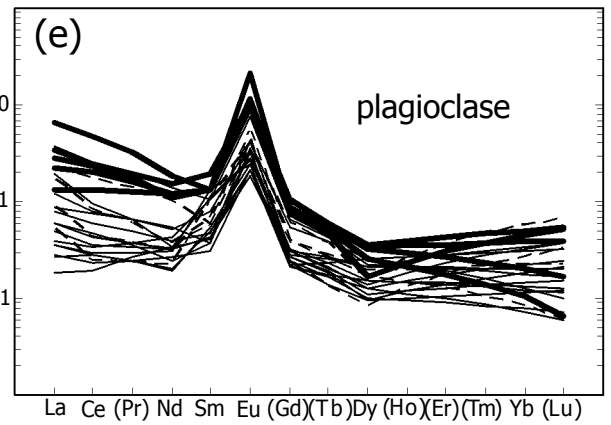
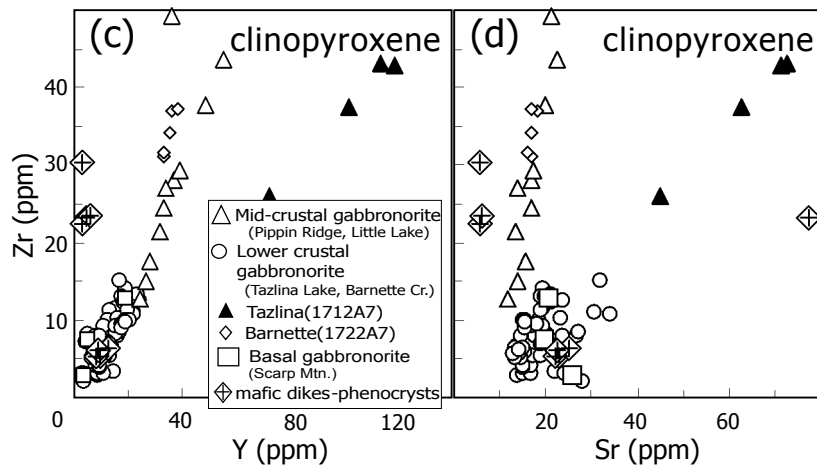
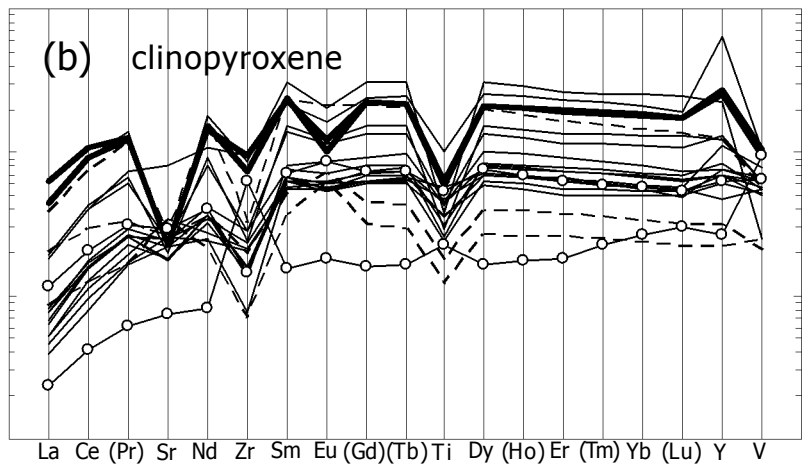
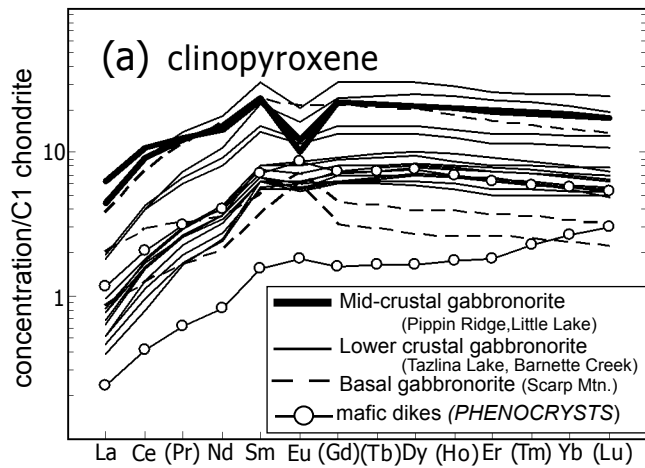
Figure 12. Eu anomaly versus chondrite-normalised Yb concentration and Sr anomaly for whole rocks. (a) Correlation between Eu/Eu^* (log scale) and $\text{Yb}(\text{N})$ reflects the strong effect of plagioclase fractionation and minimal effect of trapped liquids on $\text{Yb}(\text{N})$. (b) Eu/Eu^* and Sr/Sr^* correlate positively, indicating plagioclase accumulation is responsible for variation in Sr/Sr^* . $\text{Sr}/\text{Sr}^* = \text{Sr}(\text{N})/\sqrt{(\text{Pr}(\text{N}) \times \text{Nd}(\text{N}))}$ and $\text{Eu}/\text{Eu}^* = \text{Eu}(\text{N})/\sqrt{(\text{Sm}(\text{N}) \times \text{Gd}(\text{N}))}$, using MORB-normalised data.

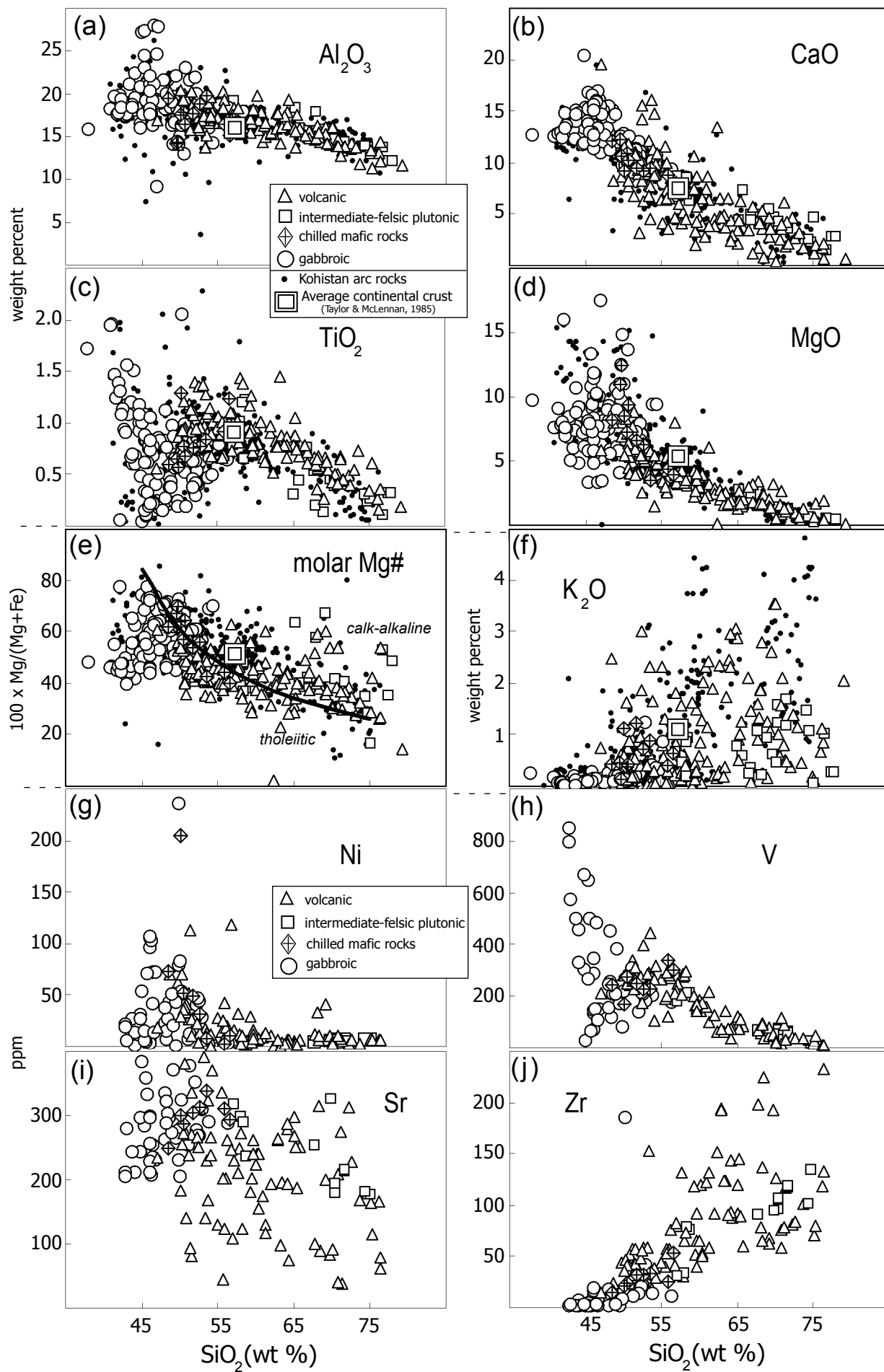
Figure 13. Summary of least squares fractional crystallisation modeling. Clinopyroxene Mg# is plotted in a panel adjacent to a plot of Mg# versus SiO_2 for volcanic and chilled mafic rocks, with the scale of the clinopyroxene Mg# axis calculated to correspond to the lava Mg# axis using the Fe/Mg Kd cpx/liquid of 0.23 calculated with total Fe(liquid) (Sisson & Grove, 1993). Clinopyroxene which could be in equilibrium with a liquid with the composition of a particular volcanic or chilled mafic rock is connected with horizontal lines. (a) Clinopyroxene is separated by lithology/crustal level. Note the vertical axis for the clinopyroxene Mg# is not linear, since it is fixed by the partitioning relationship of Fe/Mg between liquids and clinopyroxene. (b) Three steps of the least squares fractionation modeling are illustrated using arrows and numbers, with results presented in Table 7. The lines labeled ‘estimated primary magma’ represent results from pyroxenite addition calculations (Table 8). Results from fractional crystallisation MELTS models (Ghiorso & Sack, 1995) at 0.5 and 1 GPa and temperatures from ~1250 to 1000 °C are also shown. Using the parent composition from step 1 of the least squares fractionation modeling, MELTS models are shown for 2 wt % H_2O and $f\text{O}_2$ of NNO+1 (squares) at 0.5 GPa and 1 wt % H_2O and $f\text{O}_2$ of FMQ+1 (circles), 2 wt % H_2O and FMQ+2 (pluses), and 3 wt % H_2O and FMQ+2 (dashes) at 1 GPa. Solid assemblages are discussed in the text. (c) Calculated phase proportions (modes) in gabbronorites (Table 6) are compared to the proportions from solutions in least squares modeling from steps 2 and 3 (Table 7). Phase proportions are in weight %. Legend for the symbols is to the right of panel c. Outputs from least squares fractionation models are consistent with calculated phase proportions in basal and lower crustal gabbronorites. (d) Observed versus calculated REE for the three steps of least squares modeling. Calculated REE (dashed lines) are based on mass balance using phase proportions from the least squares solutions and crystal/liquid partition coefficients of McKenzie and O’Nions (1991). The parent-daughter pairs for each step are the same for both least squares and REE modeling.

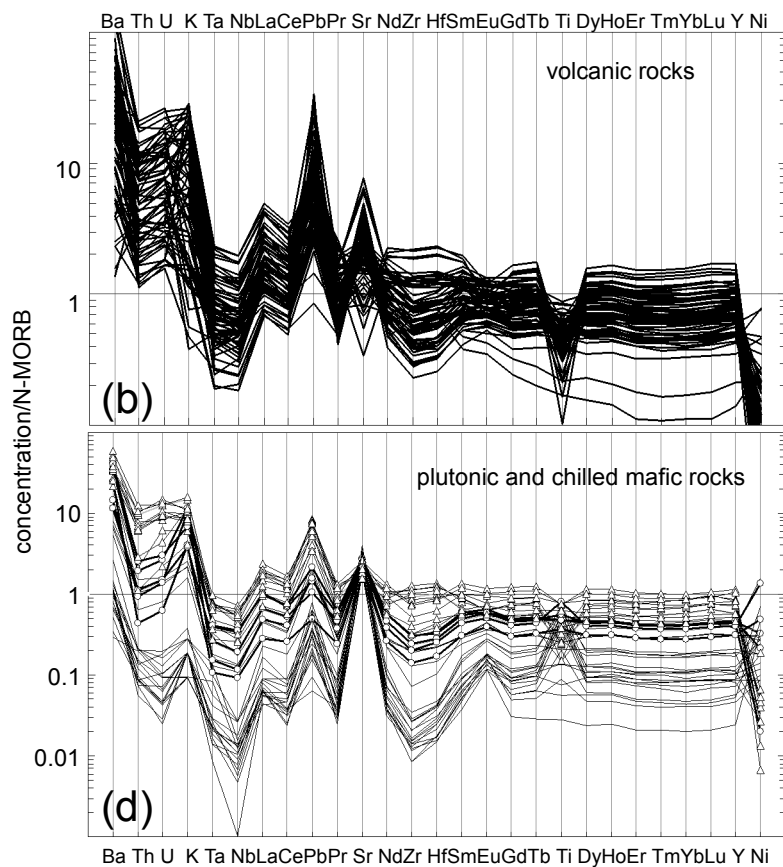
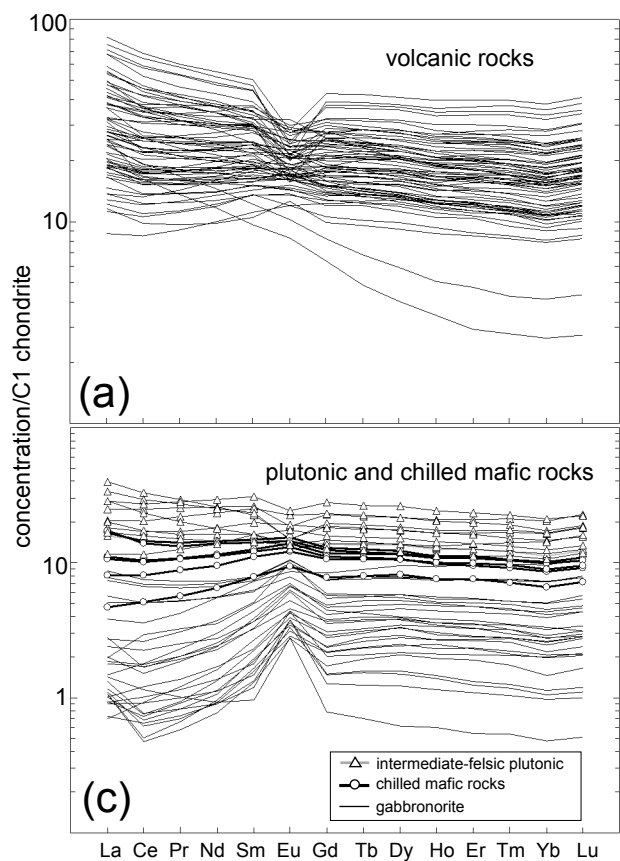


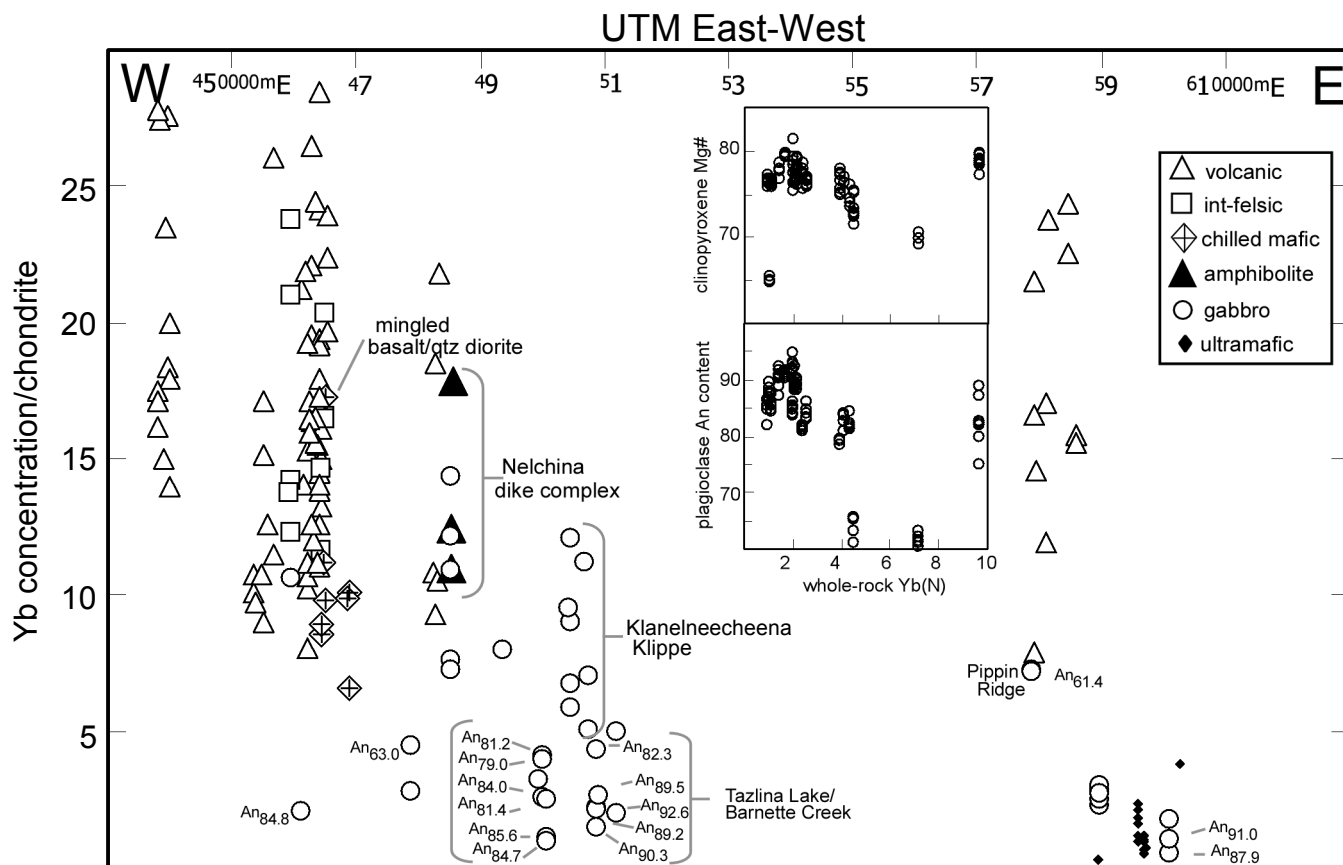


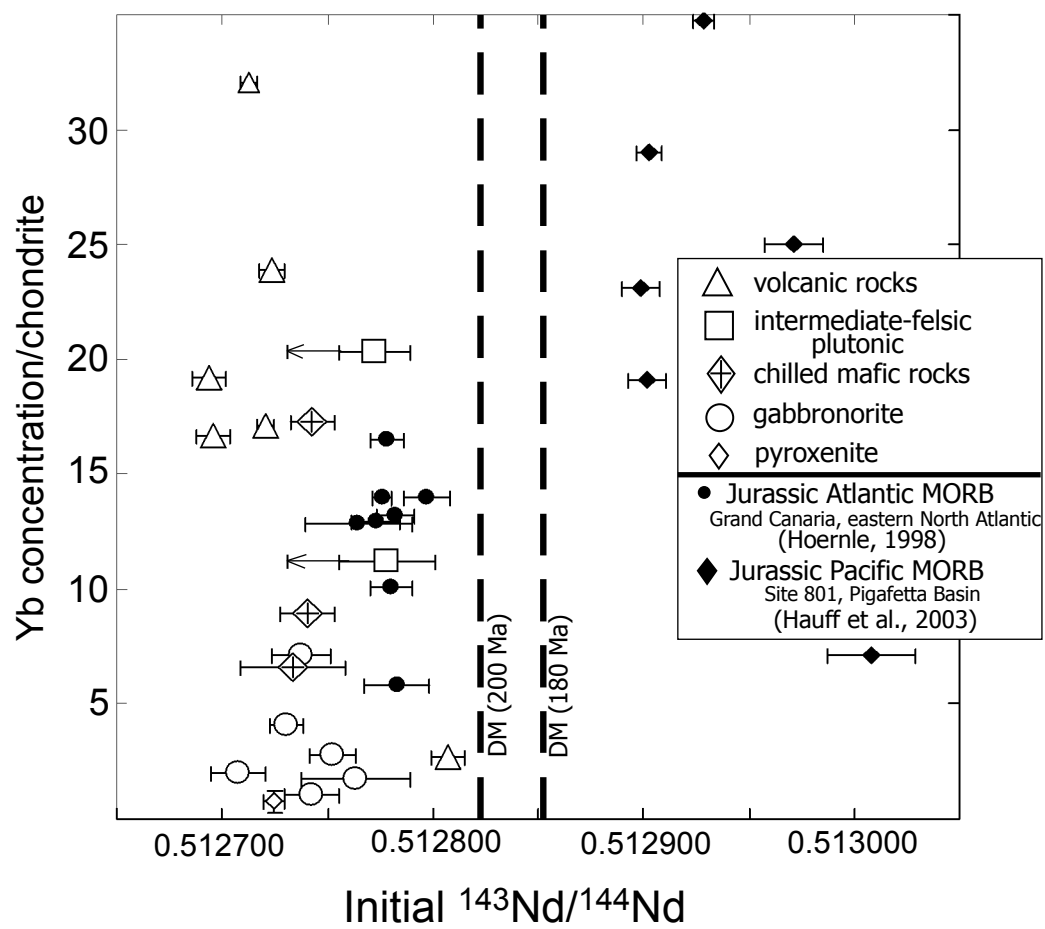


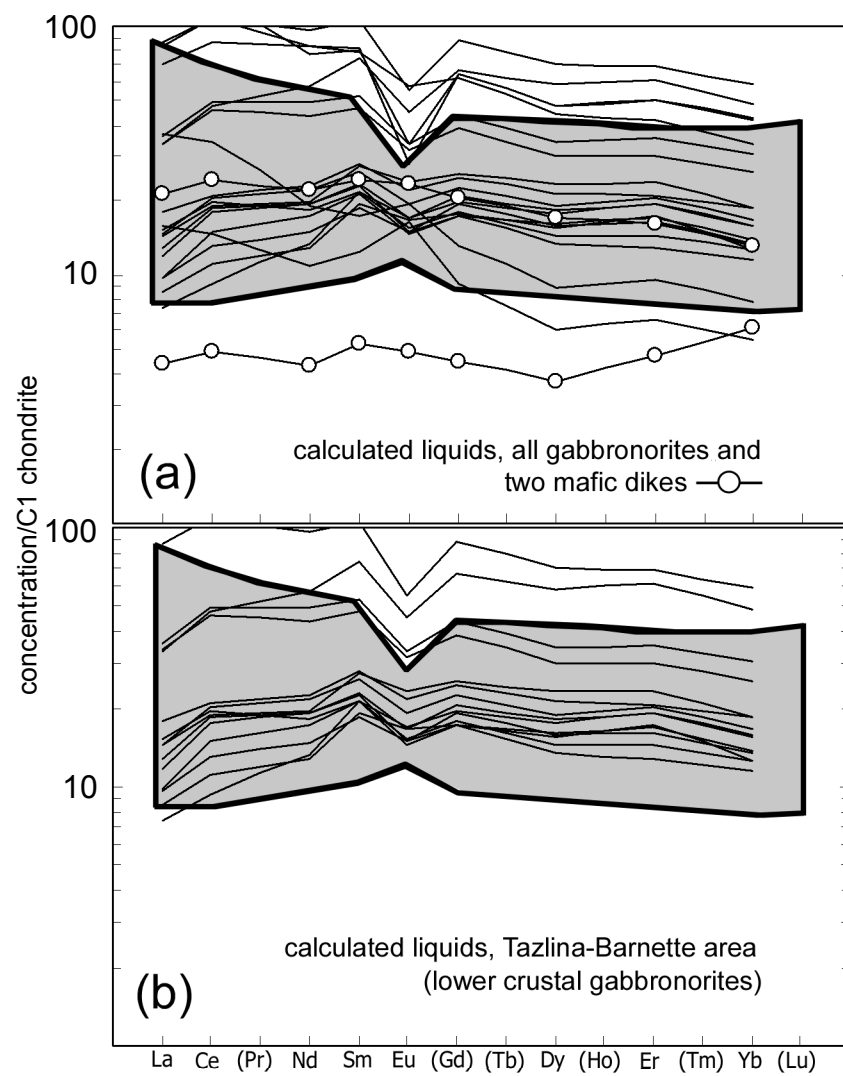


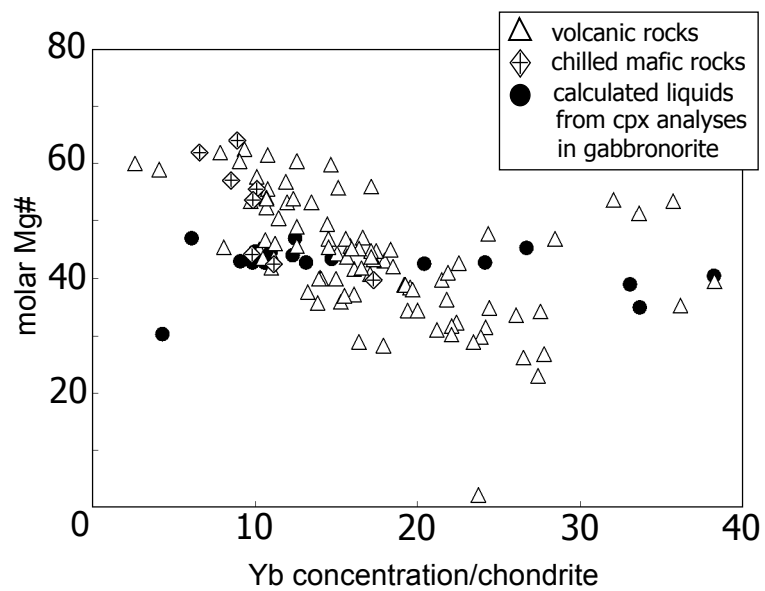


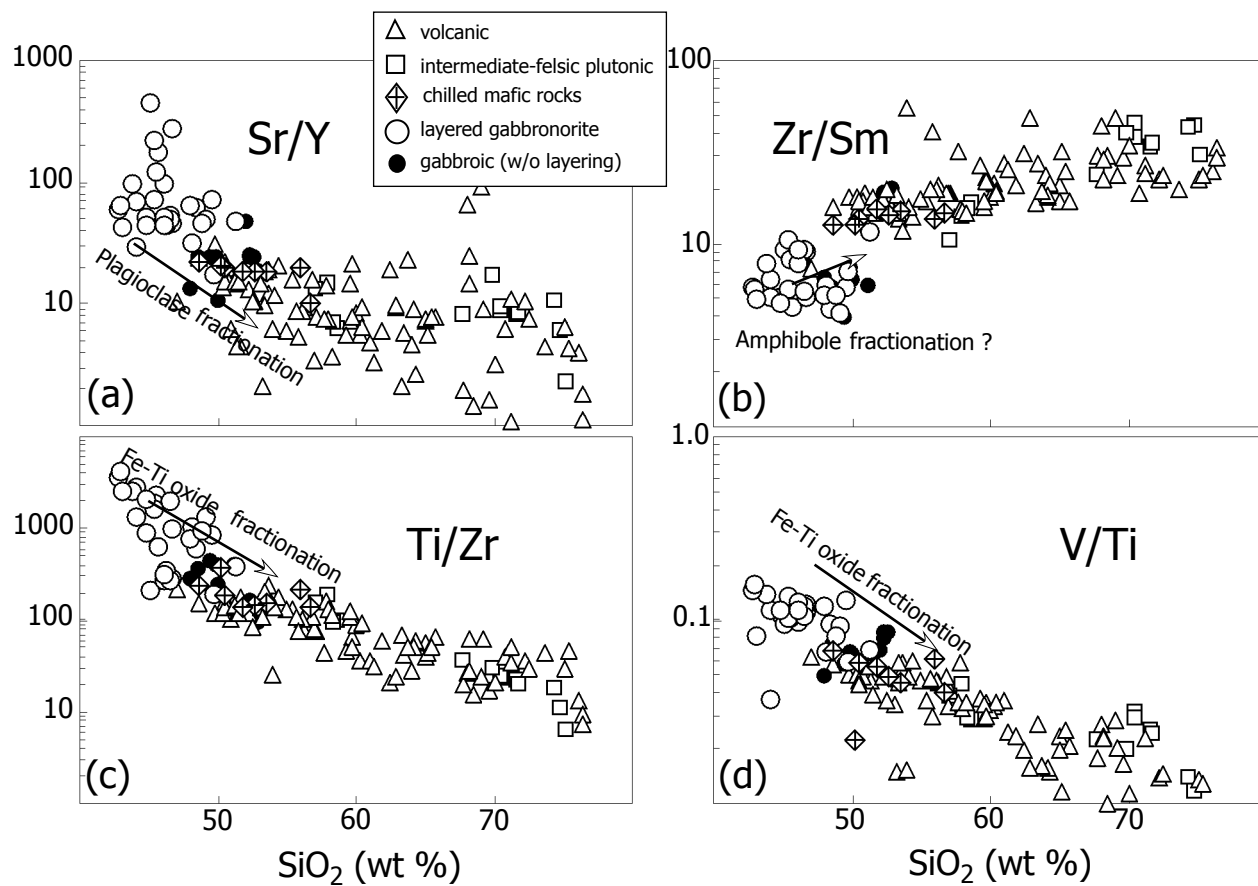


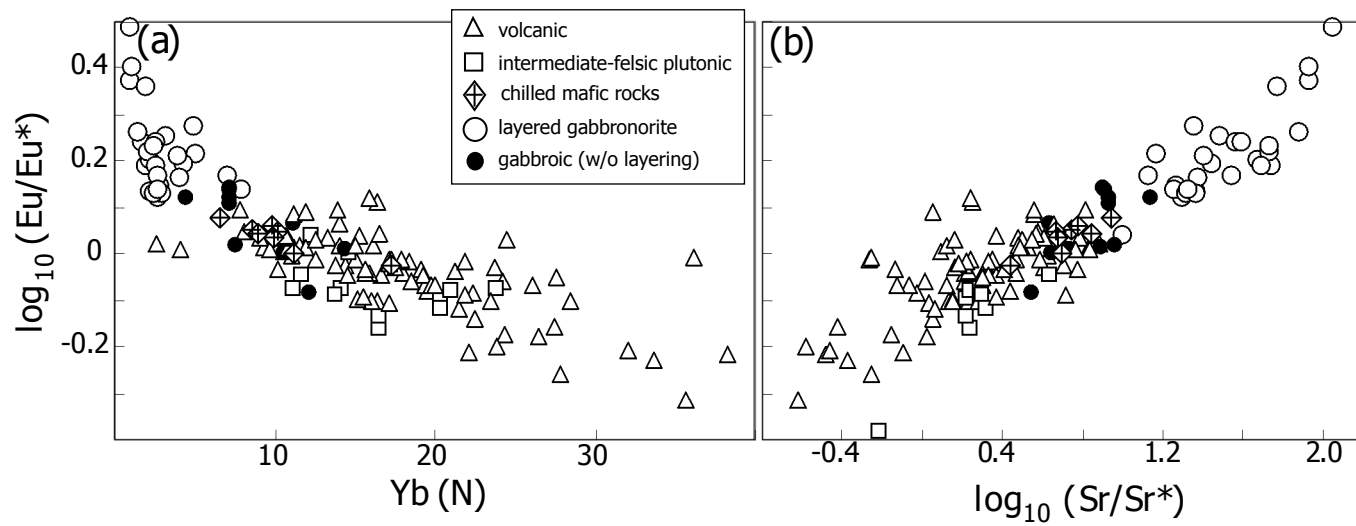












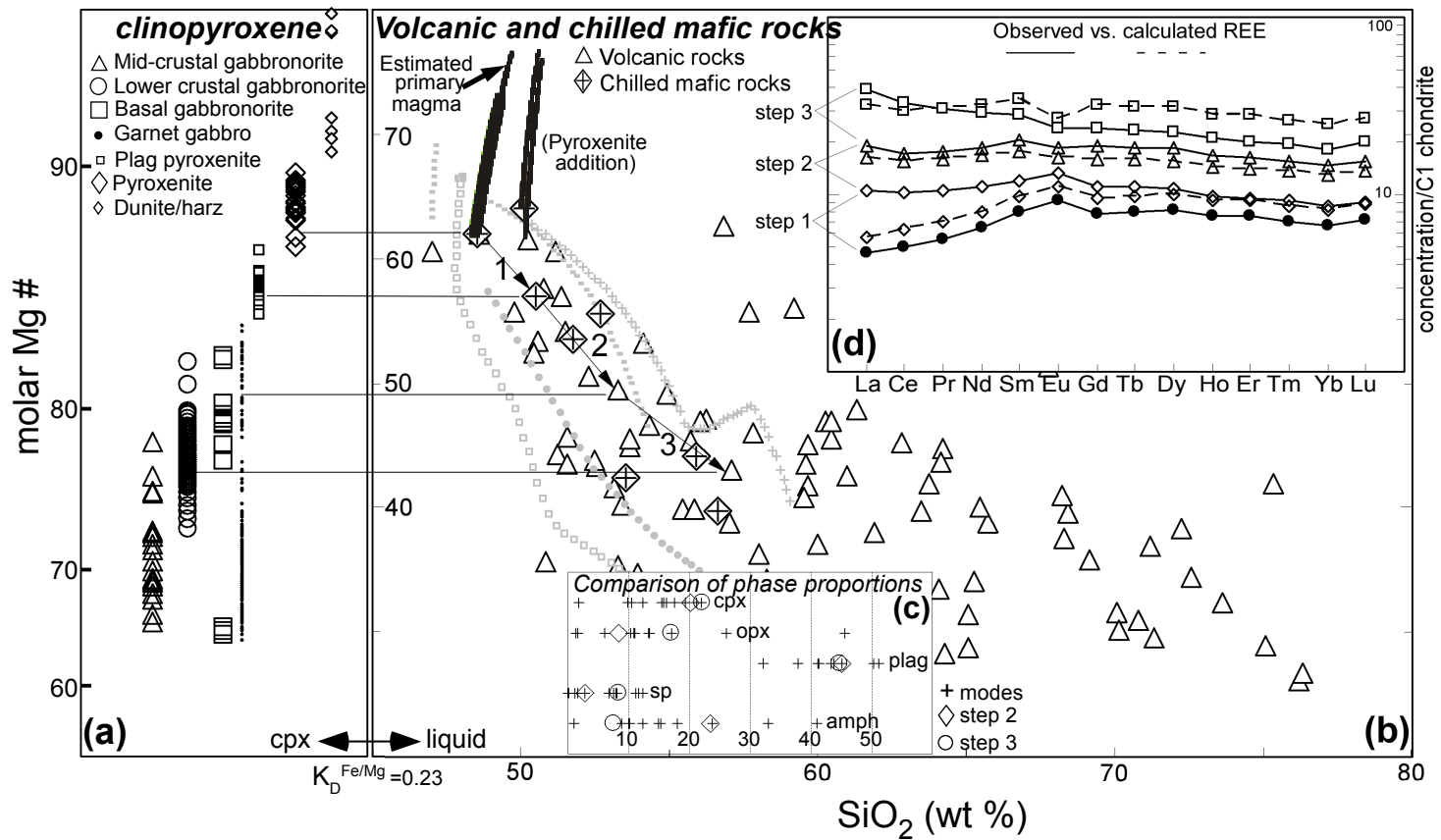


Table 1. Petrographic summary

Lithology	Petrographic characteristics	Phase proportions*
<i>Chilled mafic rocks</i>	Seriate intergranular texture. Abundant euhedral Plag phenocrysts (<3mm) and Px microphenocrysts. The groundmass is dominantly randomly-oriented, lath-shaped Plag and intergranular Px. Plag is often partially enclosed by Px in a subophitic manner. Blocky specks of Sp occupy intergranular spaces.	40-60% Plag (An 54-91) 20-30% Cpx (Mg # 66-80) 10-15% Opx (Mg # 68-81) 5-15% Fe-Ti Sp
<i>Intermediate to felsic plutonic rocks</i>	Isotropic granular texture. Subhedral to anhedral Plag, Amph, Qtz, and Bio preserve mutually-interfering grain boundaries. Quartz grains display a consertal texture. Plag is faintly zoned and granophyric textures are locally present. Oxides occur interstitially and as inclusions within Amph.	40-50% Plag 20-30% Amph 5-20% Qtz 0-5% Bio 0-5% Fe-Ti Sp
<i>Mid-crustal amphibole gabbronorites</i>	Subhedral granular texture. Subparallel network of prismatic and tabular Plag with Amph rimming and poikilitically enclosing Px, and occurring interstitially. Px and Plag display mutually-interfering relationships. Px often has undulate margins where rimmed by Amph. Plag is faintly zoned and also occurs interstitially. Oxides are Magn and Ilm pairs, and exsolution lamellae of orthopyroxene in clinopyroxene are prevalent.	50-70% Plag (An 59-85) 5-20% Cpx (Mg # 69-78) 10-15% Opx (Mg # 57-65) 10-15% Amph (Mg # 59-73) 0-2% Fe-Ti Sp
<i>Lower crustal gabbronorites</i>	Primarily layered gabbronorite. Equilibrated equigranular to unequilibrated cumulate texture (after Hunter, 1996). Locally varies from granular Plag with texturally equilibrated geometry to partly equilibrated geometry with notched grain boundaries to aligned laths and tablets of Plag with unequilibrated geometry. Penetrative fabric is defined by bands and intergrown clusters of Px, and varying proportions of Plag. Px often has undulate margins and is often rimmed or enclosed by Amph. Exsolved Px lamellae are present and zoning is absent in all phases. Oxides (usually Magn and Ilm pairs) occur interstitially, as inclusions in Px, and occasionally as symplectite intergrowths with Px. Olivine is present in one sample (1712A4). Accessory and subsolidus minerals include apatite, titanite, biotite, pyrite, chalcopyrite, and hematite. Ilmenite exsolution lamellae occur in orthopyroxene and magnetite, and amphibole, often replaces orthopyroxene lamellae in clinopyroxene.	30-80% Plag (An 75-95) 5-35% Opx (Mg # 65-78) 0-30% Cpx (Mg # 71-81) 0-10% Amph (Mg # 61-76) 0-15% Fe-Ti Sp
<i>Basal gabbronorites</i>	Granoblastic-equilibrated equigranular texture. Mosaic of highly densified granular Plag and Px with texturally equilibrated geometry. Mm-scale banding is defined by connected clusters of Px. Green, Mg-Al spinel occurs interstitially within the Px clusters and as bleb-like intergrowths with Px. Amph occurs locally. One sample, a hornblende granulite (1710A4d), contains Fe-Ti spinel.	30-60% Plag (An 77-92) 5-20% Cpx (Mg # 64-79) 0-30% Opx (Mg # 58-75) 10-50% Amph (Mg # 53-73) 0-10% Mg-Al Sp

Mineral abbreviations: Plag- plagioclase; Cpx- clinopyroxene; Opx- orthopyroxene; Amph- amphibole; Fe-Ti Sp- Fe-Ti spinel;

Px- pyroxene; Mg-Al Sp- Mg-Al spinel; Bio- biotite; Qtz- quartz; Magn- magnetite; Ilm- ilmenite; Sp-spinel

*Phase proportions are expressed in volume %, based on visual estimates.

Table 2. Average electron microprobe analyses

Clinopyroxene	N ^a	SiO ₂	TiO ₂	Al ₂ O ₃	Cr ₂ O ₃	FeO	MnO	MgO	CaO	Na ₂ O	Total	En	Fs	Wo	Mg #
<i>Plagioclase pyroxenite</i>															
1709P11	16	51.81	0.08	5.36	0.02	4.55	0.05	15.17	23.52	0.43	100.99	43.80	13.11	48.83	85.59
<i>Basal gabbronorites</i>															
1710A4b	4	49.22	0.18	6.87	0.14	6.26	0.17	13.54	22.36	0.51	99.24	40.87	10.61	48.52	79.39
1710A4d	3	50.28	0.12	6.01	0.05	6.82	0.17	13.75	21.99	0.54	99.74	41.17	11.47	47.35	78.21
1710A4e	3	49.04	0.54	5.77	0.00	11.25	0.39	11.80	19.82	0.63	99.24	36.47	19.51	44.02	65.15
<i>Lower crustal gabbronorites</i>															
0718A4	6	52.04	0.30	2.28	0.00	6.87	0.28	14.83	22.69	0.17	99.46	42.37	11.02	46.61	79.37
1712A3a	3	51.62	0.35	2.54	0.03	7.94	0.27	15.56	21.13	0.21	99.64	44.20	12.65	43.14	77.75
1712A3b	12	52.62	0.31	2.13	0.02	7.55	0.24	14.95	22.69	0.26	100.77	42.13	11.93	45.94	77.95
1712A4	4	52.56	0.31	2.50	0.03	7.92	0.21	14.75	22.42	0.31	101.00	41.77	12.58	45.65	76.86
1712A7	4	53.04	0.28	1.66	0.03	8.67	0.31	14.24	22.65	0.32	101.21	40.24	13.75	46.00	74.55
1722A2	4	51.93	0.24	1.91	0.00	7.81	0.28	14.20	22.42	0.35	99.16	40.92	12.63	46.45	76.42
1722A4b	6	51.26	0.41	3.02	0.02	7.68	0.23	13.89	22.69	0.41	99.60	40.25	12.49	47.26	76.32
1722A4c	4	51.31	0.36	2.48	0.02	7.67	0.23	14.02	22.45	0.36	98.89	40.69	12.49	46.82	76.52
1722A5a	4	52.37	0.36	2.27	0.05	7.31	0.19	14.01	22.63	0.41	99.60	40.75	11.93	47.32	77.35
1722A7	8	52.86	0.41	2.32	0.13	7.03	0.20	14.38	22.69	0.42	100.44	41.51	11.39	47.10	78.48
1722A11	4	52.47	0.32	2.52	0.00	7.75	0.23	13.97	22.67	0.38	100.32	40.36	12.57	47.08	76.25
1722A16	6	51.79	0.24	2.16	0.04	7.87	0.20	14.31	22.15	0.43	99.19	41.30	12.74	45.96	76.43
<i>Mid-crustal amphibole gabbronorites</i>															
1709A2	2	52.08	0.37	2.01	0.09	10.17	0.29	13.27	21.91	0.35	100.53	38.20	16.44	45.36	69.92
1723A5	6	51.51	0.47	2.41	0.06	8.74	0.25	13.48	22.49	0.34	99.75	39.01	14.20	46.79	73.33
1721A1	4	52.13	0.19	1.75	0.00	7.86	0.27	14.24	22.64	0.37	99.45	40.76	12.63	46.60	76.35
<i>Mafic dikes</i>															
1728A2	6	51.55	0.46	3.04	0.11	8.55	0.22	15.85	20.36	0.21	100.35	44.88	13.61	41.51	76.72
1728A3	4	50.72	0.46	4.11	0.37	7.58	0.13	15.50	20.77	0.17	99.81	44.64	12.26	43.09	78.43

Table 2. continued

Orthopyroxene	N ^a	SiO ₂	TiO ₂	Al ₂ O ₃	Cr ₂ O ₃	FeO	MnO	MgO	CaO	Na ₂ O	Total	En	Fs	Wo	Mg #
<i>Plagioclase pyroxenite</i>															
1709P11	14	54.04	0.00	4.52	0.10	12.26	0.15	28.93	0.69	0.02	100.71	79.68	92.20	1.37	80.79
<i>Basal gabbronorites</i>															
1710A4b	4	50.15	0.03	5.48	0.05	15.72	0.29	25.78	0.70	0.03	98.24	73.44	25.13	1.43	74.51
1710A4d	3	50.79	0.02	5.47	0.02	16.69	0.34	25.13	0.65	0.00	99.12	71.88	26.79	1.33	72.85
1710A4e	3	49.79	0.10	3.33	0.00	24.79	0.74	20.25	0.59	0.00	99.59	58.55	40.22	1.22	59.29
<i>Lower crustal gabbronorites</i>															
0718A4	6	52.52	0.15	1.76	0.00	18.05	0.59	25.06	0.83	0.00	98.94	70.04	28.30	1.66	71.22
1712A3a	3	52.00	0.16	1.38	0.01	17.24	0.50	26.49	1.05	0.01	98.83	71.76	26.21	2.03	73.25
1712A3b	4	53.89	0.15	1.23	0.00	19.21	0.56	24.84	0.89	0.01	100.78	68.50	29.73	1.77	69.74
1712A4	4	55.40	0.11	1.36	0.00	16.73	0.49	27.03	0.63	0.02	101.75	73.31	25.46	1.23	74.23
1722A2	6	51.52	0.09	1.26	0.00	21.54	0.65	23.30	0.61	0.01	98.98	65.03	33.75	1.22	65.84
1722A4b	4	51.86	0.10	1.48	0.00	20.10	0.49	24.75	0.59	0.01	99.39	67.89	30.94	1.17	68.70
1722A5a	2	53.70	0.12	1.30	0.03	20.40	0.46	23.49	0.57	0.00	100.08	66.46	32.38	1.16	67.24
1722A7	10	54.14	0.14	1.53	0.08	18.25	0.42	24.69	1.01	0.01	100.27	69.25	28.71	2.04	70.69
1722A11	2	53.79	0.07	1.22	0.00	20.07	0.53	23.91	0.50	0.00	100.08	67.29	31.70	1.01	67.98
1722A16	2	52.34	0.08	1.49	0.05	20.72	0.54	23.33	0.54	0.05	99.13	66.01	32.89	1.09	66.75
<i>Mid-crustal amphibole gabbronorites</i>															
1709A2	4	51.13	0.14	0.96	0.03	25.26	0.63	19.80	0.80	0.00	98.76	57.31	41.03	1.66	58.28
1723A5	5	50.60	0.20	1.17	0.04	24.34	0.61	21.10	0.78	0.01	98.84	59.72	38.70	1.58	60.69
1721A1	4	51.88	0.10	1.06	0.00	21.62	0.63	23.20	0.65	0.01	99.14	64.81	33.89	1.30	65.66

Table 2. continued

Plagioclase	N ^a	SiO ₂	Al ₂ O ₃	FeO	MgO	CaO	Na ₂ O	K ₂ O	Total	An
<i>Plagioclase pyroxenite</i>										
1709P11	13	46	36.36	0.10	0.01	18.94	0.83	0.02	101.91	92.53
<i>Basal gabbronorites</i>										
1710A4b	6	44.69	35.52	0.12	0.03	18.71	1.01	0.01	100.08	91.03
1710A4d	6	47.68	33.75	0.15	0.02	16.37	2.29	0.02	100.28	79.69
1710A4e	6	45.99	35.22	0.12	0.02	17.96	1.37	0.01	100.68	87.88
<i>Lower crustal gabbronorites</i>										
0718A4	6	44.66	35.73	0.31	0.01	18.84	0.82	0.01	100.38	92.63
1712A3a	6	44.81	35.11	0.33	0.02	18.41	1.08	0.02	99.78	90.27
1712A3b	7	45.44	35.10	0.38	0.02	18.20	1.22	0.01	100.38	89.15
1712A4	8	45.93	35.58	0.34	0.01	18.34	1.18	0.01	101.39	89.53
1712A7	4	47.55	34.41	0.38	0.01	17.09	2.03	0.01	101.47	82.27
1722A2	6	46.39	34.34	0.24	0.01	17.30	1.82	0.01	100.11	83.97
1722A4b	6	45.48	34.08	0.28	0.01	17.39	1.61	0.01	98.86	85.59
1722A4c	4	45.98	34.34	0.18	0.01	17.47	1.71	0.05	99.74	84.74
1722A5a	6	47.47	34.10	0.25	0.01	16.61	2.09	0.02	100.55	81.36
1722A7	6	47.44	34.62	0.16	0.02	16.90	1.97	0.01	101.11	82.56
1722A11	4	48.52	32.49	0.20	0.01	15.70	1.94	0.04	98.90	81.22
1722A16	2	47.93	33.40	0.33	0.00	15.96	2.33	0.02	99.97	79.00
<i>Mid-crustal amphibole gabbronorites</i>										
1721A1	6	47.04	34.97	0.26	0.00	17.39	1.72	0.02	101.39	84.75
1709A2	6	52.78	30.75	0.41	0.02	12.99	4.36	0.25	101.56	61.36
1723A5	4	51.94	30.46	0.22	0.00	12.96	4.06	0.17	99.82	63.18
<i>Mafic dikes</i>										
1728A2	6	47.01	33.60	0.67	0.08	16.82	1.79	0.03	100.00	83.72
1728A3	4	47.68	33.28	0.67	0.14	16.32	1.88	0.24	100.21	81.55
1728A4	6	50.72	31.11	0.63	0.08	13.93	3.39	0.06	99.92	69.39

Table 2. continued

Spinel	N ^a	SiO ₂	TiO ₂	Al ₂ O ₃	Cr ₂ O ₃	FeO	MnO	MgO	CaO	NiO	Total	FeO	Fe ₂ O ₃	total
<i>Plagioclase pyroxenite</i>														
1709P11	12	0.09	0.03	64.26	1.56	17.54	0.06	16.40	0.02	0.08	100.04			
<i>Basal gabbroonorites</i>														
1710A4b	6	0.01	0.02	60.50	1.08	24.76	0.15	12.74	0.03	0.08	99.36	21.73	3.37	99.70
1710A4e	6	0.43	0.03	59.85	0.37	26.15	0.17	12.72	0.05	0.08	99.84	22.33	4.25	100.26
<i>Lower crustal gabbroonorites</i>														
0718A4	5	0.01	4.11	2.07	0.15	87.08	0.20	0.48	0.07	0.00	94.18	34.23	58.73	100.06
1712A3a	6	0.01	4.50	1.88	0.33	86.02	0.25	0.81	0.07	0.01	93.88	33.87	57.96	99.68
1712A3b	7	0.03	6.27	2.37	0.15	83.85	0.27	0.96	0.12	0.01	94.03	35.26	54.00	99.44
1712A4	8	0.05	5.21	1.91	0.12	85.98	0.24	0.58	0.05	0.01	94.16	35.01	56.65	99.83
1712A7	4	0.02	1.88	1.29	0.09	90.95	0.15	0.18	0.07	0.02	94.64	32.84	64.57	101.11
1722A2	6	0.03	2.35	1.45	0.12	88.24	0.13	0.39	0.04	0.00	92.76	32.42	62.03	98.97
1722A4b	6	0.03	1.43	1.54	0.43	87.68	0.02	0.10	0.04	0.00	91.27	31.68	62.23	97.50
1722A4c	4	0.04	1.19	1.09	1.25	88.03	0.04	0.18	0.07	0.00	91.89	31.43	62.90	98.19
1722A5a	3	0.12	2.08	1.05	2.00	86.04	0.33	0.25	0.11	0.00	91.98	31.90	60.16	98.00
1722A7	4	0.26	1.36	2.55	7.48	81.30	0.19	0.56	0.09	0.00	93.79	31.82	54.98	99.29
1722A11	4	0.03	24.06	0.80	0.12	69.12	0.59	0.76	0.05	0.00	95.53	40.81	62.92	98.68
1722A16	4	0.12	1.32	1.43	1.44	86.50	0.13	0.31	0.02	0.00	91.26	31.26	61.39	97.41
<i>Mid-crustal amphibole gabbroonorites</i>														
1709A2	6	0.10	1.56	1.15	1.39	89.25	0.18	0.19	0.07	0.15	94.05	32.28	63.31	100.39
1723A5	4	0.03	22.89	0.58	0.20	69.35	1.30	0.03	0.05	0.00	94.43	40.15	64.89	97.68
1721A1	6	0.34	16.49	2.24	0.09	75.39	0.66	0.74	0.11	0.00	96.05	38.01	62.31	100.21
<i>Mafic dikes</i>														
1728A2	4	0.17	0.21	0.11	0.08	91.41	0.03	0.02	0.19	0.00	92.21	30.84	67.30	98.95
1728A3	4	0.31	0.26	0.12	0.05	89.51	0.04	0.04	0.25	0.00	90.58	30.45	65.62	97.15
1728A4	6	0.23	0.03	0.12	0.22	89.92	0.02	0.01	0.13	0.00	90.69	30.37	66.18	97.32

Table 2. continued

Amphibole	N^a	SiO₂	TiO₂	Al₂O₃	Cr₂O₃	FeO	MnO	MgO	CaO	Na₂O	K₂O	Total	Mg #
<i>Plagioclase pyroxenite</i>													
1709P11	7	42.47	0.24	18.30	0.08	6.55	0.04	15.50	12.26	2.49	0.15	98.08	80.86
<i>Basal gabbronorites</i>													
1710A4b	6	42.33	0.53	15.79	0.13	9.73	0.12	14.39	11.63	2.76	0.11	97.51	72.51
1710A4d	6	40.85	2.55	14.61	0.07	15.46	0.26	10.57	10.91	2.77	0.23	98.25	54.93
1710A4e	6	41.64	0.42	16.17	0.06	10.34	0.12	14.04	11.58	3.03	0.05	97.45	70.78
<i>Lower crustal gabbronorites</i>													
0718A4	6	47.97	1.11	9.36	0.04	9.98	0.19	15.95	12.30	1.19	0.04	98.12	74.01
1712A3a	6	45.63	1.22	11.18	0.04	10.25	0.16	15.69	11.89	2.01	0.06	98.12	73.18
1712A3b	6	47.80	1.41	8.40	0.06	10.59	0.17	16.23	12.12	1.48	0.09	98.32	73.21
1712A4	6	45.18	1.48	12.14	0.04	10.33	0.14	15.42	12.00	2.32	0.10	99.15	72.67
1712A7	4	49.63	0.84	7.06	0.02	12.64	0.24	15.55	11.32	0.84	0.05	98.20	68.76
1722A2	6	46.40	1.53	9.19	0.05	11.91	0.21	14.92	11.85	1.46	0.21	97.74	69.06
1722A4b	6	45.14	1.69	10.52	0.09	12.15	0.17	13.90	11.85	1.79	0.14	97.44	67.09
1722A4c	6	46.73	1.36	9.17	0.14	11.47	0.18	14.57	11.96	1.25	0.15	96.98	69.33
1722A5a	4	50.02	0.93	5.32	0.13	16.61	0.34	18.42	6.12	0.77	0.06	98.72	66.62
1722A7	8	46.43	1.84	9.46	0.48	9.72	0.19	13.85	14.34	1.69	0.25	98.25	71.87
1722A11	2	44.36	1.92	10.78	0.09	12.01	0.19	13.63	11.59	1.92	0.20	96.68	66.91
1722A16	4	44.72	1.88	10.16	0.06	11.77	0.16	13.90	11.26	1.70	0.20	95.81	67.81
<i>Mid-crustal amphibole gabbronorites</i>													
1709A2	6	45.68	1.57	9.02	0.09	15.21	0.16	12.89	11.76	1.21	0.81	98.41	60.16
1723A5	4	48.64	0.87	5.74	0.01	13.01	0.21	13.83	14.43	0.65	0.44	97.83	65.66
1721A1	6	47.96	1.39	8.88	0.03	12.26	0.16	14.52	11.79	1.33	0.17	98.48	67.86
<i>Mafic dikes</i>													
1728A4	6	51.58	0.66	4.03	0.02	12.57	0.65	15.32	10.81	0.39	0.14	96.18	68.41
Olivine	N^a	SiO₂	TiO₂	Al₂O₃	Cr₂O₃	FeO	MnO	MgO	CaO	NiO	Total	Mg #	
<i>Plagioclase pyroxenite</i>													
1709P11	6	39.13	0.00	0.00	0.03	17.94	0.24	43.08	0.01	0.13	100.55	81.06	
<i>Lower crustal gabbronorites</i>													
1712A4	8	37.97	0.02	0.00	0.01	25.89	0.55	36.08	0.03	0.01	100.54	71.29	

Ferric iron in spinels is calculated assuming perfect stoichiometry.

Full data set can be found online at <http://www.petrology.oupjournals.org> (Electronic Appendix I) .

^a Number of analyses used for the average.

Table 3A. Average clinopyroxene REE concentrations from ion microprobe analyses

Sample	N†	La	Ce	(Pr)	Nd	Sm	Eu	(Gd)	(Tb)	Dy	(Ho)	Er	(Tm)	Yb	(Lu)
<i>Basal gabbronorites</i>															
1710A4E	8	1.99	2.92	3.24	3.56	5.00	7.04	4.47	4.21	3.95	3.83	3.71	3.52	3.33	3.14
1710A4L	5	3.78	7.42	11.53	15.65	22.90	21.12	21.25	20.43	19.61	17.90	16.18	15.34	14.51	13.67
1710A4E	6	0.84	1.25	1.64	2.04	3.61	6.00	3.12	2.88	2.64	2.61	2.58	2.46	2.34	2.23
<i>Lower crustal gabbronorites</i>															
0718A4	3	0.40	0.80	1.64	2.48	6.25	6.19	7.04	7.43	7.82	7.63	7.44	7.12	6.80	6.48
1712A3f	3	0.46	0.96	1.68	2.41	5.64	6.13	6.26	6.57	6.88	6.77	6.66	6.05	5.44	4.83
1712A3E	3	0.52	1.13	1.95	2.77	5.46	5.47	6.28	6.69	7.10	6.83	6.56	6.26	5.96	5.66
1712A4	3	0.77	1.61	2.64	3.67	8.00	8.59	9.14	9.70	10.27	9.67	9.07	8.52	7.98	7.43
1712A7	4	1.79	4.06	7.37	10.68	21.47	16.41	23.59	24.65	25.70	24.58	23.45	22.10	20.76	19.41
1712A1E	3	0.95	1.80	3.03	4.26	8.19	8.06	8.80	9.11	9.41	8.71	8.01	7.97	7.93	7.89
1722A2	6	0.78	1.73	2.91	4.09	7.54	7.10	7.98	8.20	8.42	8.14	7.87	7.51	7.15	6.80
1722A4E	3	0.68	1.60	2.61	3.63	6.62	5.50	6.79	6.88	6.97	6.63	6.29	6.02	5.76	5.50
1722A4C	3	0.53	1.28	2.27	3.25	6.20	5.34	6.07	6.00	5.94	5.46	4.98	4.98	4.97	4.96
1722A5f	2	0.63	1.53	2.58	3.63	6.70	6.16	7.38	7.71	8.05	7.74	7.43	7.08	6.72	6.36
1722A7	4	4.65	9.32	13.72	18.12	30.54	20.21	30.78	30.91	31.03	28.81	26.59	25.84	25.09	24.34
1722A11	4	1.81	3.97	6.08	8.18	13.71	11.60	13.51	13.41	13.31	12.45	11.58	11.33	11.08	10.83
1722A1E	3	1.92	4.24	6.74	9.24	15.36	12.20	15.30	15.26	15.23	14.42	13.62	13.36	13.10	12.85
<i>Mid-crustal amphibole gabbronorites</i>															
1709A2	5	6.26	10.87	12.69	14.51	23.43	12.29	22.34	21.80	21.25	20.47	19.68	18.98	18.27	17.57
1723A5	4	4.45	9.29	12.38	15.47	23.71	10.23	22.37	21.70	21.03	20.19	19.35	18.64	17.94	17.23
1721A1	3	0.82	1.69	2.57	3.44	6.22	5.61	6.29	6.32	6.36	5.98	5.60	5.49	5.37	5.26
<i>Mafic dikes (phenocrysts)</i>															
1728A2	7	1.14	2.08	3.08	4.08	7.02	8.54	7.26	7.38	7.50	6.87	6.23	5.93	5.63	5.33
1728A4	7	0.23	0.42	0.62	0.81	1.53	1.78	1.59	1.62	1.65	1.74	1.83	2.23	2.63	3.03
Anders and Grevesse (1989)		0.235	0.603		0.452	0.147	0.056			0.243		0.159		0.163	

Results for the REE are presented as concentration/chondrite, using the chondrite values of Anders and Grevesse (1989).

† Number of analyses used for the average.

Values are interpolated for elements with parentheses in the column headings.

Full data set can be found online at <http://www.petrology.oupjournals.org> (Electronic Appendix II) .

Table 3B. Average clinopyroxene trace element concentrations from ion microprobe analyses

Sample	N [†]	Ti	V	Cr	Sr	Y	Zr
<i>Basal gabbronorites</i>							
1710A4B	3	753	115	413	20	5	8
1710A4D	5	2316	307	64	21	19	13
1710A4E	4	517	134	397	26	3	3
<i>Lower crustal gabbronorites</i>							
0718A4	3	1926	281	90	17	11	3
1712A3A	4	2060	381	321	20	12	8
1712A3B	4	2457	438	146	27	17	8
1712A4	4	1845	355	108	17	12	5
1712A7	3	4391	581	217	63	102	37
1712A18	4	2055	360	472	20	13	6
1722A2	5	1111	315	67	19	13	11
1722A4B	3	1564	309	118	14	7	6
1722A4C	3	1616	293	208	14	9	6
1722A5A	4	1339	350	428	14	11	6
1722A7	4	1666	142	795	17	35	34
1722A11	4	1925	359	87	19	20	11
1722A16	4	1263	359	225	15	19	10
<i>Mid-crustal amphibole gabbronorites</i>							
1709A2	6	2592	583	594	18	42	38
1723A5	4	2762	544	423	17	39	29
1721A1	4	1047	323	60	20	11	9
<i>Mafic dikes (phenocrysts)</i>							
1728A2	4	2351	367	1689	23	10	6
1728A4	4	978	538	256	6	4	25

Values are in parts per million.

[†]Number of analyses used for the average.

Full data set can be found online at
<http://www.petrology.oupjournals.org> (Electronic Appendix II) .

Table 3C. Average plagioclase REE concentrations from ion microprobe analyses

Sample	N†	La	Ce	(Pr)	Nd	Sm	Eu	(Gd)	(Tb)	Dy	(Ho)	(Er)	(Tm)	Yb	(Lu)
<i>Basal gabbronorites</i>															
1710A4B	2	1.83	0.90	0.63	0.36	0.49	3.89	0.34	0.27	0.19	0.18	0.17	0.15	0.14	0.13
1710A4D	2	2.93	2.15	1.68	1.20	0.83	6.46	0.52	0.36	0.21	0.20	0.20	0.20	0.20	0.20
1710A4E	2	0.51	0.24	0.23	0.22	1.03	3.89	0.59	0.37	0.15	0.26	0.36	0.46	0.57	0.67
<i>Lower crustal gabbronorites</i>															
0718A4	3	0.25	0.24	0.25	0.27	0.64	2.45	0.24	0.22	0.20	0.21	0.22	0.22	0.23	0.24
1712A3A	1	0.38	0.33	0.38	0.43	1.04	2.63	0.31	0.20	0.14	0.19	0.23	0.28	0.33	0.37
1712A3B	1	0.35	0.28	0.24	0.20	0.49	2.17	0.30	0.21	0.12	0.11	0.10	0.09	0.07	0.06
1712A4	2	0.48	0.38	0.33	0.27	0.84	3.00	0.21	0.15	0.12	0.13	0.14	0.15	0.16	0.17
1712A18	2	0.55	0.39	0.36	0.32	0.43	1.94	0.27	0.18	0.10	0.11	0.12	0.12	0.13	0.14
1722A2	1	1.68	1.16	0.94	0.71	0.43	8.09	0.29	0.22	0.14	0.35	0.56	0.77	0.98	1.19
1722A4B	1	0.88	0.74	0.64	0.54	0.38	3.29	0.24	0.17	0.10	0.10	0.09	0.08	0.08	0.07
1722A4C	1	0.80	0.60	0.49	0.38	0.48	3.23	0.32	0.23	0.15	0.15	0.14	0.13	0.12	0.11
1722A11	2	2.24	1.61	1.28	0.95	0.77	6.01	0.45	0.29	0.13	0.12	0.10	0.08	0.06	0.05
<i>Mid-crustal amphibole gabbronorites</i>															
1709A2	3	3.89	3.01	2.21	1.40	1.34	14.31	0.80	0.52	0.25	0.25	0.25	0.25	0.25	0.25
1723A5	2	2.34	1.85	1.60	1.36	1.61	11.01	0.95	0.55	0.35	0.37	0.40	0.42	0.45	0.47
1721A1	1	1.22	0.78	0.65	0.52	0.81	4.06	0.53	0.39	0.25	0.27	0.28	0.30	0.31	0.33
Anders and Grevesse (1989)		0.235	0.603		0.452	0.147	0.056			0.243				0.163	

Results for the REE are presented as concentration/chondrite, using the chondrite values of Anders and Grevesse (1989).

† Number of analyses used for the average.

Values are interpolated for elements with parentheses in the column headings.

Full data set can be found online at <http://www.petrology.oupjournals.org> (Electronic Appendix II) .

Table 4. Whole-rock analyses

Lithology	Gbn	Gbn	Gbn	Gbn	Gbn	Gbn	Gbn	Gbn	Gbn	Gbn	Gbn
Sample	0717A1	0717A2B	0717A5B	0717A5C	0717A6	0718A4	0720A2	1709A1	1709A2	1710A4A	1710A4B
UTM EW	495301	495286	495274	495274	495239	521991	469553	588932	588877	610997	610997
UTM NS	6844483	6844567	6844316	6844316	6844226	6851315	6843212	6847832	6847320	6835362	6835362
<i>Unnormalized Results (Weight %):</i>											
SiO ₂	48.25	47.44	49.15	48.85	49.57	44.33	52.64	52.06	52.61	45.24	46.26
TiO ₂	0.457	0.820	0.594	0.552	0.561	0.681	0.625	0.532	0.402	0.045	0.122
Al ₂ O ₃	18.01	18.03	16.08	21.69	14.89	18.12	19.02	18.26	18.11	27.12	21.83
FeO*	7.58	9.95	9.38	8.86	8.49	12.76	7.34	8.41	8.24	4.43	6.04
MnO	0.166	0.229	0.255	0.144	0.183	0.197	0.146	0.167	0.174	0.073	0.120
MgO	8.51	7.35	9.11	3.99	10.85	8.57	5.30	6.47	6.92	7.00	10.03
CaO	14.92	12.28	11.29	10.80	12.63	14.98	8.90	10.97	11.00	15.38	14.78
Na ₂ O	1.12	2.35	2.28	3.34	1.58	0.65	4.01	2.28	2.27	0.87	0.88
K ₂ O	0.04	0.17	0.15	0.26	0.12	0.01	1.21	0.27	0.23	0.03	0.03
P ₂ O ₅	0.036	0.095	0.061	0.170	0.034	0.008	0.118	0.031	0.041	0.008	0.011
Total	99.08	98.72	98.35	98.66	98.90	100.31	99.31	99.45	100.00	100.20	100.11
Mg #	66.7	56.8	63.4	44.5	69.5	54.5	56.3	57.8	60.0	73.8	74.7
<i>XRF-Trace Elements (ppm):</i>											
Ni	42	23	79	0	83	13	28	40	44	53	106
Cr	219	127	404	15	514	88	130	139	157	88	410
Sc	47	†70	46	22	49	67	38	37	35	3	23
V	204	242	241	192	218	456	178	254	206	25	71
Rb	2	2	2	3	2	0	25	3	2	0	1
Sr	305	331	278	432	220	205	321	282	260	383	290
Zr	15	25	14	17	19	10	50	25	24	8	10
Y	13	25	13	18	18	4	16	12	11	1	3
Ga	13	17	15	20	16	13	17	16	15	15	12
Cu	57	90	†299	†233	113	180	50	29	30	37	166
Zn	46	91	84	66	67	54	61	65	67	24	35
Th	2	0	1	1	4	0	1	2	0	1	1
<i>ICP-MS (ppm):</i>											
La	1.02	2.08	1.35	2.23	1.44	0.26	3.92	2.03	1.82	0.34	0.35
Ce	3.07	6.00	3.50	5.65	5.23	0.37	9.46	4.51	4.18	0.69	0.87
Pr	0.55	1.07	0.58	0.95	1.01	0.06	1.34	0.65	0.61	0.09	0.14
Nd	3.34	6.42	3.27	5.54	6.05	0.42	6.52	3.31	3.16	0.42	0.83
Sm	1.37	2.75	1.26	1.98	2.22	0.23	2.10	1.15	1.14	0.14	0.35
Eu	0.54	1.07	0.61	0.75	0.65	0.16	0.75	0.59	0.58	0.16	0.23
Gd	1.77	3.67	1.66	2.48	2.63	0.42	2.50	1.46	1.46	0.16	0.47
Tb	0.33	0.69	0.30	0.46	0.48	0.09	0.45	0.29	0.29	0.03	0.09
Dy	2.17	4.60	2.05	3.03	3.21	0.59	2.95	1.91	1.88	0.15	0.58
Ho	0.48	0.97	0.45	0.66	0.71	0.14	0.63	0.42	0.42	0.03	0.12
Er	1.31	2.67	1.27	1.88	2.03	0.37	1.78	1.20	1.18	0.09	0.33
Tm	0.19	0.37	0.18	0.28	0.30	0.05	0.27	0.18	0.18	0.01	0.05
Yb	1.23	2.33	1.18	1.77	1.97	0.32	1.73	1.18	1.16	0.08	0.28
Lu	0.19	0.37	0.19	0.29	0.33	0.05	0.29	0.19	0.19	0.01	0.05
Ba	20	90	60	145	38	4	525	112	99	16	18
Th	0.01	0.06	0.01	0.02	0.01	0.04	0.55	0.28	0.22	0.04	0.04
Nb	0.29	0.68	0.30	0.39	0.57	0.04	1.12	0.61	0.48	0.05	0.09
Y	12.22	25.05	11.55	17.70	19.00	3.15	16.86	11.10	11.17	0.86	3.09
Hf	0.37	0.83	0.37	0.37	0.66	0.06	1.46	0.65	0.66	0.05	0.12
Ta	0.01	0.03	0.02	0.02	0.02	0.00	0.07	0.06	0.03	0.03	0.02
U	0.01	0.04	0.02	0.03	0.02	0.01	0.31	0.11	0.10	0.01	0.01
Pb	1.52	1.75	1.64	1.94	1.39	0.05	2.95	1.18	0.99	0.25	0.38
Rb	0.3	2.3	2.0	2.9	1.3	0.3	22.1	3.2	2.4	0.2	0.4
Cs	0.32	1.06	0.88	1.11	0.84	0.03	2.18	0.06	0.08	0.07	0.06
Sr	295	333	276	419	203	211	308	276	268	382	298
Sc	45.7	66.9	44.5	22.7	57.2	76.6	34.3	40.3	42.4	8.5	32.0
Zr	8	18	9	8	14	1	42	20	21	1	3

Abbreviations are: Gbn-gabbro-norite, Ch mafic- chilled mafic, I/F plut- intermediate/felsic plutonic, Bas-and-basaltic andesite

For chilled mafic rocks: 1710 samples are chilled pillows, 1728 samples are mafic dikes.

Analyses were performed at the Washington State Univ. GeoAnalytical Laboratory. Total Fe expressed as FeO.

† denotes >120% of the highest standard.

DeBari and Sleep (1991) bulk crust is bulk arc without ultramafic unit, from their Table 1.

Sample locations are given using the Universal Transverse Mercator (UTM) coordinate system; East-West (EW) and North-South (NS)

Table 4. continued

Lithology	Gbn	Gbn	Gbn	Gbn	Gbn	Gbn	Gbn	Gbn	Gbn	Gbn	Gbn
Sample	1710A4D	1710A4E	1712A3A	1712A3B	1712A4	1712A7	1712A18	1721A1	1722A2	1722A4B	1722A4C
UTM EW	610997	610997	518764	518764	518808	518911	519226	471072	510224	510654	510654
UTM NS	6835362	6835362	6853618	6853618	6853291	6852088	6849305	6854357	6849467	6849197	6849197
<i>Unnormalized Results (Weight %):</i>											
SiO ₂	41.02	45.73	43.88	42.77	43.08	43.06	48.26	45.31	45.15	45.27	47.07
TiO ₂	1.944	0.091	0.600	0.934	0.910	1.173	0.217	0.819	1.069	0.326	0.146
Al ₂ O ₃	18.10	21.38	19.82	17.20	17.44	17.54	19.20	20.35	17.21	27.21	28.07
FeO*	15.79	7.22	11.94	15.81	15.42	17.00	6.82	11.27	13.27	5.27	3.52
MnO	0.212	0.133	0.160	0.198	0.191	0.260	0.173	0.187	0.222	0.066	0.065
MgO	7.55	10.73	7.67	8.12	8.41	7.06	9.26	7.22	8.17	3.33	3.37
CaO	12.46	13.61	15.09	14.06	14.06	12.59	15.53	13.03	13.11	16.75	16.97
Na ₂ O	2.23	1.04	0.87	0.71	0.75	1.17	0.86	1.16	1.00	1.36	1.44
K ₂ O	0.15	0.01	0.02	0.02	0.01	0.02	0.01	0.02	0.04	0.02	0.02
P ₂ O ₅	0.222	0.006	0.005	0.007	0.006	0.008	0.006	0.011	0.010	0.007	0.006
Total	99.68	99.95	100.06	99.83	100.28	99.88	100.33	99.38	99.25	99.61	100.68
Mg #	46.0	72.6	53.4	47.8	49.3	42.5	70.8	53.3	52.3	53.0	63.1
<i>XRF-Trace Elements (ppm):</i>											
Ni	19	70	27	21	18	5	37	4	5	15	13
Cr	24	166	140	88	77	30	114	36	47	65	97
Sc	67	19	58	64	62	62	57	40	†56	18	14
V	520	63	496	795	848	574	152	†499	†647	263	106
Rb	0	0	0	1	0	0	1	0	0	1	0
Sr	284	315	233	207	197	270	267	347	271	423	430
Zr	16	9	8	9	10	12	9	10	11	8	8
Y	30	3	4	4	4	7	5	3	4	3	2
Ga	22	16	16	13	17	21	12	19	15	17	18
Cu	496	7	832	534	570	201	50	23	83	24	5
Zn	87	42	48	64	63	115	38	71	82	24	17
Th	1	0	1	1	0	0	0	1	3	2	0
<i>ICP-MS (ppm):</i>											
La	1.54	0.17	0.25	0.24	0.25	0.47	0.27	0.22	0.24	0.21	0.31
Ce	5.38	0.39	0.29	0.41	0.30	0.92	0.46	0.61	0.73	0.55	0.46
Pr	1.10	0.07	0.05	0.07	0.06	0.17	0.08	0.10	0.12	0.09	0.07
Nd	7.68	0.41	0.35	0.48	0.44	1.08	0.60	0.62	0.77	0.51	0.41
Sm	3.35	0.20	0.19	0.29	0.24	0.57	0.33	0.26	0.34	0.22	0.18
Eu	1.35	0.19	0.15	0.19	0.18	0.37	0.22	0.24	0.25	0.21	0.21
Gd	4.95	0.29	0.34	0.47	0.43	0.92	0.57	0.40	0.55	0.29	0.25
Tb	0.87	0.06	0.07	0.10	0.09	0.17	0.11	0.08	0.11	0.06	0.05
Dy	5.81	0.36	0.50	0.70	0.60	1.20	0.80	0.52	0.80	0.38	0.30
Ho	1.23	0.08	0.11	0.15	0.13	0.27	0.17	0.12	0.16	0.08	0.06
Er	3.28	0.20	0.30	0.42	0.37	0.75	0.45	0.33	0.45	0.21	0.17
Tm	0.45	0.03	0.04	0.06	0.05	0.11	0.07	0.05	0.07	0.03	0.03
Yb	2.70	0.17	0.24	0.36	0.34	0.70	0.42	0.33	0.42	0.18	0.16
Lu	0.40	0.03	0.04	0.06	0.05	0.11	0.07	0.05	0.07	0.03	0.02
Ba	37	10	11	9	5	13	7	15	20	16	14
Th	0.04	0.03	0.02	0.03	0.02	0.04	0.02	0.02	0.03	0.01	0.02
Nb	0.80	0.04	0.04	0.05	0.04	0.09	0.02	0.03	0.05	0.00	0.03
Y	30.53	1.90	2.57	3.66	3.18	6.65	4.10	2.95	4.05	2.03	1.67
Hf	0.48	0.05	0.05	0.08	0.07	0.12	0.09	0.09	0.14	0.05	0.04
Ta	0.03	0.02	0.00	0.01	0.00	0.01	0.00	0.00	0.00	0.00	0.00
U	0.01	0.01	0.00	0.00	0.00	0.01	0.00	0.01	0.01	0.00	0.00
Pb	0.27	0.10	0.15	0.15	0.09	0.17	0.03	0.17	0.31	0.28	0.09
Rb	0.5	0.1	0.4	0.3	0.1	0.4	0.1	0.2	0.3	0.1	0.0
Cs	0.02	0.10	0.02	0.01	0.00	0.01	0.01	0.02	0.02	0.02	0.01
Sr	295	331	243	211	204	279	262	357	282	432	455
Sc	67.5	30.4	61.8	77.5	69.5	65.7	62.9	44.3	61.7	27.1	24.7
Zr	7	1	1	2	1	3	2	2	4	1	1

Table 4. continued

Lithology	Gbn	Gbn	Gbn	Gbn	Gbn	Gbn	I/F plut	I/F plut	I/F plut	I/F plut	I/F plut
Sample	1722A5A	1722A7	1722A11	1722A16	1723A3	1723A5	0720G3	0720G2	0720A4	0720A6	0720A7
UTM EW	510889	510889	510122	510227	488891	488891	469553	469553	469553	469478	469242
UTM NS	6849161	6848864	6846862	6847214	6844348	6844348	6843212	6843212	6843212	6843405	6843978
<i>Unnormalized Results (Weight %):</i>											
SiO ₂	49.82	49.97	44.67	49.20	46.19	52.16	70.31	58.54	57.60	57.89	70.17
TiO ₂	0.226	0.237	1.000	0.434	0.676	0.332	0.406	1.220	1.002	1.191	0.386
Al ₂ O ₃	16.43	14.00	16.35	16.28	16.11	21.92	14.69	15.89	16.13	16.09	14.55
FeO*	9.04	10.22	14.34	10.30	11.70	5.80	3.46	9.18	9.56	9.13	3.64
MnO	0.204	0.265	0.224	0.234	0.222	0.120	0.091	0.238	0.281	0.223	0.099
MgO	11.05	14.87	8.76	10.73	9.88	5.05	1.35	3.11	3.42	2.94	1.26
CaO	12.56	9.73	13.24	12.13	13.40	11.99	3.66	6.20	7.49	6.87	3.83
Na ₂ O	1.14	0.88	1.00	1.16	0.91	2.61	4.48	4.06	3.30	3.62	3.96
K ₂ O	0.02	0.03	0.01	0.02	0.02	0.17	1.23	0.92	0.44	0.84	1.57
P ₂ O ₅	0.006	0.054	0.021	0.012	0.009	0.070	0.097	0.334	0.156	0.332	0.095
Total	100.50	100.26	99.62	100.50	99.12	100.22	99.77	99.69	99.38	99.12	99.56
Mg #	68.5	72.2	52.1	65.0	60.1	60.8	41.0	37.7	38.9	36.5	38.1
<i>XRF-Trace Elements (ppm):</i>											
Ni	43	235	27	51	41	27	7	1	4	2	4
Cr	190	589	87	177	168	77	4	8	18	8	10
Sc	48	39	†59	52	†57	27	20	30	42	37	14
V	171	82	†666	207	483	136	76	210	269	211	68
Rb	0	0	0	0	0	2	20	16	8	15	25
Sr	256	225	286	268	228	362	187	258	298	299	200
Zr	8	15	11	10	10	19	114	77	40	84	106
Y	3	14	7	8	5	7	21	35	21	41	21
Ga	13	12	18	13	15	18	14	19	20	18	15
Cu	12	13	29	96	36	61	17	52	151	39	4
Zn	61	106	77	74	69	45	40	94	85	82	35
Th	1	0	1	1	2	1	1	2	2	1	4
<i>ICP-MS (ppm):</i>											
La	0.22	0.90	0.35	0.66	0.16	1.19	6.68	6.73	2.74	7.31	7.31
Ce	0.44	2.17	1.08	1.02	0.56	3.03	14.04	16.44	6.95	18.01	15.36
Pr	0.08	0.38	0.20	0.18	0.11	0.46	1.79	2.51	1.12	2.77	1.93
Nd	0.51	2.51	1.36	1.16	0.74	2.52	8.11	13.25	6.24	14.71	8.78
Sm	0.28	1.08	0.65	0.54	0.39	0.92	2.38	4.53	2.38	5.13	2.53
Eu	0.20	0.48	0.38	0.35	0.24	0.44	0.70	1.36	0.97	1.56	0.71
Gd	0.46	1.66	0.96	0.81	0.61	1.13	2.71	5.48	3.09	6.24	2.81
Tb	0.10	0.32	0.19	0.16	0.12	0.20	0.50	0.97	0.56	1.11	0.51
Dy	0.68	2.31	1.28	1.11	0.84	1.34	3.32	6.33	3.67	7.20	3.32
Ho	0.15	0.52	0.28	0.25	0.19	0.29	0.73	1.34	0.79	1.55	0.73
Er	0.43	1.53	0.75	0.68	0.51	0.80	2.17	3.72	2.21	4.33	2.16
Tm	0.07	0.24	0.11	0.10	0.08	0.12	0.34	0.54	0.32	0.63	0.34
Yb	0.40	1.57	0.67	0.64	0.45	0.73	2.31	3.41	2.00	3.87	2.23
Lu	0.07	0.26	0.10	0.11	0.07	0.12	0.39	0.54	0.32	0.63	0.39
Ba	11	37	16	15	14	75	478	379	355	498	636
Th	0.01	0.04	0.02	0.02	0.01	0.12	2.00	1.18	0.21	1.12	1.80
Nb	0.02	0.10	0.05	0.06	0.02	0.38	1.51	1.93	0.91	2.09	1.62
Y	3.70	13.60	6.72	6.06	4.55	7.60	20.57	37.83	20.65	40.98	20.59
Hf	0.07	0.31	0.13	0.12	0.11	0.43	3.27	2.51	1.15	2.67	3.01
Ta	0.01	0.01	0.00	0.01	0.00	0.02	0.15	0.12	0.05	0.14	0.14
U	0.00	0.01	0.00	0.00	0.01	0.06	0.95	0.66	0.16	0.66	0.90
Pb	0.08	0.32	0.23	0.12	0.19	0.89	3.97	3.70	1.69	3.80	4.04
Rb	0.1	0.1	0.1	0.1	0.1	1.0	19.0	16.0	6.8	15.1	22.0
Cs	0.00	0.00	0.05	0.00	0.02	0.07	1.28	3.51	1.04	1.69	1.40
Sr	264	230	295	272	234	351	179	236	298	290	193
Sc	59.3	46.6	65.8	58.8	68.0	31.7	16.5	41.2	42.9	34.6	14.2
Zr	2	7	3	3	2	13	106	76	33	78	96

Table 4. continued

Lithology	I/F plut	I/F plut	I/F plut	I/F plut	I/F plut	Ch mafic	Ch mafic	Ch mafic	Ch mafic	Ch mafic
Sample	1719A3	1719A5	1719A7	1719A9	1719A12	1719A4	1719A6	1719A8a	1719A10	1728A2
UTM EW	474505	475167	475078	474959	474467	474505	475167	475078	474745	479016
UTM NS	6844810	6845119	6845191	6845221	6845168	6844810	6845119	6845191	6845226	6846824
<i>Unnormalized Results (Weight %):</i>										
SiO ₂	69.67	70.59	67.05	70.98	56.43	49.99	55.22	56.03	52.82	51.81
TiO ₂	0.453	0.414	0.526	0.391	0.774	0.764	0.902	1.228	0.832	0.755
Al ₂ O ₃	15.06	14.22	15.40	14.22	18.87	17.64	16.30	15.00	19.47	18.51
FeO*	3.99	3.28	4.46	3.15	6.97	9.62	9.81	10.43	8.41	8.76
MnO	0.080	0.068	0.115	0.073	0.154	0.183	0.204	0.202	0.163	0.204
MgO	1.40	1.25	1.51	1.21	3.04	7.16	4.35	3.85	3.47	6.16
CaO	4.70	3.69	4.91	3.56	8.57	10.84	8.67	7.92	9.35	9.02
Na ₂ O	3.60	3.81	3.71	3.63	3.18	2.20	2.81	3.39	3.10	2.25
K ₂ O	0.60	1.14	1.09	1.67	0.66	0.38	0.40	0.64	0.87	0.71
P ₂ O ₅	0.098	0.073	0.131	0.073	0.180	0.111	0.098	0.224	0.122	0.143
Total	99.65	98.53	98.90	98.96	98.83	98.89	98.76	98.91	98.61	98.32
Mg #	38.5	40.5	37.6	40.6	43.7	57.0	44.2	39.7	42.4	55.6
<i>XRF-Trace Elements (ppm):</i>										
Ni	5	6	4	4	7	52	3	10	8	32
Cr	5	5	5	9	21	125	24	28	25	67
Sc	17	10	25	20	28	42	41	38	36	35
V	54	63	71	57	181	273	339	303	229	228
Rb	10	18	24	26	13	6	8	13	19	15
Sr	335	222	262	213	316	291	319	294	329	302
Zr	102	115	98	113	37	33	32	60	39	38
Y	19	25	31	24	23	14	15	28	18	17
Ga	14	12	14	13	16	14	19	13	17	18
Cu	21	4	2	3	66	95	96	117	100	69
Zn	39	32	49	30	57	74	79	96	67	97
Th	3	4	0	2	1	1	3	3	1	2
<i>ICP-MS (ppm):</i>										
La	4.71	7.92	5.80	9.36	4.23	2.49	2.61	4.86	3.71	3.88
Ce	10.38	17.65	14.96	19.93	10.26	6.11	6.28	12.32	8.76	8.74
Pr	1.44	2.41	2.28	2.62	1.52	0.95	0.96	1.95	1.27	1.26
Nd	7.27	11.36	11.74	11.72	8.19	5.06	5.18	10.52	6.55	6.49
Sm	2.39	3.45	3.84	3.33	2.91	1.78	1.86	3.69	2.20	2.18
Eu	0.78	0.83	1.04	0.84	1.06	0.73	0.78	1.27	0.80	0.87
Gd	2.87	3.85	4.45	3.65	3.57	2.17	2.29	4.51	2.70	2.54
Tb	0.51	0.69	0.79	0.65	0.64	0.40	0.42	0.81	0.49	0.46
Dy	3.29	4.46	5.28	4.18	4.24	2.59	2.77	5.27	3.29	2.96
Ho	0.71	0.97	1.15	0.92	0.92	0.54	0.60	1.12	0.70	0.62
Er	1.99	2.74	3.32	2.65	2.55	1.52	1.74	3.16	1.99	1.77
Tm	0.29	0.42	0.51	0.40	0.37	0.22	0.26	0.46	0.29	0.26
Yb	1.89	2.68	3.30	2.68	2.38	1.39	1.60	2.81	1.82	1.65
Lu	0.31	0.45	0.55	0.44	0.38	0.22	0.25	0.46	0.30	0.26
Ba	387	685	486	816	250	149	159	299	463	565
Th	0.73	1.91	1.44	2.36	1.28	0.20	0.21	0.40	1.31	0.48
Nb	1.48	1.85	2.26	1.91	1.05	0.64	0.67	1.36	0.96	1.25
Y	19.08	26.44	30.96	25.44	23.94	14.53	15.61	29.11	18.37	16.72
Hf	2.67	3.66	2.69	3.71	1.17	0.81	0.84	1.87	1.31	1.02
Ta	0.10	0.15	0.14	0.15	0.08	0.05	0.05	0.09	0.08	0.08
U	0.44	1.06	0.58	0.88	0.44	0.10	0.11	0.44	0.76	0.21
Pb	2.53	2.73	2.52	3.16	1.69	0.75	0.52	1.78	1.97	1.05
Rb	8.0	16.0	24.3	28.0	12.9	6.2	6.9	12.0	19.3	13.6
Cs	0.57	1.15	1.03	0.78	1.33	0.37	0.74	0.61	1.34	0.49
Sr	326	212	254	215	316	288	311	294	337	312
Sc	16.1	13.4	19.2	12.6	32.3	44.0	45.8	42.9	32.3	38.4
Zr	94	116	90	118	30	24	25	54	34	31

Table 4. continued

Lithology	Ch mafic	Ch mafic	Ch mafic	Bas-and	Basalt	Basalt	Basalt	Basalt	Dacite	DeBari
Sample	1728A4	1719A11	1728A3	1723C05	1710C08	2712C05	2713C20	2723C05	1710C10	& Sleep
UTM EW	478732	474467	478947	492655	589172	463513	465065	472814	588949	bulk
UTM NS	6846830	6845168	6846771	6855257	6850355	6896358	6897859	6873367	6850448	crust
Unnormalized Results (Weight %):										
SiO ₂	50.73	49.38	48.06	56.76	47.75	50.27	51.36	46.96	67.97	52.40
TiO ₂	0.737	1.270	0.591	0.730	0.617	0.934	0.774	0.561	0.268	0.770
Al ₂ O ₃	17.29	17.24	19.26	16.31	19.93	17.12	17.80	16.97	15.80	17.67
FeO*	10.05	8.37	8.86	8.54	8.61	9.19	8.92	6.75	2.38	9.63
MnO	0.225	0.133	0.213	0.139	0.588	0.198	0.171	0.307	0.054	0.180
MgO	6.51	8.35	8.09	8.02	7.87	8.26	7.68	5.81	2.00	6.17
CaO	9.24	9.00	11.96	4.63	8.04	11.57	10.49	19.56	4.55	9.44
Na ₂ O	1.84	3.18	1.42	4.39	2.37	2.15	2.88	1.54	4.04	3.02
K ₂ O	1.21	1.10	0.43	0.21	2.42	0.12	0.18	0.75	1.23	0.59
P ₂ O ₅	0.132	0.444	0.071	0.129	0.084	0.147	0.093	0.688	0.076	0.140
Total	97.97	98.46	98.96	99.85	98.28	99.96	100.34	99.90	98.37	100.00
Mg #	53.6	64.0	61.9	62.6	62.0	61.6	60.6	60.5	60.0	53.3
XRF-Trace Elements (ppm):										
Ni	49	205	73	118	70	71	52	19	41	
Cr	189	296	188	243	107	245	173	85	41	
Sc	43	21	34	29	32	42	37	22	12	
V	249	170	245	213	214	283	260	213	47	
Rb	21	2	11	4	35	1	0	16	18	
Sr	295	1379	244	256	299	243	232	259	475	
Zr	39	158	21	49	31	52	39	24	78	
Y	17	19	11	17	12	17	15	25	6	
Ga	15	20	14	15	15	18	17	17	16	
Cu	12	71	67	70	7	56	75	73	83	
Zn	99	92	127	74	†497	73	69	135	75	
Th	0	3	4	3	3	2	3	1	0	
ICP-MS (ppm):										
La	4.06	1.90	1.10	4.45	2.71	4.48	3.21	4.76	4.77	
Ce	8.41	4.89	3.08	10.12	5.93	10.48	7.43	8.61	9.74	
Pr	1.18	0.78	0.50	1.42	0.86	1.52	1.10	1.21	1.21	
Nd	6.26	4.28	2.93	7.05	4.43	7.82	5.76	6.47	5.30	
Sm	2.08	1.64	1.16	2.20	1.54	2.57	1.99	2.10	1.41	
Eu	0.80	0.67	0.52	0.80	0.71	0.94	0.77	0.86	0.46	
Gd	2.44	2.08	1.53	2.52	1.95	2.98	2.36	2.82	1.25	
Tb	0.44	0.39	0.29	0.45	0.35	0.53	0.43	0.50	0.18	
Dy	2.84	2.55	1.98	2.89	2.23	3.34	2.72	3.41	0.98	
Ho	0.61	0.56	0.42	0.61	0.48	0.71	0.58	0.78	0.19	
Er	1.72	1.56	1.20	1.69	1.35	1.98	1.65	2.22	0.46	
Tm	0.25	0.23	0.17	0.24	0.20	0.28	0.23	0.33	0.07	
Yb	1.61	1.45	1.07	1.52	1.28	1.75	1.47	2.05	0.43	
Lu	0.25	0.23	0.17	0.24	0.20	0.27	0.23	0.34	0.07	
Ba	489	203	344	73	1243	75	72	42	642	
Th	0.36	0.18	0.08	0.46	0.25	0.40	0.27	0.09	1.76	
Nb	1.19	0.41	0.33	1.67	0.87	2.28	1.81	0.54	1.08	
Y	16.38	14.34	11.21	15.84	12.53	18.61	15.33	22.09	5.04	
Hf	0.97	0.75	0.50	1.13	0.77	1.39	1.02	0.53	2.03	
Ta	0.07	0.03	0.02	0.07	0.05	0.14	0.11	0.03	0.08	
U	0.19	0.10	0.04	0.29	0.13	0.18	0.12	0.43	1.12	
Pb	0.71	0.77	0.24	2.03	16.49	1.48	1.22	0.46	13.13	
Rb	21.3	7.5	10.1	3.7	35.1	0.4	0.8	14.4	16.3	
Cs	1.56	0.80	0.66	0.26	0.63	0.01	0.01	0.17	0.91	
Sr	303	299	249	247	301	254	238	233	458	
Sc	40.7	46.2	42.7	32.5	34.8	42.7	43.0	24.7	7.6	
Zr	32	21	15	41	24	46	32	15	68	

Table 5. Neodymium isotopic data

Lithology	Sample	$^{143}\text{Nd}/^{144}\text{Nd}$	\pm	ϵ_{Nd}	$^{147}\text{Sm}/^{144}\text{Nd}$	$(^{143}\text{Nd}/^{144}\text{Nd})_{\text{T}}$	$\epsilon_{\text{Nd(T)}}$
Volcanic*	1710C10	0.512998	8	7.02	0.160184	0.512807	7.87
Volcanic*	1710C11	0.512929	8	5.68	0.195712	0.512696	5.70
Volcanic*	1721C04	0.512919	8	5.48	0.189359	0.512693	5.65
Volcanic*	1722C15	0.512976	4	6.59	0.214083	0.512721	6.19
Volcanic*	1724C02	0.512927	4	5.64	0.179919	0.512713	6.03
Volcanic*	1725C03	0.512951	6	6.11	0.191104	0.512723	6.24
Int/felsic plutonic	1719A7	0.512981	17	6.69	0.174597	0.512773	7.21
Int/felsic plutonic	1719A8a	0.512971	10	6.50	0.190613	0.512744	6.64
Int/felsic plutonic	1719A10	0.513000	23	7.06	0.185077	0.512780	7.33
Chilled mafic	1719A11	0.512990	13	6.87	0.208759	0.512741	6.59
Chilled mafic	1728A3	0.512981	25	6.69	0.207118	0.512734	6.45
Gabbroonorite	1709A2	0.512960	14	6.28	0.185757	0.512739	6.54
Gabbroonorite	1710A4b	0.513032	26	7.69	0.224690	0.512764	7.04
Gabbroonorite	1710A4e	0.513047	13	7.98	0.254391	0.512744	6.64
Gabbroonorite	1721A1	0.512998	13	7.02	0.242755	0.512709	5.96
Gabbroonorite	1722A11	0.513041	8	7.86	0.259501	0.512732	6.41
Gabbroonorite	1723A3	0.513085	11	8.72	0.278292	0.512754	6.83
Pyroxenite [†]	0712P1C	0.513024	5	7.53	0.251068	0.512725	6.27

Age corrections were made using an age of 182 Ma for all samples.

*Volcanic analyses are from Clift *et al.* (2005).

† Unpublished analysis from J. Blusztajn.

Table 6. Phase proportions for gabbronorites (in wt %)

Sample	Cpx	Opx	Plag	Sp	Amph	Ol	Total	ΣR^2
<i>Basal Gabbronorites</i>								
1710A4b	20.4	20.8	46.9	1.5	10.4		100.0	0.0088
1710A4d	9.5	3.1	29.1	8.1	50.1		99.8	0.1190
<i>Lower crustal gabbronorites</i>								
0718A4	19.3	10.9	43.7	8.1	18.0		100.0	0.0137
1712A3a	21.2	10.9	51.1	7.9	8.9		100.0	0.0198
1712A3b	15.7	13.4	50.4	11.6	8.9		100.0	0.0028
1712A4	22.0	13.3	43.3	11.2	10.2	0.02	100.0	0.0153
1712A7	1.8	1.3	43.8	12.2	41.0		100.1	0.4140
1722A2	16.3	17.0	45.1	6.8	14.8		100.0	0.6442
1722A4b	10.5	1.7	75.0	2.8	10.0		100.0	0.0127
1722A4c	12.3	6.1	79.6	1.2	1.0		100.1	0.0105
1722A5a	15.3	10.3	41.2	0.1	32.9		99.9	0.1516
1722A7	9.9	45.7	32.1	0.0	12.3		100.0	0.0536
1722A11	17.6	13.3	37.8	7.5	23.8		100.0	0.1642
1722A16	15.8	26.1	41.3	1.6	15.3		100.1	0.0349
<i>Mid-crustal amphibole gabbronorites</i>								
1721A1	2.2	8.8	49.8	5.2	34.1		100.1	0.1353
1723A5	5.5	11.9	68.8	0.1	14.1		100.3	0.2133

ΣR^2 is the sum of the squares of the residuals for all oxides used in the mass-balance.

Results are based on a least-squares method using the whole-rock and mineral chemistry.

Results are plotted in Figure 13C, along with solutions from fractionation modeling.

Table 7. Least-squares fractional crystallisation solutions

Step 1	Sample		Proportion	SiO2	Al2O3	TiO2	FeO*	MnO	CaO	MgO	Na2O	Mg#
Parent	1728A3	mafic dike		48.54	19.45	0.60	8.95	0.22	12.08	8.17	1.43	61.9
Daughter	1719A4	chilled pillow	20.7 % crystallised	50.53	17.83	0.77	9.73	0.18	10.96	7.24	2.22	57.0
Fractionated minerals	1709P11	cpx	42.9 %	51.87	4.39	0.08	4.12	0.04	23.63	15.46	0.41	87.0
	1709P11	opx	8.0 %	53.03	5.42	0.00	12.25	0.16	0.56	28.46	0.00	80.6
	1709P11	plag	31.6 %	44.21	36.12	0.00	0.08	0.00	18.93	0.02	0.63	
	1709P11	Mg-Al sp	17.5 %	0.20	67.14	0.04	15.31	0.04	0.02	17.08	0.00	
		calculated composition		48.53	19.46	0.62	8.85	0.15	12.07	8.23	1.84	
		parent		48.54	19.45	0.60	8.95	0.22	12.08	8.17	1.43	
		difference		0.0077	-0.0083	-0.0236	0.0979	0.0605	0.0109	-0.0554	-0.4077	
		% of oxide (daughter)		0.0153	-0.0463	-3.0574	1.0059	32.6942	0.0992	-0.7661	-18.33	
		Σ R ² kd (Fe/Mg) cpx/liq(parent)		0.1833 0.24	Cumulative results: % crystallised							20.7
				% melt							79.3	
Step 2	Sample		Proportion	SiO2	Al2O3	TiO2	FeO*	MnO	CaO	MgO	Na2O	Mg#
Parent	1719A4	chilled pillow		50.53	17.83	0.77	9.73	0.18	10.96	7.24	2.22	57.0
Daughter	0709P2A	bas-andesite	38.5 % crystallised	53.30	16.96	1.05	11.04	0.26	7.81	6.05	3.04	49.4
Fractionated minerals	1709P11	cpx	20.2 %	51.31	5.31	0.08	4.51	0.05	23.29	15.02	0.42	85.6
	1712A3A	opx	8.4 %	52.61	1.40	0.16	17.44	0.51	1.06	26.80	0.01	73.3
	1709P11	plag	45.1 %	44.80	35.68	0.00	0.10	0.00	18.58	0.01	0.82	
	1712A7	mag-il	2.9 %	0.02	1.49	2.24	95.86	0.15	0.01	0.13	0.00	
	1712A3b	hbl	23.5 %	48.61	8.54	1.43	10.77	0.17	12.32	16.51	1.51	
		calculated composition		50.54	17.83	0.81	9.73	0.20	10.95	7.23	2.18	
		parent		50.53	17.83	0.77	9.73	0.18	10.96	7.24	2.22	
		difference		-0.0038	0.0025	-0.0396	0.0009	-0.0108	0.0024	0.0070	0.0436	
		% of oxide (daughter)		-0.0071	0.0147	-3.7626	0.0081	-4.1929	0.0308	0.1161	1.4315	
	Σ R ² Kd (Fe/Mg) cpx/liq(parent)		0.0037 0.22	Cumulative results: % crystallised							51.2	
				% melt							48.8	
Step 3	Sample		Proportion	SiO2	Al2O3	TiO2	FeO*	MnO	CaO	MgO	Na2O	Mg#
Parent	0709P2A	bas-andesite		53.30	16.96	1.05	11.04	0.26	7.81	6.05	3.04	49.4
Daughter	0709P2C	andesite	44.8 % crystallised	57.09	18.36	1.02	9.12	0.24	4.46	3.87	3.82	43.1
Fractionated minerals	0718A4	cpx	22.2 %	52.32	2.29	0.30	6.91	0.28	22.81	14.91	0.17	79.4
	1722A2	opx	17.0 %	52.05	1.28	0.09	21.77	0.65	0.61	23.53	0.01	65.8
	1723A5	plag	44.7 %	52.63	30.12	0.00	0.26	0.00	12.52	0.01	4.24	
	1710A4d	mag-il	8.4 %	2.43	1.86	10.57	83.38	0.43	0.58	0.53	0.00	
	1712A3b	hbl	7.6 %	48.61	8.54	1.43	10.77	0.17	12.32	16.51	1.51	
		calculated composition		53.30	16.96	1.05	11.04	0.23	7.81	6.05	3.04	
		parent		53.30	16.96	1.05	11.04	0.26	7.81	6.05	3.04	
		difference		-0.0003	0.0000	0.0009	-0.0002	0.0244	0.0003	0.0003	0.0032	
		% of oxide (daughter)		-0.0006	0.0001	0.0872	-0.0025	10.1537	0.0076	0.0074	0.0832	
	Σ R ² Kd (Fe/Mg) cpx/liq(parent)		0.0006 0.25	Cumulative results: % crystallised							73.1	
				% melt							26.9	

* Total Fe as FeO

$\sum R^2$ is the sum of the squares of residuals.

Fractionated minerals are expressed as a percentage of the percent crystallised.

Complete whole rock analyses for the parents and daughters are listed in Table 5.

Cumulative % crystallised is the sum of the % crystallised from the remaining melt for each step.

Abbreviations: cpx-clinopyroxene, opx-orthopyroxene, plag-plagioclase, mag-il-magnetite-ilmenite, hbl-hornblende,

bas-andesite-basaltic andesite

Table 8. Pyroxenite addition results

Daughter (starting comp.)								
	ch mafic	ch mafic	volcanic	volcanic	ch mafic	ch mafic	volcanic	volcanic
	1719A11	1728A3	1710C08	2712C05	1719A11	1728A3	1710C08	2712C05
Mg#	64.0	61.9	62.0	61.6	64.0	61.9	62.0	61.6
SiO ₂ ^a	50.11	48.54	48.57	50.25	50.11	48.54	48.57	50.25
Fe ³⁺ /Fe(t) used	0.14	0.14	0.14	0.14	0.14	0.14	0.14	0.14
cpx Fe ²⁺ /Mg kd used	0.27	0.27	0.27	0.27	0.33	0.33	0.33	0.33
equil. Cpx Mg#	88.5	87.5	87.5	87.3	86.2	85.2	85.2	84.9
daughter wt %	73.8	68.0	68.6	66.4	55.6	50.6	51.6	51.2
Pyroxenite (solid added)								
pyroxenite wt %	26.2	32.0	31.4	33.6	44.0	49.4	49.4	49.4
% Cpx	70.0	70.0	70.0	70.0	70.0	70.0	70.0	70.0
% Opx	28.0	28.0	28.0	28.0	28.0	28.0	28.0	28.0
% Sp	2.0	2.0	2.0	2.0	2.0	2.0	2.0	2.0
Estimated primary magma								
SiO ₂	50.41	49.33	49.34	50.59	50.61	49.70	49.72	50.73
Al ₂ O ₃	14.57	15.44	16.10	13.61	12.99	13.76	14.25	12.33
TiO ₂	1.02	0.47	0.50	0.71	0.88	0.42	0.44	0.62
FeO*	7.51	7.70	7.58	7.83	6.98	7.18	7.05	7.35
MnO	0.13	0.19	0.47	0.18	0.13	0.18	0.42	0.17
CaO	10.96	13.43	10.57	13.12	11.95	14.01	11.63	13.69
MgO	11.26	11.55	11.37	11.75	12.80	12.99	12.89	13.02
K ₂ O	0.86	0.31	1.79	0.09	0.72	0.26	1.50	0.07
Na ₂ O	2.52	1.08	1.80	1.58	2.13	0.94	1.53	1.37
Cr ₂ O ₃	0.29	0.31	0.29	0.33	0.40	0.41	0.40	0.42
P ₂ O ₅	0.35	0.05	0.06	0.10	0.29	0.04	0.05	0.09
Mg#	72.8	72.8	72.8	72.8	76.6	76.3	76.5	75.9
final equil. Cpx Mg#	92.01	92.00	92.01	92.01	92.01	91.91	91.99	91.75

* Total Fe as expressed as FeO. Mg# is calculated with total Fe, expressed as FeO.

^a Renormalized wt% with Cr₂O₃.

Full analyses for all rocks are listed in Table 4.

cpx Fe²⁺/Mg Kd's are from Sisson and Grove (1993) (0.27) and Mientener *et al.* (2001)(0.33)

DeBari and Sleep (1991) bulk crust estimate from their Table 1.

Abbreviations: cpx-clinopyroxene, opx-orthopyroxene, sp-spinel, ch mafic-chilled mafic rock, equil.- equilibrium

Table 8. continued

Daughter (starting comp.)

	ch mafic	ch mafic	volcanic	volcanic	ch mafic	ch mafic	volcanic	volcanic
	1719A11	1728A3	1710C08	2712C05	1719A11	1728A3	1710C08	2712C05
Mg#	64.0	61.9	62.0	61.6	64.0	61.9	62.0	61.6
SiO ₂ ^a	50.11	48.54	48.57	50.25	50.11	48.54	48.57	50.25
Fe ³⁺ /Fe(t) used	0.20	0.20	0.20	0.20	0.20	0.20	0.20	0.20
cpx Fe ²⁺ /Mg Kd used	0.27	0.27	0.27	0.27	0.33	0.33	0.33	0.33
equil. Cpx Mg#	89.2	88.3	88.3	88.1	87.1	86.0	86.1	85.8
daughter wt %	79.6	74.2	74.6	72.8	63.6	57.0	58.0	55.0

Pyroxenite (solid added)

pyroxenite wt %	20.4	25.8	25.4	27.2	36.4	42.6	41.8	44.4
% Cpx	70.0	70.0	70.0	70.0	70.0	70.0	70.0	70.0
% Opx	28.0	28.0	28.0	28.0	28.0	28.0	28.0	28.0
% Sp	2.0	2.0	2.0	2.0	2.0	2.0	2.0	2.0

DeBari & Sleep**Estimated primary magma****primary magma**

SiO ₂	50.32	49.17	49.18	50.50	50.52	49.55	49.55	50.68	50.97
Al ₂ O ₃	15.14	16.11	16.79	14.17	13.62	14.37	14.99	12.70	14.95
TiO ₂	1.07	0.49	0.52	0.74	0.94	0.44	0.46	0.65	0.65
FeO*	7.68	7.88	7.75	8.02	7.16	7.33	7.22	7.43	9.49
MnO	0.13	0.20	0.49	0.18	0.13	0.19	0.44	0.17	0.18
CaO	10.59	13.20	10.16	12.86	11.54	13.79	11.20	13.52	9.19
MgO	10.72	10.98	10.82	11.18	12.20	12.48	12.31	12.68	11.27
K ₂ O	0.91	0.33	1.90	0.09	0.77	0.28	1.62	0.08	0.48
Na ₂ O	2.66	1.14	1.90	1.67	2.29	0.99	1.64	1.43	2.50
Cr ₂ O ₃	0.25	0.27	0.24	0.29	0.36	0.38	0.35	0.40	0.21
P ₂ O ₅	0.37	0.06	0.07	0.11	0.31	0.05	0.06	0.09	0.11
Mg#	71.3	71.3	71.3	71.3	75.2	75.2	75.2	75.2	67.9
final equil. Cpx Mg#	92.01	92.00	92.01	92.00	92.00	92.00	92.00	92.01	

* Total Fe as expressed as FeO. Mg# is calculated with total Fe, expressed as FeO.

^a Renormalized wt% with Cr₂O₃.

Full analyses for all rocks are listed in Table 4.

cpx Fe²⁺/Mg Kd's are from Sisson and Grove (1993) (0.27) and Mientener *et al.* (2001)(0.33)

DeBari and Sleep (1991) bulk crust estimate from their Table 1.

Abbreviations: cpx-clinopyroxene, opx-orthopyroxene, sp-spinel, ch mafic-chilled mafic rock, equil.- equilibrium